UNIVERSITY OF BIRMINGHAM

MODELLING AND CONTROL OF HYBRID LCC HVDC SYSTEM

by

YING XUE

A thesis submitted to
The University of Birmingham
for the degree of
DOCTOR OF PHILOSOPHY

School of Electronic,
Electrical and Systems Engineering
The University of Birmingham
January 2016

To my parents

ACKNOWLEDGEMENTS

First of all, my deepest gratitude goes to my supervisor, Professor Xiao-Ping Zhang. It is a great honour for me to have Professor Xiao-Ping Zhang as my supervisor for my PhD study. His innovative ideas and advices formed the bases of my study, his patience and support helped me through the hardest times of my research work. Without his generosity to share with me his understanding and visions of power systems and HVDC, this research work cannot reach the same level as it does today.

I would also like to thank my colleagues Dr. Dechao Kong, Dr. Xuan Yang, Dr. Suyang Zhou, Dr. Jingchao Deng, Mr. Puyu Wang, Mr. Jianing Li, Mrs. Na Deng, Mr. Zhi Wu, Mr. Jing Li, Mr. Zuanhong Yan and Mrs. Can Li from the Power and Control Group for their advices and inspiring discussions. It has been a great experience to work with them over the past three years.

To my girlfriend and colleague, Conghuan Yang, I am grateful for all the supports and understanding I have received from her during the past three years. Thank you for the joys you have brought to my life.

Last but not least, I would like to thank my beloved parents. Thank you so much for your love and support throughout my whole research period. You brought me into the scientific world and guided me to where I am today.

ABSTRACT

Since its first application 60 years ago, Line Commutated Converter (LCC) based High Voltage Direct Current (HVDC) technology has played an important role in long distance bulk power transmission. Nowadays due to the geographical separations of generation and demand in many countries together with an ever increasing requirement of renewable power integration, LCC HVDC is playing an even more crucial role in long distance high power transmissions. However, several technical challenges still exist today which limit the further application of this technology. The notable three are 1) Commutation failures which can happen under 10% to 14% of AC voltage reduction at inverter side; 2) Significant reactive power requirements at both sides of the HVDC system; 3) Difficulty in the black start of a passive AC network. This thesis proposes a new hybrid HVDC system to solve these problems.

Unlike any existing method, the proposed hybrid HVDC configuration offers the ability of commutation failure elimination under both single-phase to ground and three-phase to ground fault at inverter AC bus. With dynamic insertion of capacitors in the commutation loops, the increase of effective commutation voltage can help the success of commutations even when there is no natural commutation voltage from the AC side such as during zero impedance three-phase fault.

The elimination of commutation failures opens up the possibility of reactive power control at inverter side. The inverter side can now be controlled to work at unity power factor without concerns about commutation failures. With the proposed new extinction angle measurement, dynamic reactive power tracking and inverter AC voltage control can also be achieved.

For the black start of a passive network, the difficult initial commutations can be successfully completed with the help of connected filter banks. A new inverter side AC voltage controller is proposed to keep the inverter bus voltage at rated value. The possibility of loss of commutation margin using the proposed controller is eliminated utilizing the proposed hybrid HVDC system.

In order to verify the performance of the proposed system and the designed controllers, simulation results from Real Time Digital Simulator (RTDS) are presented based on the modified CIGRE HVDC benchmark system.

TABLE OF CONTENTS

LIST OF FIGURES

LIST OF TABLES

LIST OF ABBREVIATIONS

HVDC	High Voltage Direct Current
FACTS	Flexible Alternating Current Transmission Systems
LCC	Line Commutated Converter
VSC	Voltage Sourced Converter
MMC	Modular Multilevel Converter
VDCOL	Voltage Dependent Current Order Limit
SCR	Short Circuit Ratio
ESCR	Effective Short Circuit Ratio
CCC	Capacitor Commutated Converter
GCSC	Gate Controlled Series Capacitor
PLL	Phase Locked Loop
DSL	DigSilent Simulation Language
DPL	DigSilent Programming Language
ASC	Automatic Switching Control
OLTC	On-Load Tap Changer Control
IGBT	Insulated Gate Bipolar Transistor
THD	Total Harmonic Distortion
PCT	Phase Controlled Thyristor
α	Converter Firing Angle

ϕ	Converter Power Factor Angle
μ	Commutation Overlap Angle
V_d	DC Voltage
E_m	AC Phase Voltage Magnitude
X_c	Transformer Equivalent Reactance
I_d	DC Current
γ	Inverter Extinction Angle
β_n	Normal Firing Advance Angle
I_{dn}	Rated DC Current
γ_n	Normal Extinction Angle
γ_m	Minimum Extinction Angle
ω	AC System Angular Frequency
f	AC System Frequency
L_c	Transformer Leakage Inductance
V_0	Initial Capacitor Voltage
i_1	Instantaneous Current through TY1

i_3	Instantaneous Current through TY3
v_p	Instantaneous Voltage for Positively Inserted Capacitor
v_n	Instantaneous Voltage for Negatively Inserted Capacitor
C	Capacitance of Capacitor Module
$I_{d\max}$	Maximum DC Fault Current
$\mu_{\max}$	Maximum Commutation Overlap Angle
L_d	Inductance of DC Smoothing Inductor
ΔV_{in}	Capacitor Voltage Increase after Commutation
ΔV_{de}	Capacitor Voltage Decrease after Commutation
ΔV_{total}	Total Capacitor Voltage Decrease in One Cycle
ΔV_{pre}	DC Voltage Increase due to Capacitor Pre-Insertion
V_{ac}	RMS Line-to-Line AC Voltage
I_{L1}	RMS Value of Fundamental Frequency AC Current
i_3'	Instantaneous TY3 Current during Single-Phase Fault
i_1'	Instantaneous TY1 Current during Single-Phase Fault
ΔV_{μ}	DC Voltage Increase due to Capacitor Insertion during Commutation

$V_{original}$	DC Voltage without Capacitor Insertion
I_{conv}	Total Inverter AC Current Injection into AC System
I_{up}	AC Current Injection from Upper 6-Pulse Bridge
I_{down}	AC Current Injection from Lower 6-Pulse Bridge

CHAPTER 1 INTRODUCTION

1.1 Research Background

1.1.1 Shift to Renewable Generations

Ever since the industrial revolution took off in 18th century, fossil fuels have been the main driving force behind social and economic growth. The fossil fuel consumption level has grown significantly to about 10,000 million tons of oil equivalents in 2012 [1]. As the global population increases and energy-intensive industries expand, the speed of consumption has reached an unprecedented level, as shown in Figure 1-1. This trend is expected to continue in the future to be in pace with social and technology developments. However since fossil fuels are finite and it takes millions of years to become so, there is the possibility of running out of fossil fuels not long in the future [2]. For example, if we carry on the rate at which we are using oil, the currently known oil deposits will be completely depleted by 2052 [3]. If an increase of gas production is used to fill the gap left by oil, it can only give us limited additional years to 2060 [4]. Similarly if the coal is used to fill the gap left by oil and gas, the known coal deposits will take us to 2088 at most [5]. The concerns for fossil fuel depletion hence become one of the reasons for a shift to renewable energy generation.

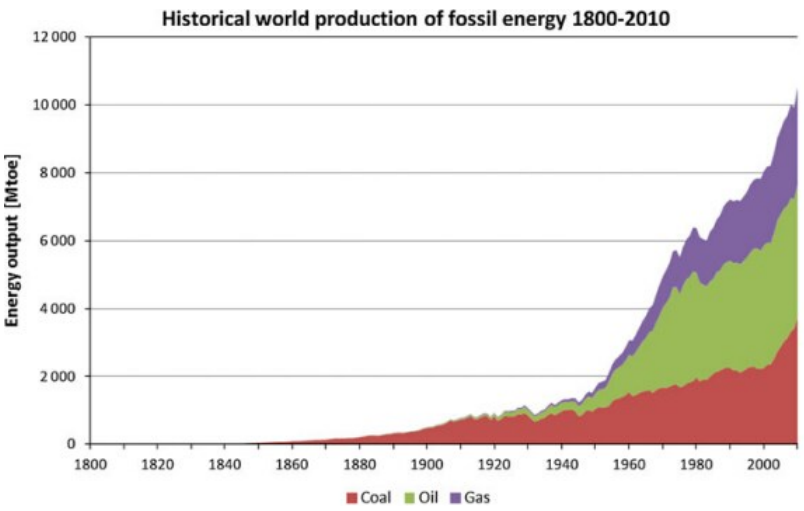

Figure 1-1 Historical production of fossil fuel from 1800 to 2010 [1]

At the same time environmental issues associated with the use of fossil fuels also raise worldwide concerns. It is well-known that the process of burning fossil fuels produces carbon dioxide (CO_2) which is one of the main greenhouse gas emissions that is contributing to global warming. The global warming directly causes an increase of the world's temperature and results in various adverse effects such as the melting of glaciers, an increase of sea levels and changes in traditional agriculture productivities [6]. Among the economic activities that lead to greenhouse gas emissions, energy supply is the largest single source as shown in Figure 1-2 [7]. Hence the energy supply sector is under pressure and has the strongest driving force in a shift to electricity generation using renewable sources to help reduce global CO_2 emissions. Consequently renewable power such as wind power, hydropower and solar power are experiencing noticeable developments in the 21st century. In this way, the vision of sustainable development can become possible. In response to this trend of shifting, different countries have set up their own targets to meet global requirements. In U.K, it has a target of 15% of energy demand being provided by renewable sources and a corresponding 34% reduction in CO2 emission by 2020 [8]. Scottish government's 2020 renewable target states that the equivalent of 100% of Scotland's electricity demand should be met by renewables [8]. In China in order to use the vast hydro power located at West part of the country, about 13

large hydro power centres are planned in the future with a total generating capacity of about 215 GW [9]. In order to reach these targets, a minimum level of renewable power integration is definitely needed. For instance in U.K, approximately 30% of UK's electricity will have to come from renewable sources by 2020.

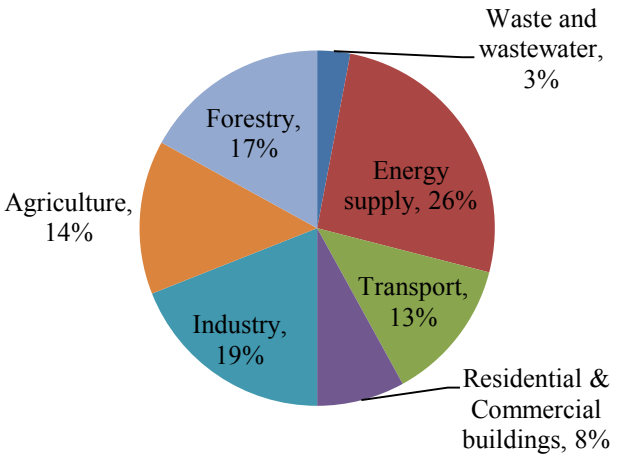

Figure 1-2 Global greenhouse gas emissions by source [7]

Beside the drives from global energy situations, other factors from within the power system sector are also contributing to the increase of renewable power integrations. Some examples of these factors are:

- Decommissioning of the aged power plants (coal and nuclear).
- Advancement of power electronic technologies applicable to power systems.
- Government incentive policies such as the *Feed in Tariffs* for solar power and *Carbon Tax*.
- Difficulty in obtaining planning permissions for traditional power plants and transmissions lines.

All of the reasons mentioned above result in a rapid development of renewable electricity generation and will certainly lead to even larger scale of integrations in the future.

1.1.2 The Need for HVDC

As discussed in last section, the continued population growth will result in higher energy consumptions and the corresponding power generations to meet the demand. However, for many countries the majority of renewable sources needed are not located at or near the load centres. For example in China, hundreds of GW of hydroelectric power and wind power are located at the west part of the country. Most of the industrialized load centres, on the other hand, are located at the east and south part of the country along the coast. The nominal distances between these generation sources and the load centres are in the range of 1000 km to 3000 km. Similarly in UK, most of the wind power and hydroelectric power sources are located at the Scotland area while the main load centres are located at the south of England. This geological separation of renewable sources and load centres requires the technology for efficient long distance power transmission.

Furthermore, as the interconnection of AC networks between different countries are under development such as the European Super Grid and interconnection between Asian countries [10], it can be expected that unsynchronized AC system connections are required because some of the countries with the intention of interconnection are using different frequencies.

Beside the required long transmission distances and possible unsynchronized AC system connections, from an environmental protection point of view, it is becoming more and more difficult to get planning permissions for onshore transmission corridors for renewable energies due to the limited right of way and the need to avoid sensitive ecosystems. Most of the time the best solution is to increase the transmitted power level or to use undersea/underground cables instead. So alternative solutions to traditional AC transmission to meet the above needs are required and these requirements can be met by High Voltage Direct Current (HVDC) especially when the transmission distance is longer than 700 km [11].

As a matter of fact, the history of power system started with DC transmission when Thomas Edison built the first low voltage DC transmission back in 1882 [12]. However at that time, due to the reasons that AC voltages can be easily stepped to different levels for transmission and circuit breakers can be applied taking advantage of natural current zero crossing, DC was quickly taken over by AC. Despite the fact that AC transmission in power system has been dominating the power system industry for most of the time, the interests on DC transmission still remained [13]. Ever since the commission of first commercial HVDC in 1954, the number of HVDC projects around the world were steadily increased and are experiencing a dramatic increase in recent years [14]. This wide application of HVDC technology is justified by the ability of HVDC to meet the aforementioned transmission requirements:

- *Bulk power transmission over long distances.* For long distance AC overhead line transmissions, most of the AC voltage is needed to compensate the voltage drop and phase angle shift due to the line inductances and this limits the AC transmission distance. Otherwise series compensations or Flexible Alternating Current Transmission Systems (FACTS) devices need to be used which will introduce more cost. On the other hand for DC transmission, thanks to the fewer and smaller transmission lines and smaller towers, although the converter station costs more than the AC substation, the per km distance cost is smaller than that of the AC option. Also there is no stability limitation for DC transmission over long distances. So there is a break-even distance beyond which it is more economical to transmit power using DC rather than AC as shown in Figure 1-3. Depending on the economic factors, the break-even distance for overhead line is normally in the range of 600 km-800 km and 40 km-70 km for cable applications.
- *Power transmission over cables.* Long AC cables are primarily capacitive and they generate a lot more reactive power than they consume. So large reactive current is needed to charge and discharge the cable as grid voltage changes polarity 50 or 60 times per

second. Since both active power and reactive power use the thermal limit of cables, the practical length for high voltage AC transmission over cable is limited. On the other hand DC cable does not draw any reactive charging current hence power can be transmitted over any distance only limited by the cost of the cable and losses.

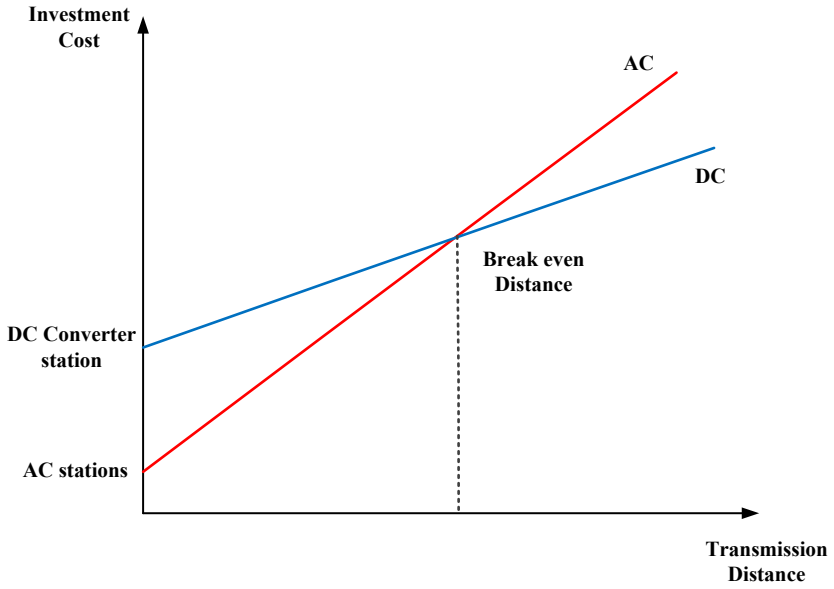

Figure 1-3 HVDC and AC break even distance [11]

- *Unsynchronized AC interconnection*. In AC transmission, safe power transmission is only possible between systems with similar nominal frequency. However for DC transmission, since the power being transmitted is in the form of DC current, no requirement on the connected AC system frequency is imposed.

Beside the above three fundamental advantages over the AC system, there are other benefits of having HVDC systems built into the existing AC system such as improving the power system stability and acting as firewalls between the interconnected AC systems. These abilities of HVDC in meeting power system challenges result in a wide application of this technology and it is likely to play an even more important role in future power systems.

1.1.3 LCC (Line Commutated Converter) vs VSC (Voltage Sourced Converter)

LCC HVDC.

The first commercial HVDC built in 1954 was based on the LCC technology [15, 16]. Ever since the development of thyristors in 1960s, which overcame many of the problems with mercury-arc valves, all the LCC HVDC projects are based on the thyristor power semiconductors. Thyristor power switches can be actively switched on by applying a gate signal but has to depend on natural current zero crossing to switch off. Therefore it relies on the external AC commutation voltage to drive the current down to zero for successful commutations and this is why it is called line-commutated converter. To achieve accurate firing of thyristor switches, Phase Locked Loops (PLL) are widely used to provide reference phase signal synchronized with the AC system [17, 18]. This reference signal is used as a basic carrier wave to derive valve firing pulses for converter controllers. The actual firing instants are then obtained by adding the desired firing angle to the PLL outputs. Figure 1-4 shows the basic module for LCC HVDC - the 6-pulse full-wave Graetz bridge [19]. Since the thyritors can only conduct in one direction, the direction of DC current is determined by the orientation of the bridge. Hence in order to achieve power transmission in two directions, DC voltage, rather than the DC current, needs to be reversed. The reverse of DC voltage is achieved by controlling the firing angle. A firing angle less than 90^0 results in a positive 6-pulse DC voltage and a firing angle between 90^0 to 180^0 generates a negative 6-pulse DC voltage. A firing angle larger than 180^0 cannot be achieved under natural commutation since the AC commutation voltage cannot drive down the outgoing phase valve current. LCC HVDC has the advantage of easy implementation and robust operation when connected to a relatively strong AC system, which makes its application successful over the years.

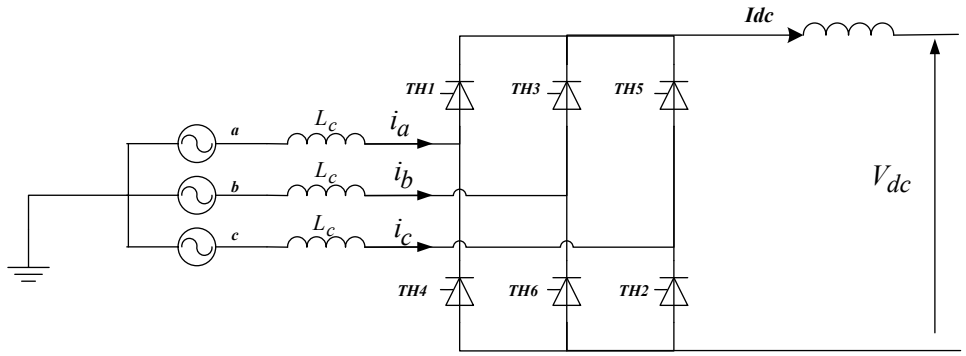

Figure 1-4 6-pulse Graetz bridge

The main application areas of LCC HVDC are bulk power transmission over long distance [20] and interconnection between two AC grids. With the mature thyristor technology, current LCC systems have a typical rating of up to 8000 MW [21, 22]. The introduction of 8.5 kV Phase Control Thyristor (PCT) is one of the main factors that improves the performance of this technology [23-25]. It has a current rating up to 4000 kA and has the lowest conduction losses among all the semiconductor switches, which results in a typical 0.7% of losses per converter station [26, 27]. These two features - low losses and high power ratings, together with its mature and time proven technology have made it the best choice of long distance bulk power transmissions.

VSC HVDC.

The newly introduced VSC technology was first put into commercial operation in 1997 in Sweden and experienced dramatic developments thereafter [28-36]. Unlike LCCs, where thyristor power switches are used, it uses Integrated- Gate Bipolar Transistor (IGBT), which offers the abilities of active switch on and switch off. It gives VSC the advantages of independent AC voltage magnitude and phase angle control hence enabling independent active and reactive power control. In recent years, due to the development of Multilevel Modular Converter (MMC) [37-46] technology and better switching strategies, the losses of

VSC have been reduced from the initial 3.7% down to less than 1% and operation without any harmonic filters at converter AC bus can be achieved [47, 48]. These flexibilities offered by VSC have made it very attractive in applications like connecting to weak AC systems and offshore wind farms[49]. However the limited power handling capabilities and relatively high conduction losses of IGBTs have made it less suitable for long distance bulk power transmissions. For example, the highest power rating of VSC link in operation today is the 500 MW interconnector between Ireland and UK [50, 51]. So it can be expected that in the near future, both the LCC and VSC installations will grow depending on the practical applications.

In this thesis, the focus will be on the traditional LCC HVDC technologies and trying to solve the problems associated with it. Some of the major inherent weaknesses of LCC HVDC will be described in the next section.

1.1.4 LCC Weaknesses

Commutation failures. The problem of commutation failure at inverter side of LCC HVDC system has been with it since its first application using mercury-arc valves [52-54]. In recent years, due to the increasing number and higher ratings of new LCC projects around the world, its adverse impacts on the connected AC system and the HVDC system itself are becoming ever more prominent [55]. Commutation failures are caused by one important characteristic of thyristor which is that it needs a negative voltage across it for certain duration of time before regaining its forward voltage blocking capability [56]. So a commutation margin is needed at inverter side to guarantee successful commutations. However, due to reasons like sudden decrease of AC commutation voltage or sudden increase in the DC current or malfunctioning of firing systems, commutation failures are unavoidable. Once happened, the faulty bridge acts as a short circuit on the DC side and the transmitted power drops down to

zero. Preliminary study results are shown in Figure 1-5, where a short duration single-phase to ground fault is simulated, commutation failure happens with a rise in DC current and zero DC power.

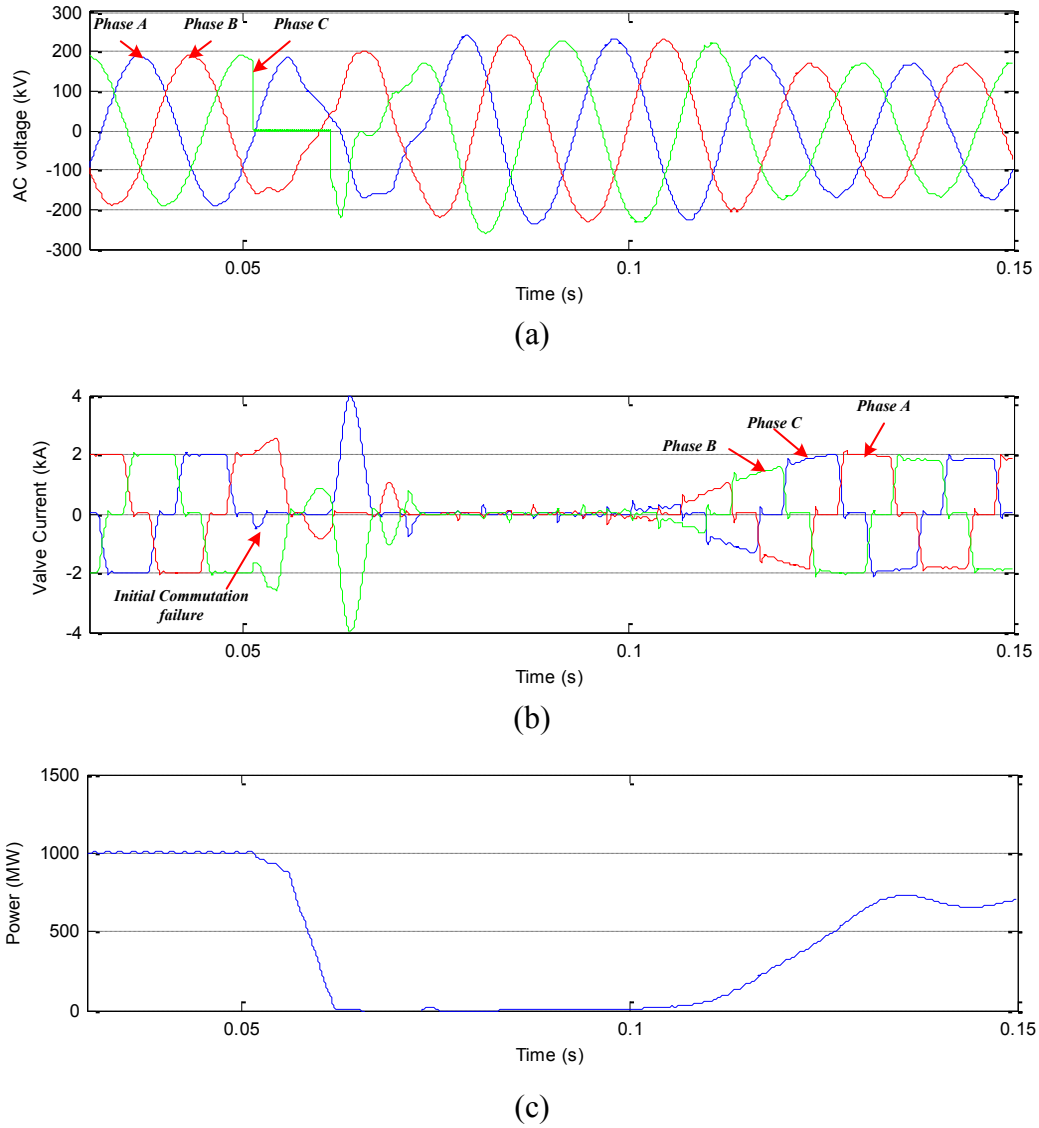

Figure 1-5 Commutation failure with single-phase fault

Due to the very high rating of LCC HVDC, it usually takes up a considerable portion of the total power being delivered to the heavily industrialized load centres. At the same time, the multi-infeed HVDC configuration has become more popular, where two or more LCC HVDCs are terminated at the same load centre such as the four LCC HVDC lines with a total rating of more than 10 GW terminating at Guang Zhou, China [57, 58]. Consequently, in the

case of commutation failures, where there is a cessation of active power being transferred, the frequency of receiving end system and the neighbouring AC system stability can be adversely affected [59]. From the point of view of the converter stations, since a DC short circuit is formed during commutation failure, it results in a significant increase of the DC current going through two of the inverter valves. In addition to the increase of DC current magnitude, the prolonged conduction time of that current during commutation failure can cause serious overheating of the valves. It can damage the semiconductor switches and increase cost on the protection systems. In some serious cases where successive commutation failures are happening, the whole converter station may need to be blocked until the fault has been cleared. Further adding to the seriousness of the problem is that commutation failures can happen under only 10% to 14% of AC voltage reduction. It means that a remote single-line fault can cause commutation failures [60]. In some earlier studies, it had been concluded that AC disturbances will cause nothing worse than a single or a double commutation failures, which are self-recoverable and do not have serious impact on the connected AC power systems [61]. However as the ratings of LCC and number of installations are increasing, the consequences of commutation failures will become more severe. Therefore it is of importance to study commutation failures and try to mitigate or even eliminate it.

Converter reactive power consumption. Since the thyristors can only conduct in one direction and cannot be actively switched off, the firing pulses can only be applied after the valve voltage becomes positive at rectifier side and be disengaged before the valve voltage becomes positive at inverter side. This in effect delayed the AC current waveform with respect to the AC commutation voltage waveform as shown in Figure 1-6, which results in both sides of the converter stations absorbing reactive power. In Figure 1-6, phase A at rectifier side is considered and commutation overlap is neglected for simplicity. At point A onwards phase A voltage becomes the largest and firing pulse can be issued after a delay

angle α to turn on *TH1* as shown in Figure 1-4. So the fundamental frequency component of i_a is in effect delayed by α, which can be seen from the phasor diagram. Therefore, viewed from the AC side, rectifier behaves like an inductor and absorbs reactive power.

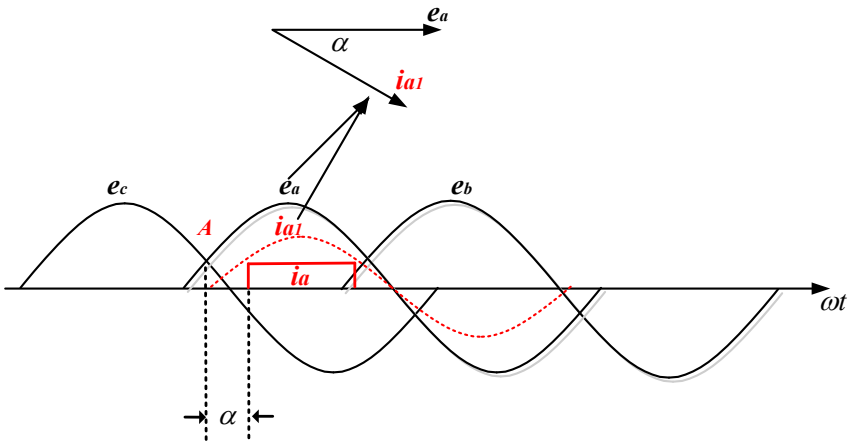

Figure 1-6 Phase displacement between voltage and current for phase A

The power factor of rectifier AC bus can be approximated by the following equation [62]

$$\cos\phi \approx \frac{\cos\alpha + \cos(\alpha+\mu)}{2} \tag{1.1}$$

where μ is the overlap angle.

Given the normal firing angle under the rated condition at rectifier side to be about 15^0, and overlap angle to be about 25^0, the power factor is 0.866 lagging. It means that the reactive power absorption is 57.7% of the active power being transferred at normal operating condition. Similarly, at inverter side of the system, due to the fact that extinction angle has a minimum value of about 15^0 to mitigate commutation failures, the resulting power factor and reactive power consumption at rated condition is very similar to that of rectifier side. Reactive power consumption of either converter station at different active power levels can be obtained as shown in Figure 1-7. The calculations are based on the CIGRE HVDC

benchmark model with system parameters obtained from [117]. A power base of 1000 MVA is used.

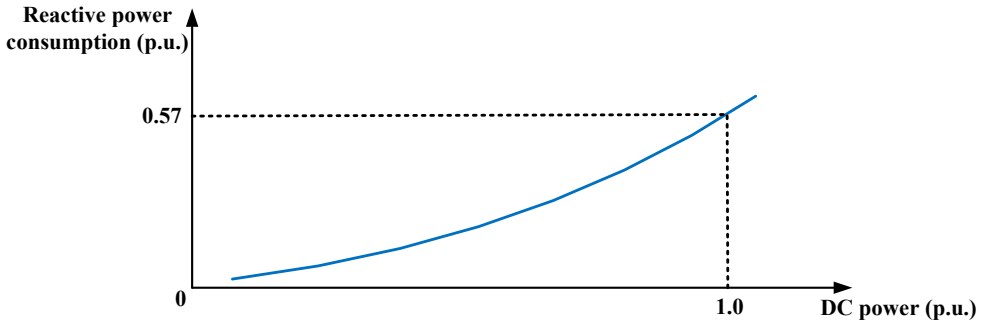

Figure 1-7 Variation of converter reactive power consumption

This requirement of considerable reactive power consumption largely limits the reactive power controllability of LCC system. Also, since large reactive power exchange with the AC system is highly undesirable, ideally all of the reactive power should be compensated locally. It is normally achieved by installing large capacitor and filter banks at the converter AC bus. Those reactive power compensations not only increase the investment cost but also accounts for a considerable amount of space of the converter station. If LCC is used for offshore windfarm integration, the extra space needed of the sea platform will be economically prohibitive. Furthermore, because the reactive power output of these passive elements largely depends on the level of the AC voltage and they tend to produce much less reactive power at reduced AC voltage level when reactive power is mostly needed, synchronous condensers are installed to provide additional reactive power controllability [63]. Last but not least, in some projects where reactive power exchange with the network is strictly limited, design of reactive power compensation imposes great technical challenges [62]. So it is highly desirable that the reactive power consumption level of LCC HVDC can be reduced.

Black start capability. For VSC HVDC systems, since the AC voltage is produced by the DC voltage and it does not rely on AC voltage for successful commutation, it can operate into an AC network with very small Short-Circuit Ratio (SCR) or even energise a passive network [64]. This is normally referred as the black start capability. However, for LCC HVDC technology, commutation is driven by the AC voltage and current always lags the voltage for normal operation, the black start is considered to be very hard [63].

For successful initial commutation, the equivalent impedance of AC network at fundamental frequency has to be capacitive [65]. Most of the time, diesel generator is needed to supply auxiliary power to the converter station, and starting motors are needed to energize the synchronous condensers. During start up process, complex and careful coordination between the converter station and those auxiliary devices are required so that a smooth energization of the dead network can be achieved. These additional investment and complexities puts the LCC technology at a disadvantage, particularly in some special cases such as connecting to an island system or very weak system where a timely and cost effective black start capability is required.

It will be a significant improvement for the LCC technology if less expensive and simpler black start scheme can be developed, because the other end of the system has a high possibility of not experiencing a blackout given the normally long distance of the transmission. Also as the ratings of LCCs become higher, it will be much more economically beneficial to improve the LCC HVDC black start strategies. Hence the motivation is high and potential benefits of improving LCC HVDC black start is large.

From the above analysis, it can be seen that the LCC HVDC technology brings both opportunities and challenges for future power systems. If its advantages can be wisely used and problems can be dealt with appropriately, it can surly bring more benefits to the world.

1.2 Literature Reviews

1.2.1 Commutation Failures

As explained in former sections, commutation failures are frequent dynamic events happened at the inverter side of the LCC HVDC system mainly due to AC side disturbances [60]. It can either be the AC voltage magnitude drop or phase shift [56]. Not all AC side disturbances can cause commutation failures and the actual behaviour of DC system is a function of the equivalent Thevenin impedance of the inverter AC network [62]. If the Thevenin impedance is small, then the variation of AC bus voltage will be small, hence the probability of commutation failure will be low. On the other hand, if the equivalent Thevenin impedance is large, the risk of commutation failure subject to AC disturbances will be large. In order to quantify the impact that AC disturbance has on the DC system, an index called the Short-Circuit Ratio (SCR) was proposed [66-70]. SCR is defined as the short circuit MVA of the AC bus divided by the rated DC power. Normally an AC system with SCR less than 2.5 is called a weak system and it can pose significant challenges in HVDC controller design. Later on, a new index called the Effective Short Circuit Ratio (ESCR) was proposed in [71] which took into account the reactive power generation of AC filters. This makes the ESCR smaller in magnitude than SCR for the same system. Normally a system is classified as weak or strong according to the ESCR values shown in Figure 1-8 [62].

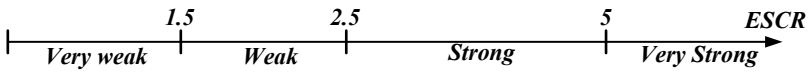

Figure 1-8 System strength against ESCR [62]

In addition to the use of sensitivity index of SCR or ESCR, mitigation functions embedded into HVDC control systems were also designed. It is called the Voltage Dependent Current

Order Limit (VDCOL) and is incorporated into the rectifier current controller [72-74]. A typical VDCOL characteristic together with the HVDC static V-I curve and are shown in Figure 1-9. During normal operations the inverter side is controlling the DC voltage (I-J) or minimum extinction angle (J-K), and rectifier side is controlling the DC current (C-D). When commutation failure happens, it causes the thyristor valves to be in conduction with a large DC current for more than 120^0. Since all the valves are designed only for the rated current with a conduction period of 120^0, they may suffer from overheating problems. So the current order at the rectifier side is designed to be about 1/3 of the rated value during fault cases to make the valves work close to their thermal rating during fault conditions. However by lowering the current orders, VDCOL is only useful to prevent the system from successive commutation failures by reducing the commutated DC current. It does not affect the onset of initial commutation failures.

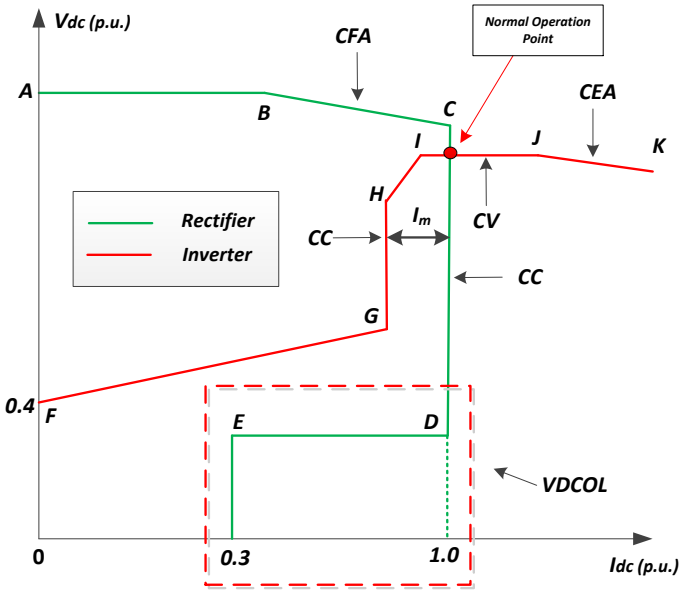

Figure 1-9 VDCOL and LCC HVDC static characteristic

In early days, most of the LCC HVDC systems had a small rating of a few hundred of MW. So commutation failures due to remote fault did not have serious impact on the connected AC systems as long as they can automatically recover. However, in the past two decades, as the

number and rating of the system increases, its impact on the connected AC power systems becomes larger, which results in a series of research on the analysis and possible mitigation methods of commutation failures [75-86]. Reference [60] perhaps shows the best theoretical analysis of commutation failures. It concludes that commutation failure can happen even under modest AC voltage reductions and it is the voltage magnitude reduction that has the largest effect on the onset of commutation failure rather than phase shift. Also it shows that other than increasing the rated extinction angle settings, modifications to control systems are not effective in reducing the probability of commutation failures. It is mainly because once the firing angles are issued, the initial commutation failures thereafter cannot be detected by the control system.

Nevertheless, a number of ways by modifying the controllers are proposed in literature in an effort to reduce the probability of commutation failure. In [80], a predictive extinction angle control method was proposed. This method utilized the measurement of AC voltage to predict if commutation failure is going to happen or not. If the calculation shows that commutation will happen under the prevailing AC voltage, the firing angle will be immediately advanced to give a larger commutation margin. In [76], similar predictive type using the AC voltage measurement was used, but with a different prediction algorithm. Later on in reference [87], without complex predictive calculations, a simple detection method is used to detect whether the AC voltage drop will cause commutation failures. The firing angle is also advanced upon detection of the faults. A fuzzy logic controller based controller modification was proposed in [75]. Extensive simulations need to be run to create the look-up-table for the fuzzy control system. The result of this method is to modify the PI controller gains depend on different system operating conditions. Another paper [79] also used fuzzy logic controller to improve the performance but the emphasis is placed on minimising the impact of commutation failure has on the connected AC system. Reference [81] proposed a predictive current controller at

rectifier side to lower the current order during disturbances. It effectively decreases the commutated DC current, which can definitely help the commutation process, but the communication delay is not considered. Simulation results have shown that the DC fault current has already reached its peak value when the control signal is send back to the rectifier control system. The most recent advances in control modification is published in [85] which utilizes a novel power component fault detection method and improved VDCOL to mitigate commutation failures. Improvement over [87] is probably obtained but practical implementation is still not justified.

From the above descriptions, it can be seen that most of the proposed control modification methods finally result in the advancement of firing angles at inverter side. The main differences are that they use different algorithms to calculate the advancement angle and to determine whether this advancement is needed or not. Due to the time delay of the control system and communication system, these methods are most useful to prevent successive commutation failures or help the recovery of system after commutation failures. When the fault is electrically close to the converter AC terminal, commutation failures can still happen. In terms of the detection method improvements, the signals with higher sensitivity on commutation failure are helpful, provided that the computational burden is not huge.

In parallel with the developments in control modifications, system topology modifications are also adopted. Reference [78] proposed a method by adding additional passive filters at the inverter AC bus sharply tuned to the 2^{nd} order harmonics. This method works by modifying the frequency spectrum of the AC network so that additional commutation margin can be achieved during cases of voltage distortions. However the effectiveness of the method is limited, since the harmonic voltage excited under different fault cases are highly unpredictable. Additional capacitors connected in parallel with the thyristors are used in [88]

to force turn off the thyristors once commutation is complete. It also utilizes the resonance between smoothing inductor and additional capacitors at DC side to lower the commutation currents. The use of resonance can easily suffer from detuning problems and the additional parallel capacitors will add significant voltage stress to thyristor valves. Also the DC voltage is going to experience high voltage spikes, which can add cost to the protection systems. Simulation studies have also shown that the choice of the parallel capacitor is very limited. One of the promising configurations is the Capacitor Commutated Converter (CCC), which results in less commutation failure and better power factor [89-97]. In this topology the actual commutation voltage is no longer the AC bus voltage but the valve side voltage, which equals to the sum of AC voltage and the voltage induced on the capacitors. The result is that the commutation margin measured against the AC voltage can be very small while the real commutation margin measured using the actual commutation voltage is much larger. So by increasing the actual commutation margin, commutation failure probability can be reduced. But the voltage stress added to thyristor valves by the series connected capacitors can be up to 2-3 p.u. before acceptable performance is achieved. That is why all of the practical CCC systems are built with a decreased DC voltage level and mostly back to back configurations [98-100]. The most recent advancement in this field is shown in [101, 102] where the concept of hybrid HVDC system is proposed. In the proposed topology, rectifier side uses the traditional LCC converter and inverter side uses the MMC converter technology, which does not have problems of commutation failure. However due to the use of high-power diodes, power flow direction cannot be reversed and given the current MMC rating, it is not compatible with the rectifier LCC rating. So by connecting the two together, the advantage of high LCC rating is lost. Furthermore, the control coordination between the two converter stations needs to be thoroughly studied.

It can be clearly seen that the application of power electronic devices/capacitors to the system do bring some benefits but the increase of voltage stress over thyristor valves and justifications for the additional investment need to be dealt with properly.

1.2.2 Reactive Power Consumption

The commutation from one valve to another has to be driven by the natural commutation voltage from the AC side. So this kind of commutation can only be started after the voltage positive crossing point at rectifier side and must be completed before the voltage negative crossing point at inverter side [62]. The consequence is that both rectifier side and inverter side draw reactive power from the AC network. Due to the amount of the reactive power requirement, most of it is compensated locally by means of filter and capacitor banks.

At rectifier side a series capacitor voltage injection method proposed by [103] is adopted to reduce the reactive power consumption. An assisting-polarity voltage is injected into the incoming phase before natural positive zero-crossing of AC voltage. If injection is carried out at the instant when voltage difference between two phases are the same as the voltage level on the capacitors, the valve connected to that phase can be turned on. The effect of this is that valves at rectifier side can be turned on earlier which make phase shift between voltage and current smaller. By proper choice of capacitor voltages, reactive power can be favourably controlled. It should be noted that reactive power reduction at rectifier will be advantageous when it is used for offshore wind farm connection, due to the smaller sea platform. On the other hand, for onshore transmission, from the sending end point of view, the rectifier side acts as a load and it is natural that it absorbs some reactive power so the reactive power requirement is not that high. The recent development of both shunt and series connected active compensators [104-108] opens up new opportunities for reactive power support, but they have not been implemented yet for such applications. It can be expected that shunt

connected devices, for example static compensator (STATCOM) and series connected gate-controlled series capacitor (GCSC), will play an important role in improving the reactive power performance of LCC HVDC, given that the additional cost and losses can be justified.

The reactive power characteristic at inverter side is very similar to that at rectifier side, but additional considerations to commutation failure should be taken into account. In theory, reactive power can be controlled by controlling the firing angle at inverter side, but small extinction angle tends to cause commutation failures. So reactive power control through control modification is very limited and is mostly achieved by switching of capacitor banks and filter banks according to different DC power levels [109]. The most promising method with practical implementations is the aforementioned CCC. The additions of fixed series capacitors naturally shift the actual valve commutation voltage so that a leading AC current can be realized with respect to the AC bus voltage. It has been demonstrated in [90] that if the capacitor voltage is high enough, the reactive power consumption can be 10%-15% of the active power being transferred. With these advantages, the increase of harmonic content and valve voltage stress are the main drawbacks of this topology [110]. Similar to the rectifier side, dynamic reactive power support from FACTS devices such as Static Var Compensators (SVC) and STATCOM are also used for better reactive power control. It is worth mentioning that to the receiving end AC system, the inverter side acts as a power producer and as such should take its share of reactive load. But instead of producing, it consumes reactive power. So its consumption level should be minimized. Thus it is of more importance for the reduction of reactive power consumption at inverter side than that at rectifier side.

From the above analysis it can be observed that reactive power control, similar to the reduction of commutation failure, is of significant importance at inverter side. Since most of

the works being done are focusing on the reactive power compensation rather than reactive power reduction, potentials are huge to reduce the converter reactive power consumption.

1.2.3 Black Start Capability

The first HVDC link built in 1954 (Gotland 1) had black start capability [63]. The link is supplying power to Gotland Island and due to limited generating capacity on the island the HVDC link is required to have black start capability. Synchronous condensers are essential to build up the AC voltage for successful commutations. The starting motors are thus needed to energize the synchronous condensers. The additional equipment not only adds to the cost but also complicates the start-up sequence. Other problems associated with the traditional way of black start are:

- If the demand on the receiving network increases, additional synchronous condensers are needed to control the AC voltage.
- During start-up process when HVDC link is supplying the auxiliary load and station losses, the DC current is very low. At this current level with the harmonic current ripples, the DC current will be discontinuous and refiring of the valves is needed. The operation in this condition cannot last long and load must be connected within 5 minutes [63].
- Extensive communications between the inverter station and island network are needed for a smooth start-up.

Later on, with the introduction of CCC, it is proposed to help the DC connection to remote load [110]. Three different configurations are discussed in the paper. The first configuration is a 6-pulse bridge with fixed series capacitor insertion and auxiliary diesel generators at inverter side while the rectifier side is using the traditional 6-pulse bridge. The second configuration is similar to the first one except the diesel generators are not present. The third

configuration is using a 12-pulse bridge with fixed series capacitors at inverter side and traditional 6-pulse bridge at rectifier side. The third configuration is finally chosen, which shows superior capability for initial commutation and active/reactive power coordination. Simulation results in [111] show that the system is able to black start a dead network with no rotating machines and no fast telecommunication networks are required. However since the system is using two 6-pulse converters independently, harmonic content in the AC network is large, hence more filters are needed. Also traditional issues with CCC which is increased voltage stress over the valves cannot be solved and in this case, the stress tends to be higher than normal, since wide range of control over the injected current is needed for acceptable performance. Nevertheless, it provides a promising direction for future research.

With the advancement of semiconductor technologies, various kinds of fast dynamic reactive power control devices such as SVC and STATCOM are being proposed in [111, 112] to help HVDC link invert into a very weak AC system. It was concluded in [111] the SVC and synchronous compensator (SC) used together have the best overall dynamic performance but the additional cost involved is comparable to the synchronous condensers. The use of STATCOM at inverter side was first proposed in [112] but no investigation into the black start capability was made at that time. It was later in [113] that the same system topologies using CCC with different control strategies are being studied connecting to an island network. In that system, the STATCOM and inverter are viewed as one controlled unit, with STATCOM controls the AC bus voltage and inverter controls the system frequency. Good overall performance can be achieved at both start up and load switching. The disadvantage of the scheme is that a fairly large STATCOM needs to be used to control the AC bus voltage and provide dynamic active power support. Similar ideas are being used in [114] with traditional LCC inverter and a STATCOM.

Over the last decade, because of the fast development in VSC technology, a number of topologies with the help of VSC were proposed. A double infeed HVDC system supplying a passive network is proposed in [115] with one LCC link and one VSC link terminated at the same AC bus. With the help of reactive power control from VSC, the system is able to successfully transfer power into a dead load with good dynamic performance. In [63], a comprehensive review of the current technology using VSC for black start purpose was carried out. Furthermore, several practical experiences of black start with VSC were shown to demonstrate the performance. The different stages of network restoration are described in detail with actual filed testing plots using VSC HVDC. In [64], the energization of a large nearby transformer, a remote transformer, a 200 km long transmission line, a shunt reactor bank and a large steam-turbine generator are carefully described with respect the field testing results. It validates that VSC can indeed be used as a power standby facility for black start purpose. The fully controllable IGBTs do offer a lot more flexibility in terms of control. But due to the limitations in rating, its application in bulk power transmission over long distances is difficult to achieve in the near future.

Very recently, the advancement of black start capability using the traditional LCC HVDC without additional power electronic devices was published in [116]. It was identified in [65] that thyristor based HVDC do have some unexploited potentials such as the black start capability, which has been traditionally ignored. In the proposed method, the fixed 50 Hz or 60 Hz pulsing scheme is used at inverter side to control the frequency of the network. The voltage magnitude at AC side is controlled by varying the current injected into the AC system. Simulation results of both no-load start up and load pick-up cases were shown, and the results demonstrated acceptable performances. However, there are two aspects needing further improvement, which are that extremely high extinction angle operation mode is required before the load is picked up, and relatively large extinction angle at steady state is required to

avoid commutation failures. The consequences are higher losses in steady state and additional protection level in surge arresters. Another novel control scheme for black start using 12-pulse bipolar LCC HVDC was proposed in [116]. The novelty of this method is that it uses lower 12-pulse bridge to work in rectifier mode drawing current from the AC network to control the AC voltage. The upper12-pulse bridge uses a fixed 50 Hz or 60 Hz scheme. In this way, the high extinction angle operation during no-load start up can be eliminated. At the same time, by slightly lowering the tap changer of upper 12-pulse bridge, a higher than nominal extinction angle can be used without violating the allowed valve stress. So for the initial start up to no load case, the extinction angle of the inverter side upper 12-pulse bridge can be controlled to about 30^0 before the load starts to pick up. The main drawbacks of this configuration are listed as follows:

- The maximum power that can be delivered to the AC system is about 0.45 p.u. of the bipolar capacity. This is due to the different power flow directions of two poles.
- When load starts to pick up, the transient extinction angle is expected to be very small, which may result in commutation failures.

Also further transient studies including fault analysis need to be carried out to test the robustness of the method.

From the above analysis, it can be seen that although the emergence of VSC technology enables reliable black start of the system, the potentials from LCC HVDCs is still waiting to be exploited. If the current issues associated with LCC black start are appropriately solved, even at the cost of additional investment, it can open up much more opportunities for the application of this technology.

1.3 Project Objectives, Contributions and Thesis Outline

1.3.1 Project Objectives

The main objectives of the project are to:

1. Develop an advanced model of LCC HVDC with Automatic Filter Switching (ASC) and On Load Tap Changer (OLTC) control.
2. Develop a novel HVDC circuit configuration which has the ability of commutation failure elimination.
3. Investigate various issues with reactive power control at inverter side with the proposed HVDC configuration.
4. Investigate various issues with black start capability of the proposed HVDC configuration.

1.3.2 Scientific Contributions of the Thesis

The main contributions of the work shown in this thesis are summarized as follows:

- A new HVDC circuit configuration with dynamic capacitor insertion is proposed. By increasing the effective commutation voltage, elimination of commutation failure is achieved.
- A new way of extinction angle measurement which accommodates negative extinction angles is proposed for reactive power controller design.
- A cascaded reactive power controller which generates extinction angle reference for the inner controller is proposed for reactive power tracking.
- A new black start sequence of the proposed system is proposed which can potentially solve most of the issues with traditional black start strategy.

- A new inverter side AC voltage controller is proposed which is able to control the voltage at rated value under various loading conditions.

1.3.3 Project Outline

The project is carried out using both theoretical analysis and time domain simulations in RTDS. The outline of the thesis is as follows:

Chapter 2 The implementation of an advanced model of LCC HVDC with ASC and OLTC are described. The traditional control methods of LCC HVDC are described first, and then the ASC and OLTC functions being added to the model are explained in detail.

Chapter 3 A new Hybrid HVDC configuration with controllable capacitors is proposed for the elimination of commutation failures. The principles of operation and capacitor balancing method are explained first and then the simulation results in RTDS are presented to validate the effectiveness of the proposed method.

Chapter 4 Reactive power control of the proposed system is analysed. Theoretical analysis is carried out to investigate how the capacitor voltage level is related to the reactive power output ability. Then a simple outer reactive power control loop is designed with simulation results showing dynamic reactive power tracking performance of the system. In addition, an inverter AC voltage controller is designed to keep the inverter AC voltage at constant level.

Chapter 5 Black start sequence and control methods are developed for the proposed hybrid HVDC system. The notable problems and issues exist in traditional method are analysed and then lead to the solutions of them using the proposed system. Simulation results of the system connecting an entirely passive network are presented.

Chapter 6 This chapter concludes the thesis and discusses possible future works.

The relationships between chapters are as follows:

Chapter 2 describes the operation of traditional LCC-HVDC system and lays the foundation for later chapters.

Chapter 3 proposes the hybrid HVDC system based on the traditional LCC-HVDC system described in **Chapter 2** to eliminate commutation failures.

Chapter 4 and **Chapter 5** are dedicated to the solution of two technical challenges in LCC-HVDC system using the hybrid HVDC system proposed in **Chapter 3**.

CHAPTER 2 DEVELOPMENT OF AN ADVANCED LCC-HVDC MODEL

2.1 Introduction

In this chapter, the development of a comprehensive LCC-HVDC model with filter bank switching control and converter transformer tap changer control is presented. In section 2.2 the motivation for Western HVDC link in UK and the need for such a model are discussed. In section 2.3 and section 2.4, the control method for traditional LCC HVDC system is reviewed which leads to the need for tap changer control and filter bank switching control. In section 2.5, the developed system configuration and the calculated filter switching strategy are presented. In section 2.6, the DSL models of filter bank switching and tap changer control are described. Simulation results are then presented to justify the controller designs in section 2.7. A summary of the main results of this chapter are included in section 2.8.

2.2 Background and Motivation

As mentioned in chapter 1, the development of renewable energy generation in UK is playing an important role in the nation's effort to reduce the production of greenhouse gas emissions and decarbonise the economy [8]. As a result of the European Union Renewable Energy Directive, the UK has a target of more than 15% of the energy to be generated from renewable sources by 2020. By taking into account the renewable target and other electricity reinforcement scenarios, the Electricity Networks Strategy Group (ENSG) varies the electricity being generated by renewable sources in Scotland from at least 6.6 GW by 2016. Currently the main transmission corridor between the Scotland and England are the 400 kV

AC lines and they are working at their maximum stability limit. The additional installations of series and shunt compensations will increase the existing limit to their thermal limit of 4.4 GW by 2015. Other onshore AC reinforcements are considered to meet the 6.6 GW generation capacities but due to the relatively high cost and difficulty to get planning permissions in time, the offshore cable schemes are chosen. Because of the limited transmission distance of AC cable mentioned in last chapter, the DC undersea cable is adopted. When it comes to the choice of HVDC technology, due to the gap of 2.2 GW and given the offshore distance between Scotland and England, LCC HVDC is the better choice over VSC because of its higher power transmission capability at longer distance. Consequently the Western HVDC link is proposed based on LCC HVDC technology to accommodate the increasing renewable energy generation in Scotland.

Since most of the LCC HVDC models do not take into account the effect of filter bank switching control and on-load tap changer control, an advanced 12-pulse bipolar LCC HVDC model with both control functions is developed which can be used for power flow studies, network stability studies and dynamic studies. In the developed model, reactive power control utilizing the filter bank switching and tap changer control of converter transformer are designed so that the system is able to operate over a wide range of active power transfer with minimum reactive power exchange with the connected AC system.

2.3 Review of Conventional LCC HVDC control

In order to show how reactive power control and tap changer control are fitted within the converter station control systems, classic LCC HVDC control systems at both rectifier side and inverter side are briefly reviewed.

2.3.1 Rectifier Control & The Need for Tap Changer Control

The most commonly used rectifier controller is shown in Figure 2-1. The main control loop is the fast current control loop where the DC current is controlled by controlling the rectifier DC voltage. The relationship between the DC voltage and rectifier firing angle can be shown as:

$$V_d = \frac{3\sqrt{3}}{\pi} E_m \cos\alpha - \frac{3}{\pi} X_c I_d \tag{2.1}$$

Where V_d is the DC voltage, E_m is the AC phase voltage magnitude, α is the rectifier firing angle, X_c is the transformer equivalent reactance and I_d is the DC current. It can be seen from (2.1) that the DC voltage can be effectively controlled by controlling the firing angle.

The main reason that the rectifier terminal is used to control the DC current not DC voltage is that if it is used to control the DC voltage, the DC fault current can be very large during inverter side grounding fault. When it is controlling the DC current, the fault current can be effectively limited by lowering the rectifier side DC voltage through an increase of its firing angle. The actual current order I_{ord}^* is obtained by taking the minimum value of the current order from outer power control loop I_{ord} and the current order from VDCOL which is I_{ord_VDCOL}. The outer power control loop is normally used to generate I_{ord} so that the transmitted DC power can be adjusted. During normal operation when the DC voltage is around the rated value, I_{ord_VDCOL} is higher than I_{ord} so that I_{ord}^* takes the value of I_{ord}, which is normally 1 p.u., to generate the firing angles. Then the PI controller produces the rectifier firing angle by minimising the difference between actual current order I_{ord}^* and measured DC current I_{dc_meas}. The control of DC current is realized by modifying the

rectifier DC voltage through adjusting the output firing angles from controllers. The Phase-Lock Loop (PLL) is used together with firing angle α to determine the actual firing instant.

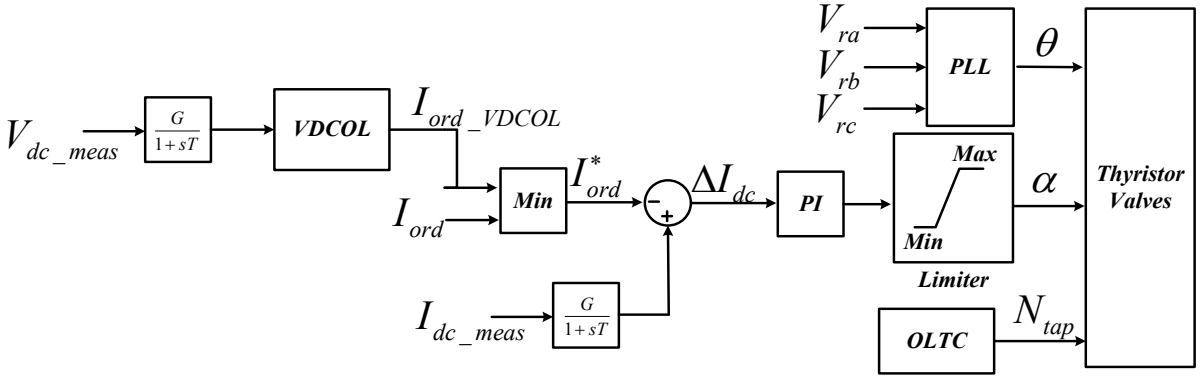

Figure 2-1 Rectifier side controller

The relationship between rectifier firing angle and its reactive power consumption is described in (1.1). It can be observed from this equation that minimum reactive power consumption can be achieved at the smallest firing angle. Therefore it is desirable to operate the system at the smallest firing angle possible during rated condition so that additional reactive power compensation can be minimised. Considering that the thyristors need a certain level of voltage for turning on, and that it should have some control over DC current by increasing its DC voltage when the inverter side DC voltage increases, the rated rectifier firing angle is normally set to be about 15^0.

However during practical operations, it is inevitable that the operating point moves around due to the changes in the connected AC networks such as AC voltage disturbances. If the system is constantly working at a non-rated condition, the rectifier firing angle can either be too large or too small to keep the rated transmitting power. A larger firing angle brings down the DC voltage and increases the reactive power consumption level. With lower DC voltage the operating DC current need to be higher than normal for rated power transfer. The persisting high DC current can affect or damage the system components. A too small firing

angle leaves no room for rectifier side to control the DC current when there is an increase of DC voltage at inverter side. Also there is the possibility that thyristors may not be successfully turned on. So some mechanisms need to be in place to modify the rectifier firing angle if it is working at abnormal values for a certain period of time. This is the main reason that On Load Tap Changer Control (OLTC) is equipped at the converter transformer. It works by applying step changes to transformer tap changer so that the rectifier firing angle can be brought back to nominal value. Compared with the normal rectifier current controller, OLTC can be considered as a slow supplementary controller for the steady state firing angle.

2.3.2 Inverter Controller & The Need for Tap Changer Control

The normally used inverter side controller is shown in Figure 2-2. It has a current control loop, a constant extinction angle γ control loop and a Current Error Control (CEC) between the two loops. The inverter side V-I characteristic is similar to the rectifier side and is given by the following equation:

$$V_d = \frac{3\sqrt{3}}{\pi} E_m \cos\gamma - \frac{3}{\pi} X_c I_d \tag{2.2}$$

where γ is the inverter side extinction angle. The inverter controller mainly controls the minimum extinction angle which determines the DC link voltage level. From Figure 1-9 it can be seen that under normal conditions the inverter side is controlling the DC voltage, and this is achieved by controlling the extinction angle via firing angle as demonstrated in (2.2). The *CEC* is used to make a smooth transition between extinction angle control and current control. Under normal operating conditions, the current error ΔI_{inv} will be zero and the firing angle order coming out of the current loop PI controller is biased to its maximum value by the current margin I_m. So under the rated condition inverter side is on constant extinction angle control. The current controller takes over the constant γ control when the DC current

error ΔI_{inv} is larger than 0.1 p.u. In this case, the DC current cannot reach rated value because the rectifier firing angle is at its minimum value and cannot decrease the DC current by further increasing its DC voltage. So now rectifier side determines the DC voltage level and inverter current controller is controlling the DC current to be 0.9 p.u. This situation is normally encountered when the rectifier side terminal is experiencing an AC voltage drop. It is not desirable for the system to work in this mode for a long time because the extinction angle can be quite large when inverter side is in current control mode. In normal operation, by observing the converter static characteristic as shown in Figure 1-9, the inverter side is working at its voltage ceiling with minimum extinction angle. A large extinction angle results in higher reactive power consumption and higher active power losses. Consequently the OLTC is also equipped at inverter side to control the DC voltage level. The aim of OLTC at inverter side is to bring back the extinction angle to its minimum value by adjusting the DC voltage.

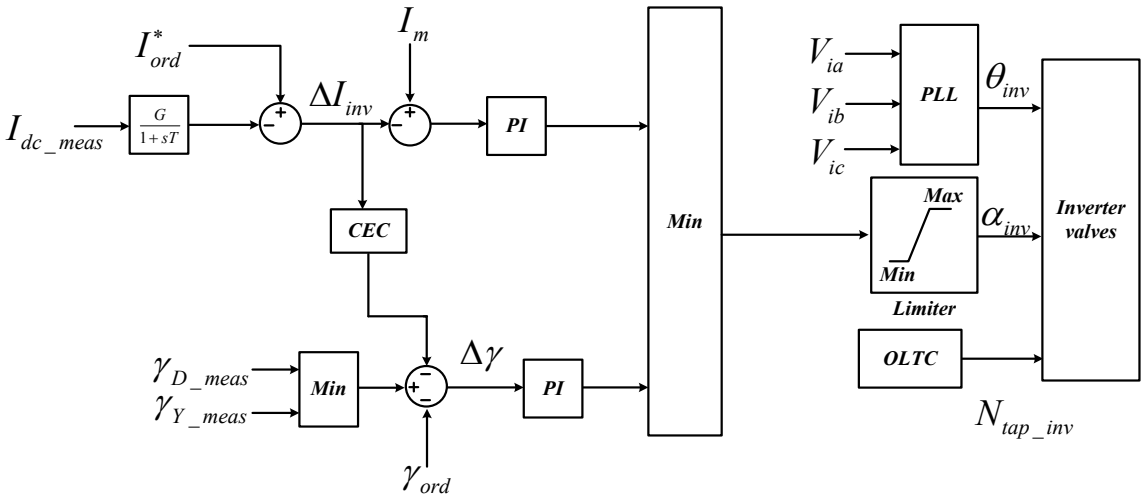

Figure 2-2 Inverter side controller

From the above descriptions it can be seen that the pole controllers at both sides are mainly used to deal with fast transients resulting from AC and DC side disturbances. The role of OLTCs is to control the steady state firing angle at the rectifier side and extinction angle at

the inverter side so that the reactive power consumption and active power losses can be minimised. Due to the speed of mechanical movement of tap changers, OLTCs are dealing with much slower dynamics.

2.4 Filter Bank Switching Control

Both rectifier and inverter side controllers and OLTCs are used to minimise the reactive power consumption but their control range is rather limited and are not able to cover the whole range of active power transfer level. In order to meet the reactive power exchange limit for a wide range of active power levels, filter bank switching controls are adopted to control the reactive power compensation level in a much larger scale.

Normally the passive filters are designed so that its equivalent impedance is very small at certain harmonic frequencies. At the fundamental frequency, its impedance is mainly capacitive and can be used to supply the needed reactive power. Normally the whole MVar rating of the filter bank should match the rated reactive power consumption but since the active power level and reactive power consumption have the relationship as shown in Figure 1-7, the filter connections to the AC bus cannot be fixed. This necessitates the need of flexible filter bank switching for different active power levels.

The points at which the actual switching actions are taking place depend on the measured active power transfer level. The aims of the switching actions are to limit the reactive power exchange with the network within acceptable limits at all possible active power transfer levels. It should be noted that in order to minimise the number of mechanical switching actions and avoid the hunting of switching signals, the switching-in point and switching-out point are made different.

2.5 System Setup

2.5.1 Circuit Configuration

The developed system configuration in single line diagram is shown in Figure 2-3. It is a bipolar LCC-HVDC system rated at 2000 MW and ±500 kV. Both sides of the AC systems are modelled as infinite bus systems with constant line-to-line RMS voltage of 400 kV and constant frequency of 50 Hz. For each 12-pulse bridge, two 6-pulse bridges are connected in series and are connected to the AC system through a YY and a YD transformer for partial harmonic cancellation. The nominal transformer turns ratio between the secondary side and primary side is at 0.48, with a rating of 543.06 MVA. The leakage inductance of transformer is 0.18 p.u., which matches that of the benchmark system [117]. The transformer rating is calculated according to the following equation [62]:

$$MVA_{rated} = 1.0472 \times \frac{3\sqrt{3}}{\pi} E_m \times rated\_DC\_current \tag{2.2}$$

where the rated DC current is 2 kA.

Smoothing reactors are connected at each DC terminal to smooth out the DC current harmonics and limit the DC fault current. The value of smoothing reactor being used is 1028 mH to limit the DC current ripple [56]. To calculate the value of smoothing reactor, the normal firing advance angle β_n is calculated using:

$$\cos\beta_n = \cos\gamma_n - \frac{I_{dn}}{I_{s2}} \tag{2.3}$$

where γ_n is the normal extinction angle which is set at 15 degrees for 50 Hz system [62] and I_{dn} is the rated DC current. I_{sn} is given as:

$$I_{s2} = \frac{\sqrt{3}E_m}{2\omega L_c} \tag{2.4}$$

where ω is the AC system angular frequency and L_c is the transformer leakage inductance. The change of DC current is then calculated using:

$$\Delta I_d = 2I_{s2}\left[\cos\gamma_m - \cos(\beta_n - 1)\right] - 2I_{dn} \tag{2.5}$$

where γ_m is the minimum extinction angle, and is set to 8 degrees [56]. Finally the smoothing reactor value can be calculated using:

$$L_d = \frac{V_d \dfrac{(\beta_n - 1 - \gamma_m)}{360 \times f}}{\Delta I_d} \tag{2.6}$$

where V_d is the rated voltage per 6-pulse bridge and f is the rated AC system frequency of 50 Hz.

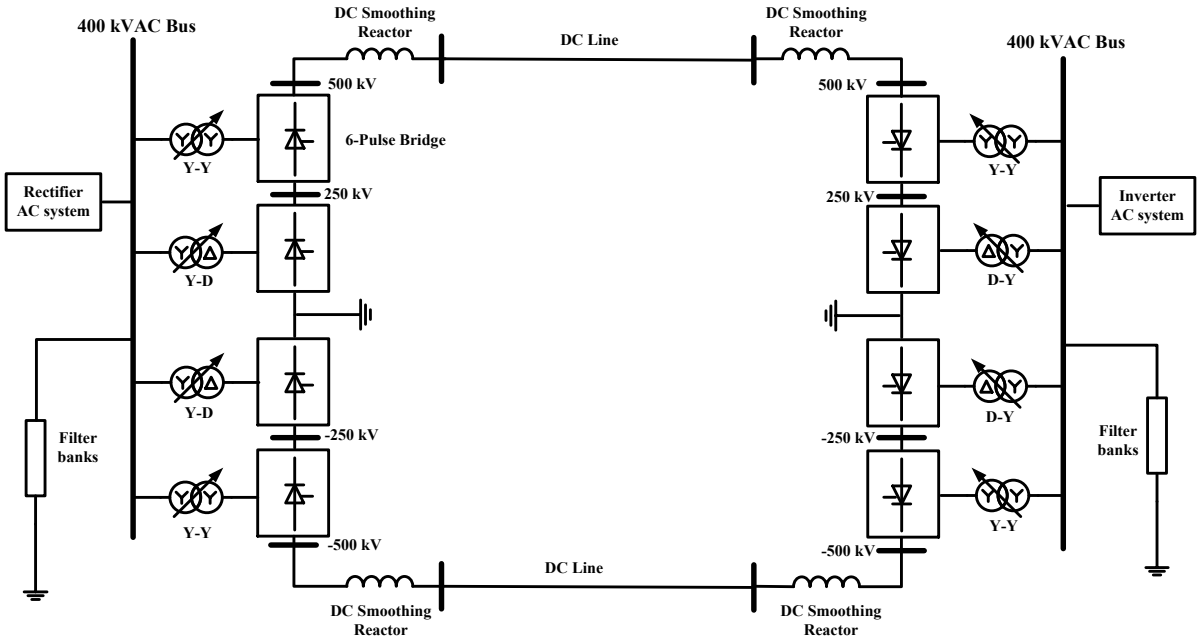

Figure 2-3 HVDC system configuration

Two identical sets of passive harmonic filters are connected at AC bus at both ends to filter out the dominate harmonic currents for 12-pulse operation which are 11^{th}, 13^{th}, 23^{rd} and 25^{th}. The detailed configuration of the filter bank for each bipole (1000MW) is shown in Figure 2-4. The values of filter components and their reactive power compensation levels are set to match the Western Link HVDC project. It can be seen from the figure that for each bipole four filters are used to compensate for the converter reactive power consumption. Among them 2 are **B** type which are C-type high pass filters tuned at 3^{rd} harmonic frequency and the other 2 are **A** type which are high pass filters tuned at 11^{th} harmonic frequency. The high pass filters are used to filter out the characteristic harmonics and the C-type filters are used to avoid the low-order harmonic resonances. Also for the C-type filter by choosing a tuned filter section $L_b - C_{b1}$ at the fundamental frequency, almost all fundamental current is excluded from the resistor and the fundamental frequency loss is negligible.

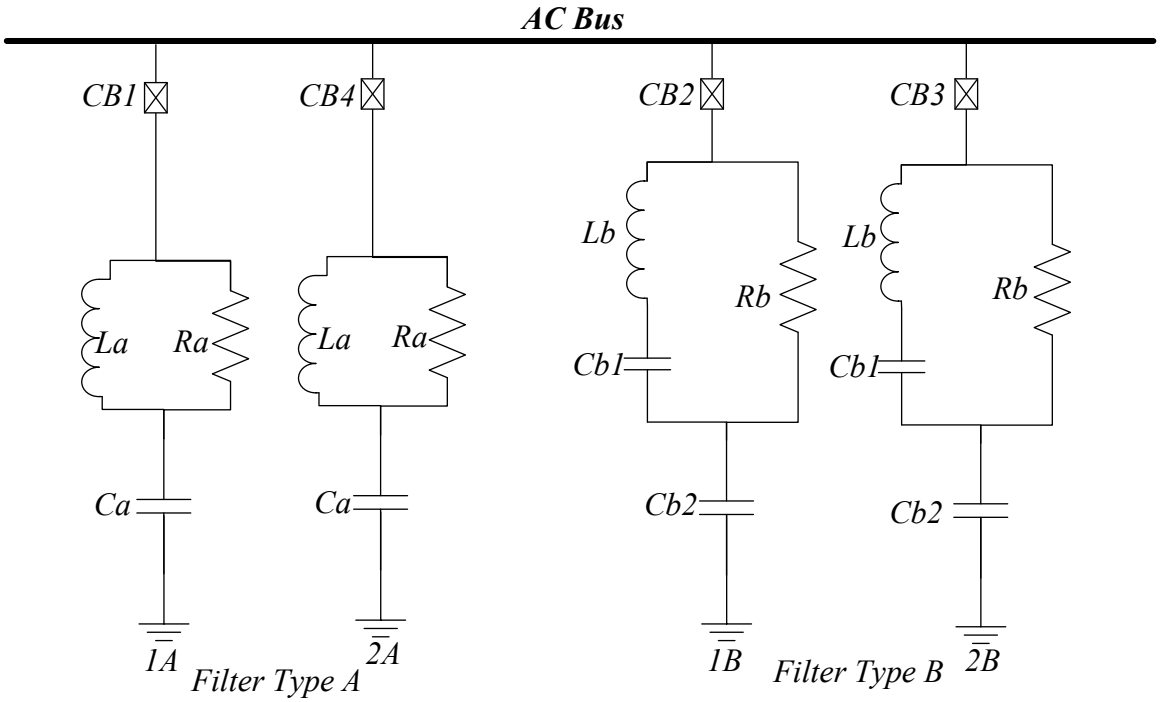

Figure 2-4 Filter bank for each bipole

The fundamental capacitive MVars of the filters are such that the reactive power requirement of converter can be met at various active power levels. The component parameters and the size of capacitors are listed in Table 2-1.

Table 2-1 Parameters of filter banks

Type	**Rated Q (*MVar*)**	**Parameter values**		
		R (*ohm*)	L (*mH*)	C (μF)
A	131.17	214	35.4	2.586
B	130	666	424	Cb_1: 23.89 Cb_2: 2.586

2.5.2 Filter Control

As mentioned in the last section, filters are energised and de-energised to keep reactive power exchange with the AC network within defined limits. So in order to determine how many filters should be in service at a certain active power flow level, load flow studies for a wide range of active power levels are carried out. Then the detailed switching points for switching-in and switching-out modes can be obtained. The switching-in points are listed in Table 2-2, and the switching-out points are listed in Table 2-3. It should be noted that the active power level shown in the tables are for one pole which is half of the total active power flow of the DC link.

Table 2-2 Switching-in points

Switching-in Points (*MW*)	**Filters in Service**
[0-280]	1A
[280-440]	1A, 1B
[440-820]	1A, 1B, 2B
[820-1000]	1A, 1B, 2B, 2A

Table 2-3 Switching-out points

Switching-out Points (*MW*)	**Filters in Service**
[1000-770]	1A, 1B, 2B, 2A
[770-410]	1A, 1B, 2B
[410-250]	1A, 1B
[250-0]	1A

So based on the calculated two switching modes, control signals for all the circuit breakers can be obtained as shown in Table 2-4 and Table 2-5. Only the results for four filters in one pole are shown for illustration since all the other poles have identical filter bank structures.

Table 2-4 Circuit breaker status for switching-in

P (*MW*)	**CB1**	**CB2**	**CB3**	**CB4**
[0-280]	ON	OFF	OFF	OFF
[280-440]	ON	ON	OFF	OFF
[440-820]	ON	ON	ON	OFF
[820-1000]	ON	ON	ON	ON

Table 2-5 Circuit breaker status for switching-out

P (*MW*)	**CB1**	**CB2**	**CB3**	**CB4**
[1000-770]	ON	ON	ON	ON
[770-410]	ON	ON	ON	OFF
[410-2500]	ON	ON	OFF	OFF
[250-0]	ON	OFF	OFF	OFF

The power measurements for circuit breaker control are taken at the primary side of transformers. For each 6-pulse bridge one measurement is taken as shown in Figure 2-5.

When using the look up table for switching actions, the total active power level for one pole is obtained by adding the relevant two measurement results together.

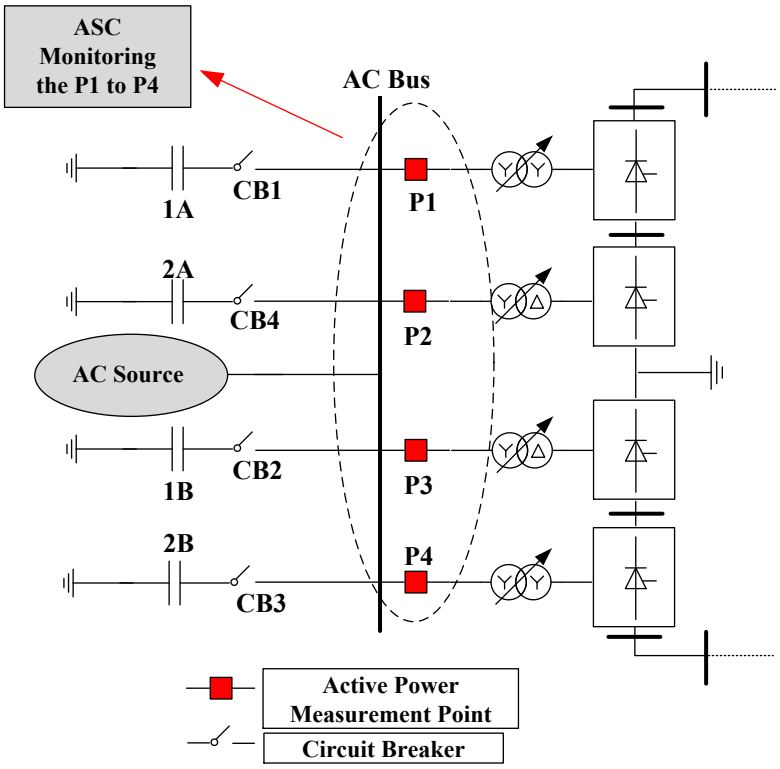

Figure 2-5 Power measurements at rectifier side

Now the filters are able to be switched in and out according to the predefined power thresholds using the active power measurements so that the reactive power exchange with the connected AC network is limited to be within 200 MVars.

2.5.3 HVDC Setup in DigSilent Programming Language (DPL)

In order to make it easier for the user to setup the HVDC system for simulation studies a DPL command object is designed which is shown in Appendix A.2. It works in similar ways as a graphical user interface with some initial conditions as input entries. Some of the main input entries and detailed descriptions of them are listed as follows:

DIR: It sets the initial power flow direction of the system by taking values of either 1 or 0. At the same time it prepares the control system to control the active power at rectifier side and

DC voltage at inverter side. The transformer tap changers are used so that the initial firing angle at rectifier and extinction angle at inverter are at their rated values.

P: It determines the initial total active power flow of the HVDC system.

Vdc: It activates the inverter controllers to control the DC voltage level.

Before carrying out the power flow studies and dynamic simulations the DPL command object is always run first to help the system set up the correct initial condition.

2.6 Design of DigSilent Simulation Language (DSL) Model for Dynamic Simulations

2.6.1 DSL Model for Automatic Switching Control (ASC)

In order to realize dynamic switching of filter banks under, a DSL model for ASC needs to be designed [118]. Firstly a composite frame object which is a pure graphical representation of the whole controlled dynamic system including the controller and controlled units is designed. The designed composite frame for the circuit breaker control is shown in Figure 2-6. Each block in the figure represents a "slot" inside which the physical elements can be filled. So the *active power measurements* slot is filled by four measurement devices with measured values as the output signal. The *circuit breakers* slot is filled by all the circuit breaker elements in the system and the outputs are the current circuit breaker status. The output signal of measurements and CB status are fed to the *switching control* slot which is filled by the designed DSL model of ASC. The model in this case does not have any graphical representations and is realized in codes. For this specific system, the switching information contained in Table 2-4 and Table 2-5 are included in the codes. Finally by adding the composite frame with filled slots to the designed HVDC system, the controller is able to

dynamically switch the filters to meet reactive power requirements. The composite frame is shown in Appendix A.3.

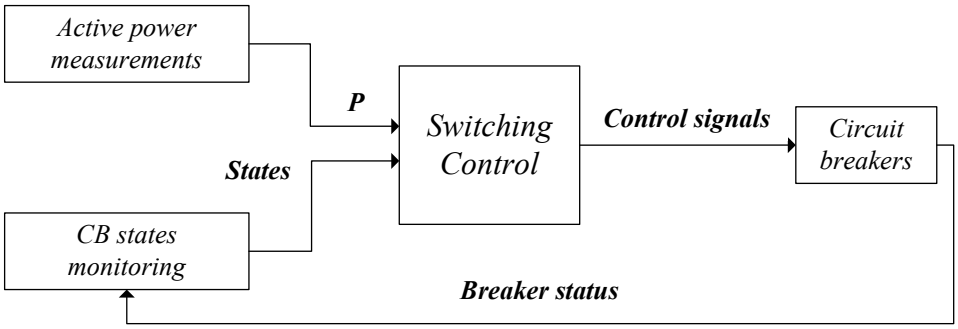

Figure 2-6 Composite frame for ASC

2.6.2 DSL Model for OLTC

As discussed earlier, the OLTC forms part of the whole HVDC pole control system. So unlike the design of ASC, only a separate DSL model for tap changer control needs to be designed and placed into the composite model for the whole HVDC controller. It receives its input which is the firing angle from the main current controller at rectifier side and DC voltage level at inverter side. Its output is the tap order in p.u. to the relevant converter transformers. When it comes to the implementation in, similar to the ASC, a composite frame is used to illustrate how the controller works as shown Figure 2-7. It can be seen from the figure that a high frequency clock signal is added to the frame which is used to realize the digital tap control.

The design of tap changer control can be designed using either codes or graphical representations and in this project it was realized using codes. The controller works by dynamically comparing the firing angle to the pre-defined thresholds. If the feedback firing angle is outside the limits, the controller sends a tap changing signal to the converter transformers to bring back the firing angle. It is important to note that a dead band should be

designed for the controller so that the possibility of tap hunting is minimised. For the developed system, the dead band of 2% is chosen to prevent hunting and wearing of mechanical components [119]. In addition in order to represent the slow mechanical movement of tap changers a delay time is added for each actual tap changing action. The flow chart describing the operating method of OLTC is shown in Appendix A.4.

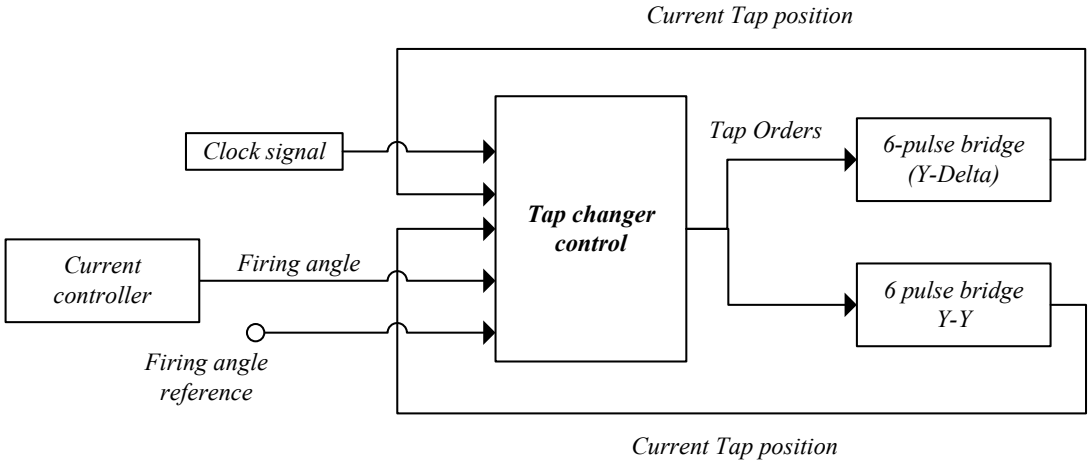

Figure 2-7 Composite frame for OLTC

2.7 Simulation Results

2.7.1 ASC Results

Figure 2-8 shows the power flow results for switching-in mode. The data is obtained by doing power flow studies for a wide range of active power flow levels with measured reactive power consumption of converter station and reactive power compensation from the connected filters. The power order at rectifier side is increased from 0 MW to 1000 MW for each pole and power flow results are taken for each power order value. It can be observed from the figure that by switching in different numbers of filter for different active power flow levels, the net reactive power exchange with the AC network is effectively limited.

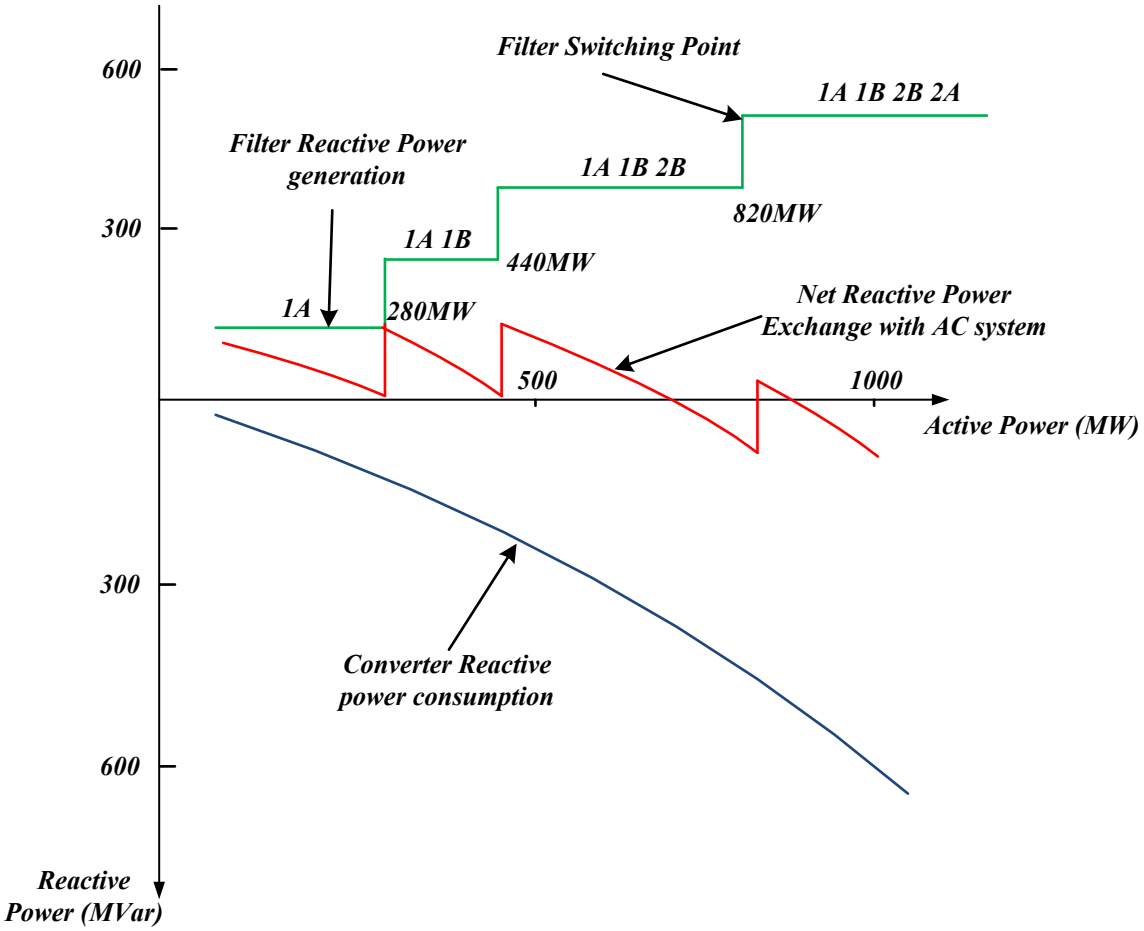

Figure 2-8 Reactive power vs. active power characteristics with filter switching

2.7.2 OLTC Results

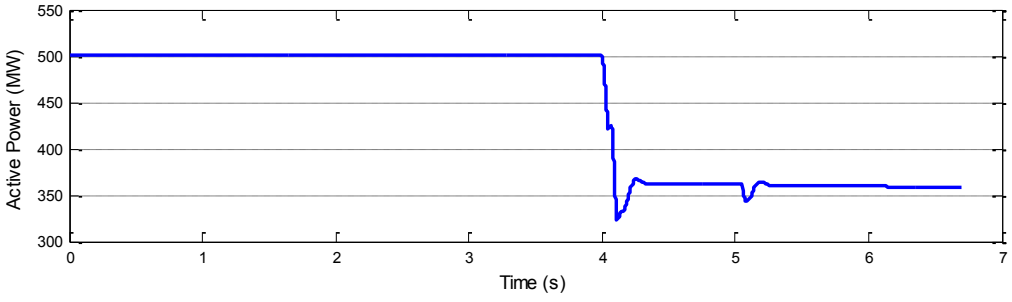

(a)

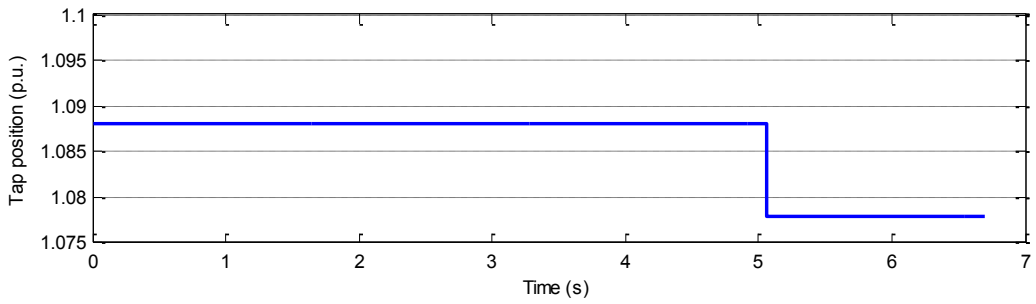

(b)

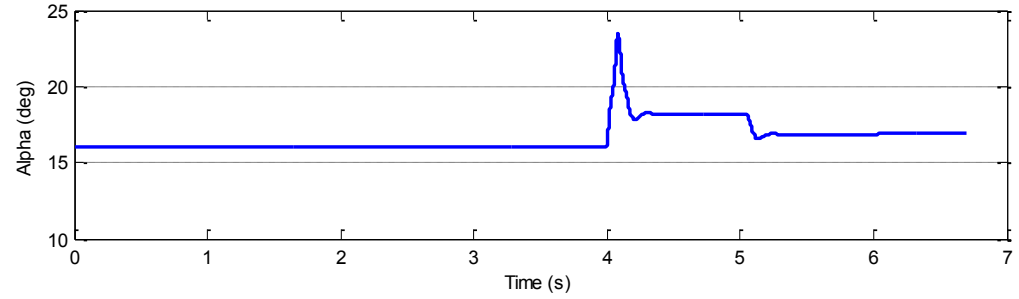

(c)

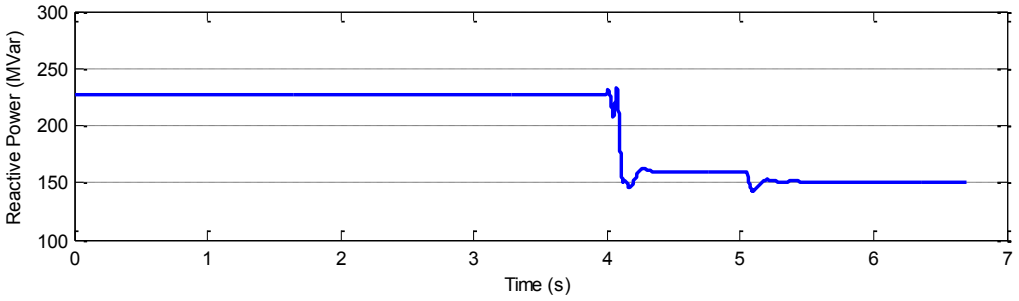

(d)

Figure 2-9 Responses of active power step change. (a) Active power per 6-pulse bridge; (b) tap position; (c) firing angle; (d) reactive power consumption per 6-pulse bridge.

The simulation results of OLTC are shown in Figure 2-9. In order to demonstrate the operation of tap changer controller, tap position of the rectifier side converter transformer is set to 1.088 p.u. as shown in Figure 2-9(b). The initial power order is set to 2000 MW and at 4s a step change is applied to change the power order down to 1400 MW. 2000 MW is chosen to represent the system under normal working condition, and 1400 MW is chosen to represent a sufficiently large increase of firing angle at rectifier side so that tap changer will be activated. With DC current at its rated value, 1400 MW indicates a steady-state voltage of 175 kV for each 6-pulse bridge. By substituting back to (2.1) it can be calculated that firing angle is about 40 degrees and will activate the tap changer movement. This decrease of power order leads to a sudden decrease of current order to the rectifier current controller. Then the current error drives the output firing angle up in order to bring down the DC current which is

shown in Figure 2-9(c). Once the firing angle increases out of the dead-band, the OLTC activates to move the tap changer so that the firing angle is brought down and reactive power requirement is decreased. From Figure 2-9(d) it can be seen that as the firing angle is brought down by tap changer action, the reactive power decreases. The transients of reactive power at 4s in Figure 2-9(d) is because of the transient change of firing angle as shown in Figure 2-9(c). It should be noted that a 1s delay is added to represent the slow mechanical movement of tap changer.

2.8 Summary

In this chapter, the development of an advanced LCC HVDC model is presented. The lack of comprehensive model for LCC HVDC facilitates the development of the model. It has been identified that OLTC is an essential supplementary control function to the traditional pole controllers at both rectifier side and inverter side to control the steady state firing angle and extinction angle to be within desirable limits. By controlling these two angles, the reactive power consumption and active power losses can be minimised. In addition, filter bank switching is also necessary for large reactive power compensation adjustment so that the HVDC system can work over a wide range of active power flow levels with limited reactive power exchange with the AC network.

The ASC switching points are calculated by carrying out power flow studies and the controller is implemented using the DSL model for dynamic simulation. OLTC is designed as another DSL model which is fitted into the whole HVDC control system with firing angle as its input and tap changer signals as its outputs. Simulation studies have been presented to justify the performance of the controllers.

CHAPTER 3 Hybrid HVDC for Commutation Failure Elimination

3.1 Introduction

This chapter describes the proposed hybrid HVDC system. Section 3.2 explains the main reasons of choosing the series connected topology and describes the proposed system configurations. Then the principles of operation and capacitor voltage balancing method are described. In section 3.3, section 3.4 and section 3.5, detailed theoretical analysis of the commutation process with the proposed system is carried out. It then leads to the selection of capacitor voltage level and capacitor value for complete elimination of commutation failure under most serious faults. Section 3.6 presents the simulation results of the proposed system under zero impedance single-phase to ground and three-phase to ground faults to validate the performance. Section 3.7 summarizes the major results of this chapter.

3.2 Proposed Hybrid HVDC system

3.2.1 Choice of Series Capacitor Insertion

It is of significant importance to investigate the main cause of commutation failures in order to mitigate or even eliminate it. In this aspect, theoretical analysis is necessary for a full understanding of the causes and one of the most comprehensive theoretical analysis for commutation failure is presented in [60]. By carrying out a detailed mathematical analysis, it draws the following conclusions [60]:

- The inverter side AC voltage magnitude reduction is the dominant factor that contributes to the onset of commutation failures for both three-phase and single-phase grounding faults.
- The voltage phase angle shift at inverter side also contributes to the onset of commutation failure during single-phase to ground fault but to a lesser extent than magnitude reduction.
- In terms of the component parameters, the most important component parameter that affects the onset of commutation failure is the commutating reactance, which is mostly the transformer reactance. A low commutating reactance at inverter side results in a smaller commutation overlap angle, which is advantageous for the success of commutations.
- Another factor affecting the commutation failure is the rising DC current as a result of inverter side fault.
- Other than increasing the steady state extinction angle setting, other modifications to the control system cannot significantly affect the onset of commutation failures. It is mainly because the control systems do not have enough response time if the fault is electrically close to the inverter or the fault happens at the start or during the process of commutations. Therefore controller modifications are only useful for mitigating successive commutation failures and increasing recovery speed after commutation failures.

The most direct way to regulate AC voltage magnitude is to add FACTS devices at inverter AC bus. However it should be noted that parallel connected AC voltage regulation devices at inverter AC bus are mostly helpful to regulate the AC voltage during remote AC faults. For these fault cases, the inverter AC voltage can be controlled by injecting reactive power into the system. However if the fault happens at inverter AC bus, the terminal voltage of these

shunt connected devices will drop and it is hard to bring back the voltage if the fault impedance is small. During cases of serious faults or electrically-close faults, significant AC voltage drop at inverter AC bus is inevitable thus commutation failures can also happen. In addition, large MVar ratings are needed given the normally very high power rating of LCC systems. So in this work, dynamic series insertion of capacitor is adopted at inverter side to increase the effective commutation voltage in case of fault. This topology helps resolve all the three causes especially the most dominant factor for the onset of commutation failures:

1. The stored energy in capacitors can provide the necessary commutation voltage for commutation when the natural commutation voltage is limited during fault.
2. The series connected capacitors introduce additional phase shift to the valve side commutation voltage so that extra commutation margin is obtained as that in CCC scheme.
3. The inserted capacitors partially compensate the transformer commutating reactance.

Consequently if the capacitor voltage level and capacitor values are appropriately chosen and capacitor voltage balancing methods are carefully designed, commutation failures can be eliminated. All these aspects are to be discussed in detail in the following sections.

3.2.2 Circuit Configuration

The proposed converter circuit configuration and the connected AC system at inverter side are shown in Figure 3-1. The whole HVDC system is based on the CIGRE HVDC benchmark model, which is shown in Figure 3-2. All the values shown in Figure 3-2 are in, Ω, H, and μF for resistance, inductance and capacitance, respectively. The rated DC voltage is 500 kV and the rated active power is 1000 MW. The short circuit ratio at rectifier side is $2.5\angle 84^0$ and at inverter side is $2.5\angle 75^0$. The upper and lower 6-pulse thyristor bridges are connected to the

AC system through a *YY* and a *YD* transformer for partial harmonic cancellation. The parameters of the CIGRE HVDC benchmark system can be found in [117].

In Figure 3-1, *TY1-TY6* and *TD1-TD6* are thyristor valves for the upper and lower 6-pulse bridges. *CapYa, CapYb, CapYc* and *CapDa, CapDb, CapDc* are capacitor modules and *SIYa-S4Ya* are four Insulated Gate Bipolar Transistor (IGBT) switches for capacitor module *CapYa*. The same full bridge capacitor sub-module topology using IGBTs has been adopted for all the other capacitor modules. It should be mentioned that although full bridge capacitor sub-modules have been used in VSC technologies, they have not been used in LCC HVDC technologies.

The additional capacitor modules and IGBTs will lead to higher cost. However, this additional cost can be partially compensated by the significant reductions of reactive power support devices, which will be discussed in chapter 4. Also due to the reduction of reactive power consumption, the size of the converter transformer can be reduced [120], which further contributes to the cost savings. Finally, as will be explained in chapter 4, chapter 5 and this chapter, significant improvements in terms of commutation failure elimination, reactive power control and black start of LCC HVDC system are obtained.

The only additions to the original benchmark system are the capacitor modules, which are connected in series between the secondary side of transformer and thyristor valves. Each of these capacitor modules can be realized by a single module similar to that in 2-level VSC or by a number of series connected sub-modules so that a higher insertion voltage can be achieved. In the following analysis, a single module is assumed for simplicity. It should be noted that there are various topologies of capacitor modules, such as those summarized in [121-124], but in this thesis only the full bridge sub-module is discussed for simplicity. It can be seen from Figure 3-1(b) that in each full bridge module, there are four IGBT switches with

anti-parallel diode across each one of them. The left side of the module is connected to the valve side and the right side of the module is connected to transformer secondary winding.

The reference polarity of capacitor is defined as shown in Figure 3-1(b). The capacitor is inserted as a positive voltage when S1 and S4 are on and S2 and S3 are off. It is inserted as a negative voltage when S2 and S3 are on and S1 and S4 are off. The capacitor can be bypassed when S1 and S3 are on or S2 and S4 are on at the same time.

The control system in the proposed system is identical to the original benchmark system except that the rectifier side firing angle is temporarily limited when there is a high DC fault current. The rectifier is controlling the DC current and inverter side is controlling minimum extinction angle under normal operating condition.

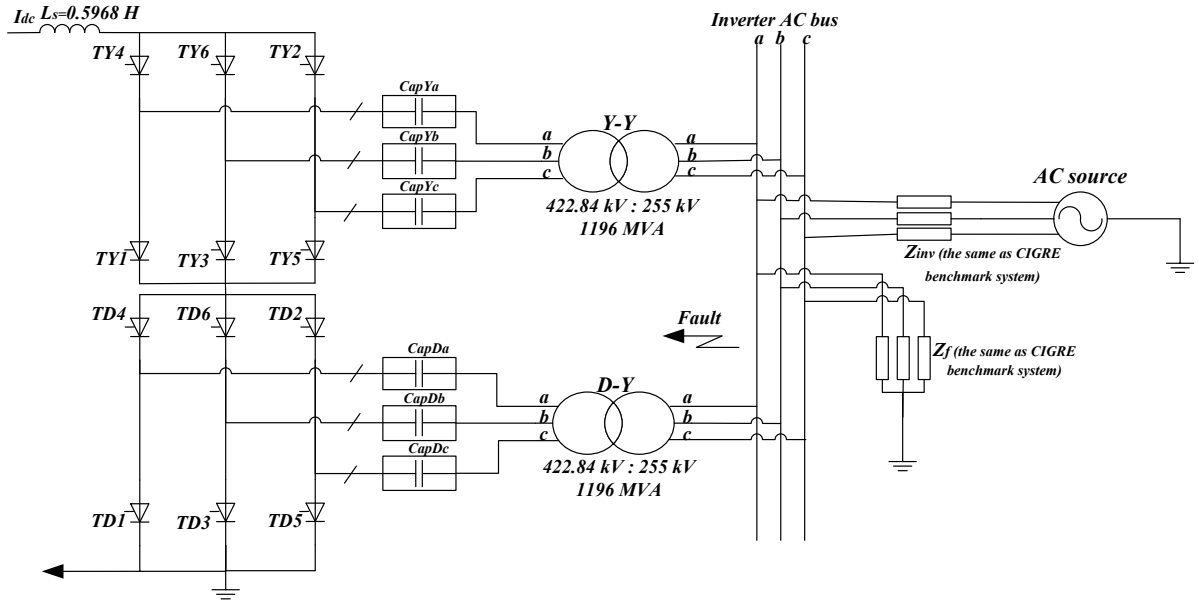

(a)

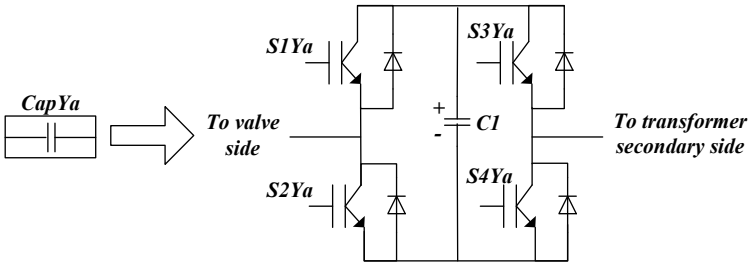

(b)

Figure 3-1 Proposed Hybrid HVDC inverter topology and the connected AC system. (a) System configuration;

(b) Capacitor module configuration

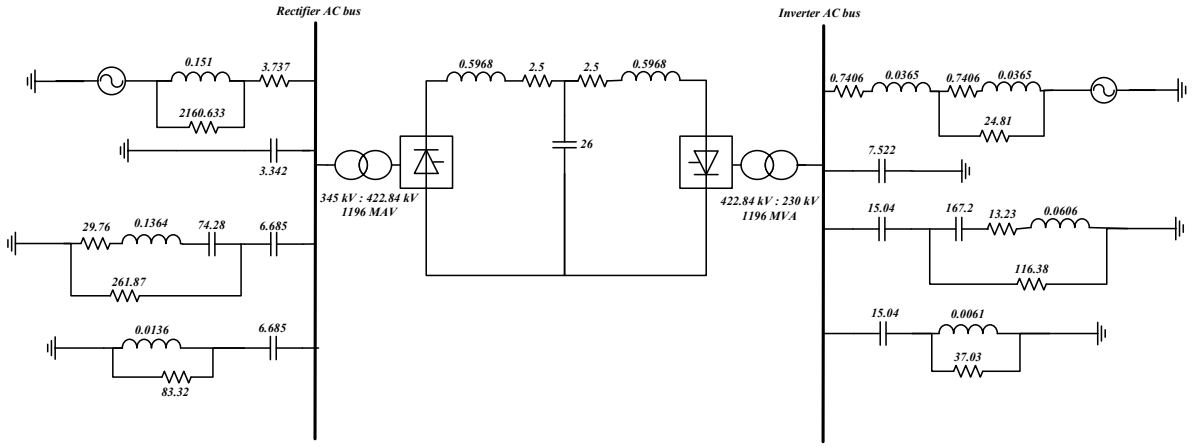

Figure 3-2 CIGRE HVDC benchmark system

3.2.3 Operating Principles

The proposed insertion strategy of the hybrid HVDC system is called the ‘push’ & ‘pull’ method. It works by inserting two capacitor modules connected to the incoming and outgoing phases at the same time. It can be best explained with reference to Figure 3-3, where the commutation from *TY2* to *TY4* is considered.

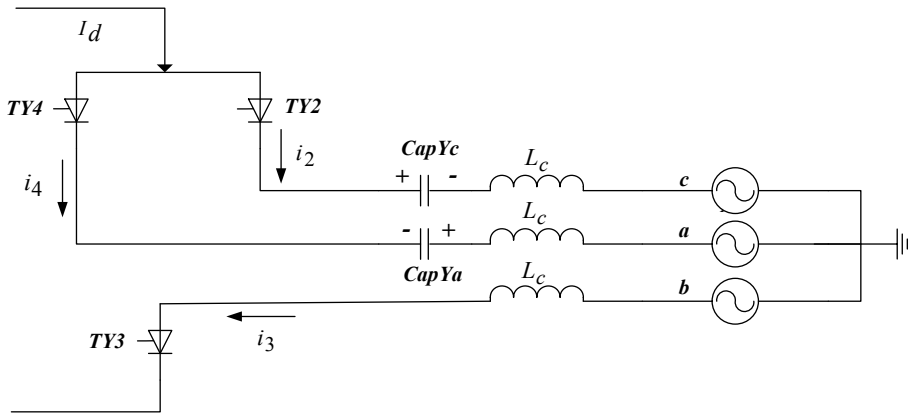

Figure 3-3 Commutation from *TY2* to *TY4*

In this case, only upper 6-pulse bridge circuit is considered for explanation but the principle for lower 6-pulse bridge is the same. Before commutation starts, *TY2* and *TY3* are conducting with all the capacitor modules being bypassed. Capacitor voltages are assumed to be charged to the rated value before insertion. When *TY4* is fired, the commutation from *TY2* to *TY4* starts and *TY2*, *TY4* and *TY3* are all conducting. At the same time, capacitor module *CapYc* in phase C is inserted as a positive voltage and capacitor module *CapYa* in phase A is inserted as a negative voltage as shown in Figure 3-3. As a consequence of the insertions, commutation voltage is increased by the sum of two capacitor voltages. Both capacitors are kept inserted into the circuit and bypassed until the commutation is complete when only *TY4* and *TY3* are conducting. In the case of fault conditions where natural commutation voltages are limited, the voltages coming from the inserted capacitors guarantee the success of commutation. At the end of commutation when both capacitors are bypassed, the voltage level in *CapYc* increases and the voltage level in *CapYa* decreases due to the direction of current flowing through them.

For the next commutation from *TY3* to *TY5*, *CapYb* will be inserted as a negative voltage and *CapYc* will be inserted as a positive voltage throughout the commutation period. It is important to mention that in this case the capacitor voltage level in *CapYc* decreases due to

the change of current direction. This means that the capacitor voltage level in *CapYc* is partially balanced thanks to the natural conducting sequence of thyristors. Thus limited balancing actions outside commutation period are needed. The change of *CapYc* voltage for the two commutation processes described above is shown in Figure 3-5. Similar to *CapYc*, all the other capacitor modules experience similar charge and discharge period for two consecutive commutations.

The described capacitor module insertion strategy for upper 6-pulse bridge can be summarised into the flow chart as shown in Figure 3-4. The same insertion strategy is used by the lower 6-pulse bridge.

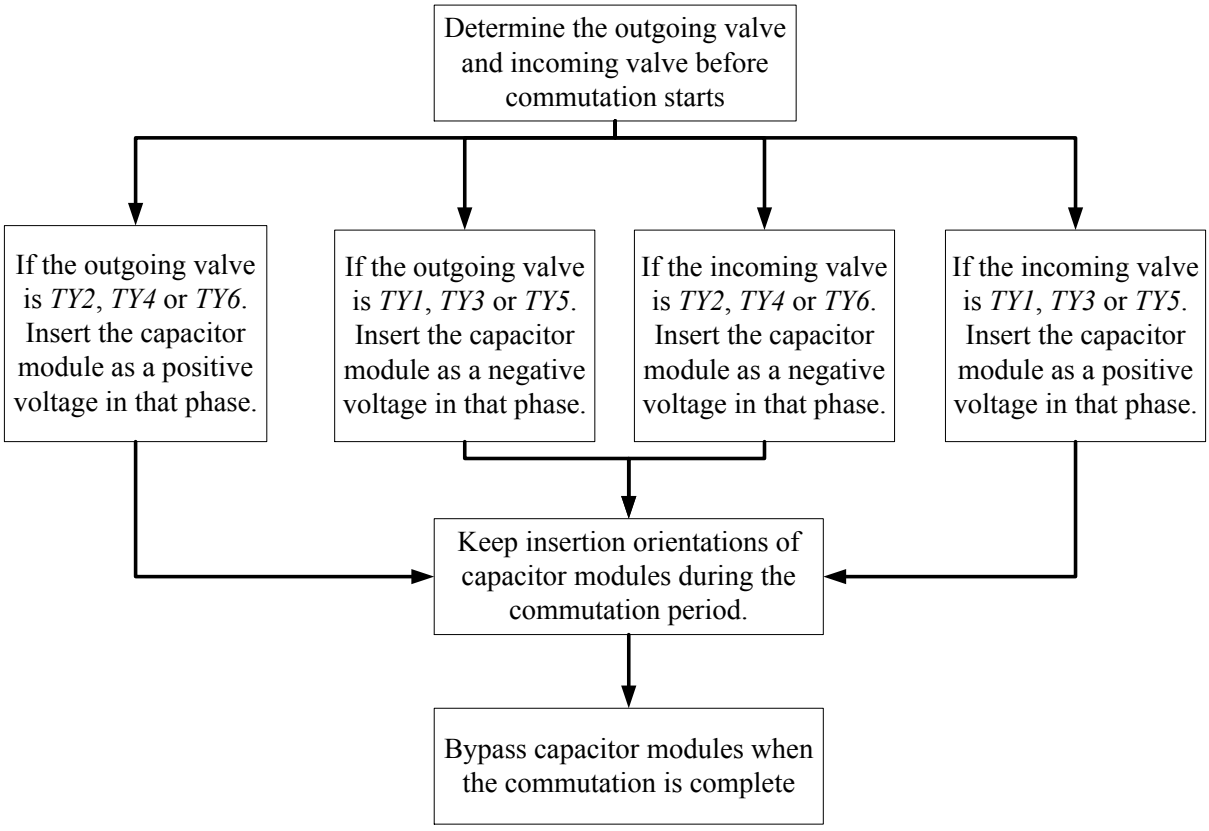

Figure 3-4 Insertion strategy for upper 6-pulse bridge

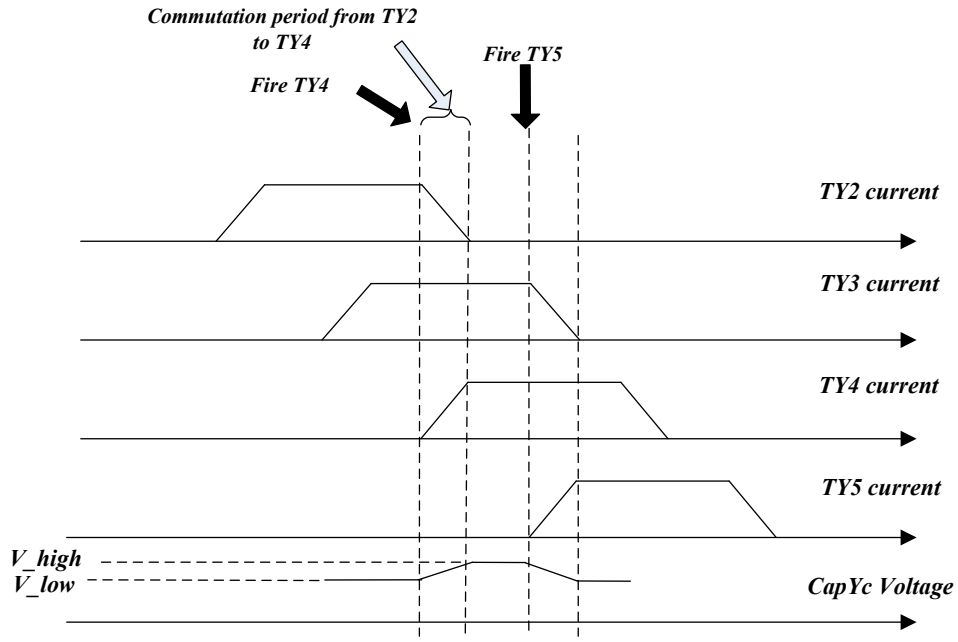

Figure 3-5 Variation of *CapYc* voltage for two successive commutations

3.2.4 Capacitor Voltage Balancing Methods

The capacitor voltage is balanced by pre-inserting the capacitor into the circuit for a short period of time before the phase it is connected to switches out. The voltage balancing controller and its main firing logics for *CapYa* are shown in Figure 3-6 for better illustration. In order to balance *CapYa*, since it is connected to *TY4* and *TY1,* it can only be charged or discharged when either *TY4* or *TY1* is fully conducting. The proposed method chooses to insert *CapYa* as a positive voltage before *TY6* is fired and keep it inserted until the commutation from *TY4* to *TY6* is complete. The point of time at which it is inserted is obtained through a PI controller as shown in Figure 3-6. Firstly the capacitor voltage reference C_{ref} is compared with the measured capacitor voltage in CapYa $VYYa_{meas}$. Then the calculated voltage error signal is processed by a PI controller to give the phase of insertion α_{YYc}. This phase angle together with the reference phase information from PLL determines the firing instant of *CapYa*. The final output of the controller is the switching word for IGBT switches associated with *CapYa*- FPYYaPos. The main firing logics for all

the other capacitor modules have similar structure with different phase reference signals from PLL. The flow chart that illustrates the balancing strategy of all capacitor modules is shown in Figure 3-7. It can be seen from the flow chart that the capacitor modules will only be inserted before the start of commutation when its voltage level is lower than the reference. If the measured voltage level is higher than the reference, capacitor modules will be inserted during the commutation period only.

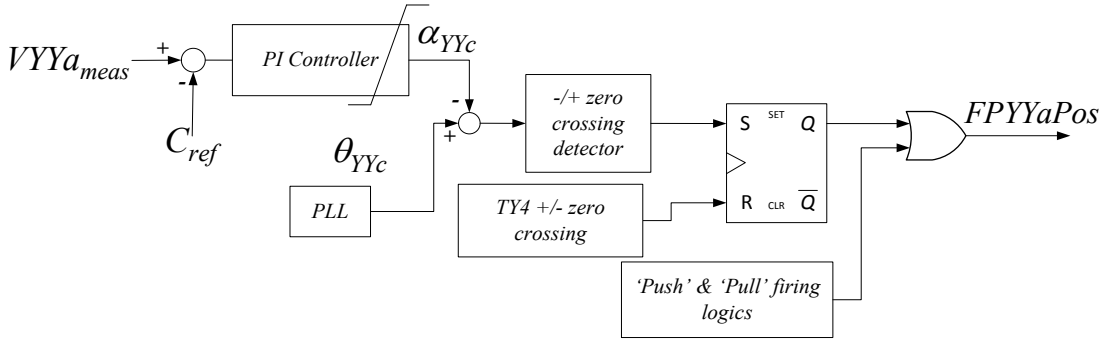

Figure 3-6 Main Firing logics for *CapYa* voltage balancing

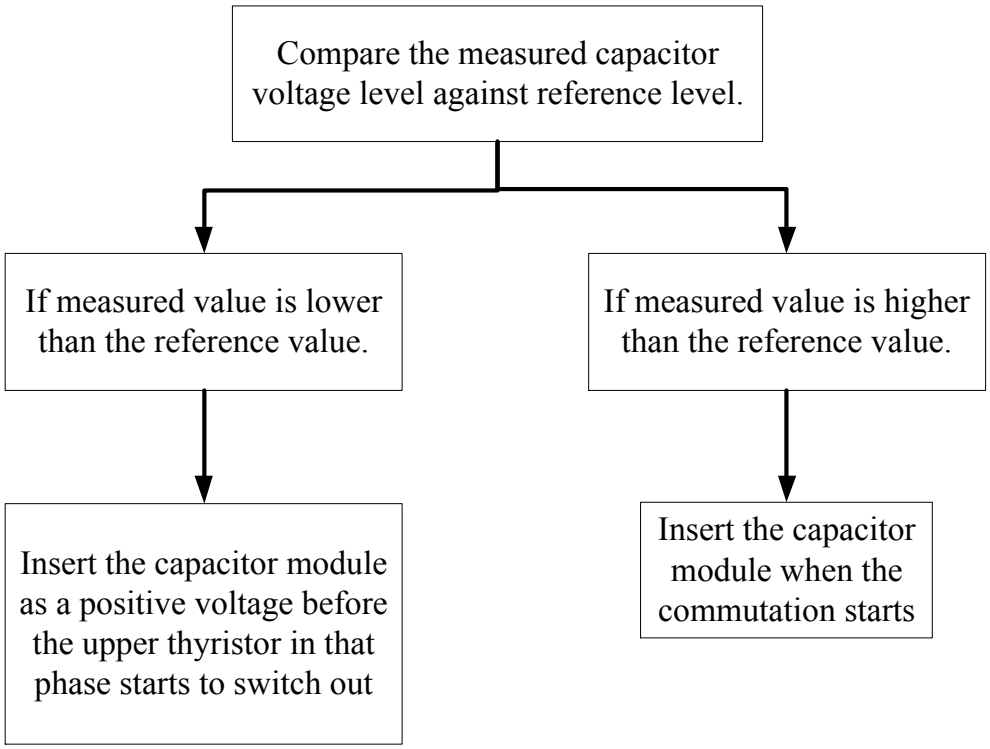

Figure 3-7 Flow chart for capacitor voltage balancing strategy

3.3 Theoretical Analysis of Commutation Process

The success of the proposed method largely depends on the selected capacitor voltage level and its capacitor values. If the capacitor voltage level is too low, it may not be able to help finish the commutation process when the AC voltage is limited. If the capacitor voltage level is too high, it can introduce more cost. The calculations for the required capacitor voltage level will be carried out later on in this section so that commutation failure can be eliminated for both single-phase fault and three-phase fault. Considering the capacitor value, if it is too small, the stored energy can quickly run out and it will be difficult to balance the voltage level. If the capacitor is too large, it will significantly increase the cost. So in order to have a better insight into these problems, theoretical analysis of commutation process with the proposed hybrid HVDC system is to be carried out in this section. In the following analysis, commutation from *TY1* to *TY3* is considered as shown in Figure 3-8. In the figure, L_c is the transformer leakage inductance, I_d is the DC current, v_n is the instantaneous voltage of capacitor inserted in the negative direction, v_p is the instantaneous voltage of the capacitor inserted in the positive direction, i_1, i_2, i_3 are the instantaneous currents flowing through *TY1*, *TY2* and *TY3*, respectively. The polarities of the inserted capacitors are also shown in the figure.

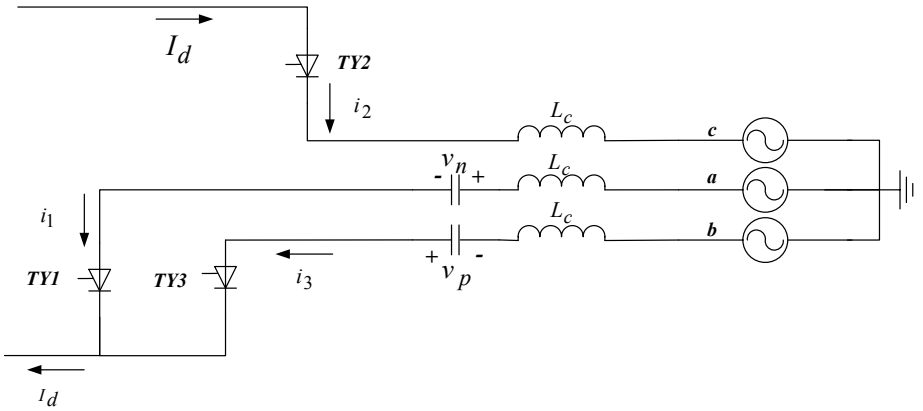

Figure 3-8 Commutation from TY1 to TY3

In the following analysis, DC current is assumed to be constant and all the capacitor voltages are charged to the initial value of V_0.

The instantaneous line-to-neutral source voltages are

$$\begin{aligned} e_a &= E_m \cos\left(\omega t + 60^o\right) \\ e_b &= E_m \cos\left(\omega t - 60^o\right) \\ e_c &= E_m \cos\left(\omega t - 180^o\right) \end{aligned} \tag{3.1}$$

where

E_m is the peak value of phase voltage;

ω is the AC system frequency.

Consider the commutation loop containing *TY1* and *TY3*, the dynamic equations can be written as:

$$i_1 + i_3 = I_d \tag{3.2}$$

$$i_1 = C\frac{dv_n}{dt} \tag{3.3}$$

$$i_3 = -C\frac{dv_p}{dt} \tag{3.4}$$

$$e_b - L_c\frac{di_3}{dt} + v_p = e_a - L_c\frac{di_1}{dt} - v_n \tag{3.5}$$

With the initial conditions of

$$v_p(t)|_{t=\alpha/\omega} = V_o \tag{3.6}$$

$$\frac{dv_p(t)}{dt}|_{t=\alpha/\omega} = -\frac{1}{C}i_3|_{t=\frac{\alpha}{\omega}} = 0 \tag{3.7}$$

where

α is the firing angle.

Solve (3.2)-(3.5), the instantaneous capacitor voltage can be obtained

$$v_p = C_1 cos\omega_n t + C_2 sin\omega_n t + Bsin\omega t + D \tag{3.8}$$

where

$$C_1 = aV_0 - Basin\alpha - \frac{bI_d}{2\omega_n C} + \frac{Bb\omega}{\omega_n} cos\alpha \tag{3.9}$$

$$C_2 = bV_0 - Bbsin\alpha + \frac{aI_d}{2\omega_n C} - \frac{Ba\omega}{\omega_n} cos\alpha \tag{3.10}$$

$$a = \cos\frac{\omega_n}{\omega}\alpha \tag{3.11}$$

$$b = \sin\frac{\omega_n}{\omega}\alpha \tag{3.12}$$

$$\omega_n = \frac{1}{\sqrt{L_c C}} \tag{3.13}$$

$$B = \frac{-\sqrt{3}E_m}{2L_c C} \times \frac{1}{\omega_n^2 - \omega^2} \tag{3.14}$$

$$D = -\frac{I_d}{2C}t + \frac{I_d \alpha}{2\omega C} \tag{3.15}$$

By substituting (3.8) into (3.4), the current through *TY3* can be calculated

$$i_3 = -C(-C_1\omega_n \sin\omega_n t + C_2\omega_n \cos\omega_n t + B\omega\cos\omega t - \frac{I_d}{2C}) \tag{3.16}$$

It will be used in later sections for the selection of capacitor voltage level.

3.4 Capacitor Voltage Selection

In this section, selection of the required capacitor voltage level is presented. The selection criterion is that commutations are still successful under zero impedance single-phase to ground fault and three-phase to ground fault. Each of these two faults is considered separately.

3.4.1 Three-phase Fault

Under zero impedance three-phase fault, the following aspects need to be considered before using (3.16) to determine the required capacitor voltage:

- All three phase voltages drop to zero, which means E_m is zero. There will be no commutation voltage from the AC side and the commutation is completely driven by the voltage from inserted capacitors.
- The DC current can be very large, due to the collapse of AC voltage. This means that the current that needs to be commutated from one valve to another is large. In this case for the benchmark system with a rated current of 2 kA, the maximum DC fault current of 4 kA is used. This value is obtained by carrying out a series of simulation studies of three-phase fault on the original HVDC benchmark system. It has been found through the simulation studies that the maximum DC fault current is around 4 kA.
- The maximum allowed commutation overlap angle μ_{max} cannot be too large. Under normal condition, thyristors are fired under a 60^0 sequence so the commutation has to be completed before the next valve fires. In this case for the commutation from *TY1* to *TY3*, it means that the commutation needs to be completed before *TY4* is fired. Further considering the recovery time of thyristors to regain forward voltage blocking

capability after the current goes through it drops to zero, a commutation safe margin of 20^0 is adopted. As a result, the maximum overlap angle is chosen to be 40^0.

Now for successful commutation under zero impedance three-phase fault, the necessary mathematical condition can be expressed as

$$i_3 \mid_{t=\alpha+\mu_{\max}, I_d = I_{d\max}} \geq I_{d\max} \tag{3.17}$$

where

$$E_m = 0\,kV \tag{3.18}$$

$$\mu_{\max} = 40^o \tag{3.19}$$

$$I_{d\max} = 4\,kA \tag{3.20}$$

In order to solve (3.17) the capacitor value C still need to be determined. It will firstly be set at 500μF to solve (3.17) and then it will be shown that different capacitor values do not significantly affect the minimum required capacitor voltage once (3.18)-(3.20) are defined. The results of solving (3.17) is shown in Figure 3-9.

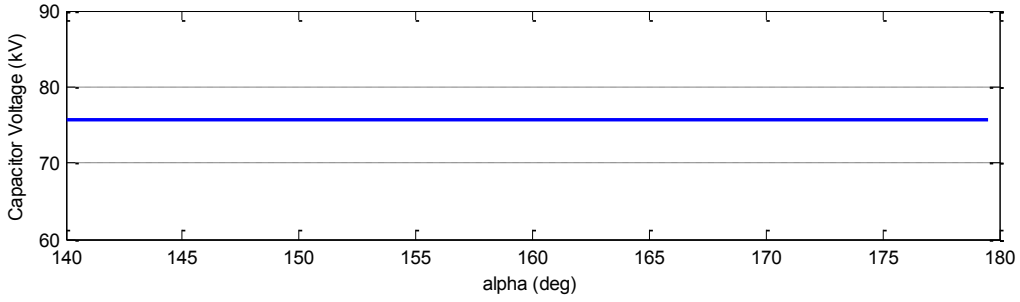

(a)

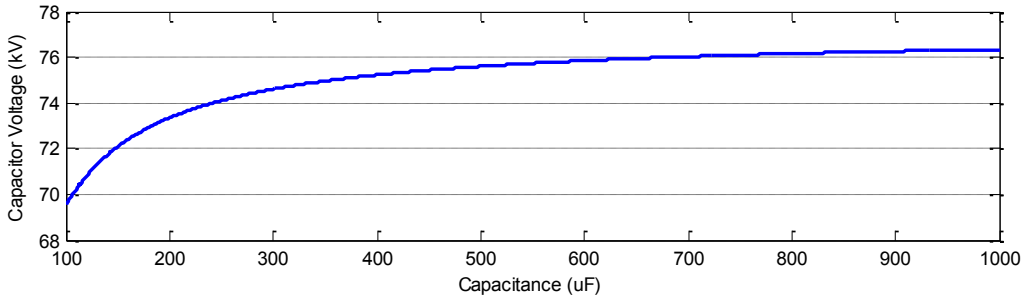

(b)

Figure 3-9 Variation of capacitor voltage for three-phase grounding faults. (a) With firing angle ranges from 140^0 to 180^0; (b) With capacitor value ranges from 100μF to 1000μF.

Figure 3-9(a) shows that the minimum capacitor voltage level required is about 76kV and is the same for all range of firing angles when there is no commutation voltage from the AC side. Figure 3-9(b) shows that the minimum required capacitor voltage level does not vary much for different capacitor values being used. So for zero impedance three-phase to ground fault, the capacitor voltage needs to be charged to at least 76 kV to guarantee successful commutations.

3.4.2 Single-phase Fault

For single-phase to ground fault, a zero impedance phase A to ground fault is considered in the following analysis. The following consequences as a result of the fault need to be considered:

- When phase A voltage drops to zero, only phase B voltage can provide the commutation voltage. Since the commutation period from TY1 to TY3 as shown in Figure 3-8 is considered, phase C voltage does not contribute to any commutation voltage. Therefore the magnitude of natural commutation voltage from the AC side is effectively halved.

- Additional phase shift is incurred on phase B due to the unbalanced fault. If the remaining two phases of voltage are kept balanced at the time of fault, then it can be calculated that the additional phase shift for phase B is 30^0.

So the instantaneous current for *TY3* under zero-impedance single-phase to ground fault can be calculated by setting $e_a = 0\ kV$ and adding additional 30^0 for phase B voltage e_b in (3.5) and then resolve (3.2)-(3.5) with initial conditions of (3.6-3.7),

$$i_3^{'} = -C\left[-C_1^{'}\omega_n \sin\omega_n t + C_2^{'}\omega_n \cos\omega_n t - B^{'}\omega \sin(\omega t - 30^o) - \frac{I_d}{2C}\right] \tag{3.21}$$

where

$$C_1^{'} = aV_0 - Ba\cos(\alpha - 30^o) - \frac{bI_d}{2\omega_n C} - \frac{Bb\omega}{\omega_n}\sin(\alpha - 30^o) \tag{3.22}$$

$$C_2^{'} = bV_0 - Bb\cos(\alpha - 30^o) + \frac{aI_d}{2\omega_n C} + \frac{Ba\omega}{\omega_n}\sin(\alpha - 30^o) \tag{3.23}$$

$$B^{'} = \frac{-E_m}{2L_c C} \times \frac{1}{\omega_n^2 - \omega^2} \tag{3.24}$$

Similar to three-phase fault, the necessary condition for successful commutation under zero impedance single-phase grounding fault is obtained as

$$i_3^{'}\Big|_{t=\frac{\alpha+\mu_{\max}}{\omega}, I_d = I_{d\max}} \geq I_{d\max} \tag{3.25}$$

(3.25) is solved with capacitor value of $500\mu F$ together with (3.19)-(3.20).

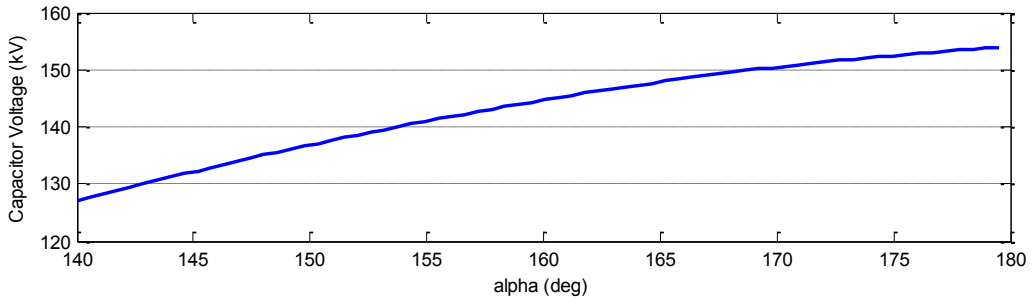

(a)

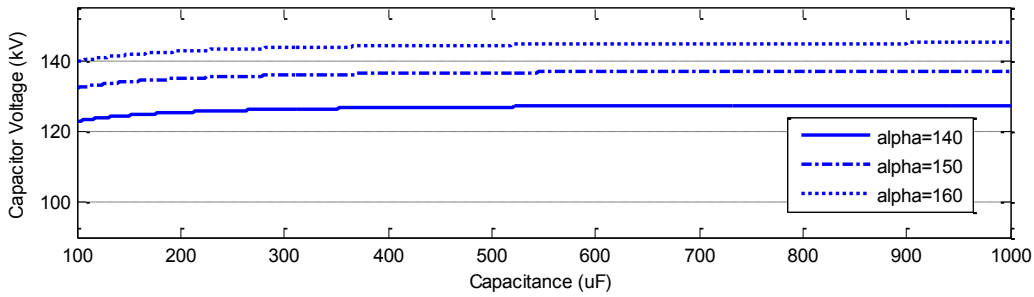

(b)

Figure 3-10 Variation of required capacitor voltage level for single-phase fault. (a) Firing angle ranges from 140^0 to 180^0; (b) Capacitor value from 100μF to 1000μF.

Figure 3-10 shows the results by solving (3.25). Unlike the three-phase fault case, it can be seen from Figure 3-10(a) that for single-phase fault as firing angle increases, the required capacitor voltage level increases considerably. The main reason for the increase of capacitor voltage is the additional phase shift of e_b. When firing angle is large, phase B voltage not only provides smaller commutation voltage but also contributes to a negative commutation voltage. It is this negative commutation from phase B that drives up the required capacitor voltage level for successful commutations. This point can be made clearer with reference to Figure 3-11. It shows phase A to ground fault during commutation from *TY1* to *TY3*. It can be clearly seen that when *TY3* is fired, the total commutation voltage from AC side is negative due to the negative phase B voltage. Also as commutation continues, this negative commutation voltage becomes larger and causes an increase of the required capacitor voltage level. The calculation results in Figure 3-10(b) further demonstrate that for single-phase to

ground fault, it is the firing angle that mainly affects the required capacitor voltage level rather than the capacitor value.

Therefore the change of inverter firing angle during fault should be considered. However the normal time constant of extinction angle control at inverter side is relatively large compared with the fast dynamics of other electrical variables during commutation failure. So firing angle does not change a lot in such a short period of time and it can be viewed as unchanged with its value the same as the steady state value.

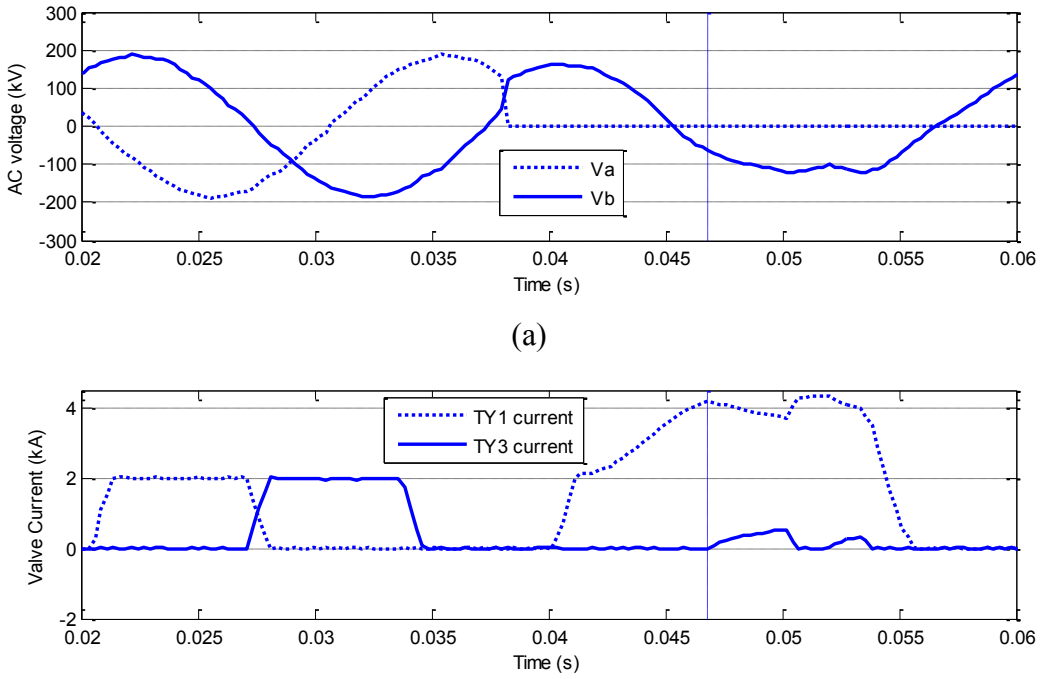

Figure 3-11 Commutation failure for phase A to ground fault. (a) AC voltage; (b) Valve currents.

Finally by combining the results from Figure 3-9 and Figure 3-10, the minimum required capacitor voltage level for successful commutation under both fault cases is chosen to be 140 kV. It is because the nominal firing angle at inverter side is around 150-155 degrees [62], and from Figure 3-10(a) it can be seen that a capacitor voltage level of at least 140 kV is required. This value is used in simulations shown in later sections.

3.5 Capacitor Value Selection

Similar to the capacitor voltage level, the choice of capacitor value is also carried out by considering the percentage of voltage change under two kinds of faults. In the following analysis, single-phase fault and three-phase fault will be considered separately for the choice of capacitor value.

3.5.1 Three-phase Fault

It should be mentioned that the voltage change on the two inserted capacitors after each commutation is different. So the changes of v_p and v_n need to be calculated separately. The percentage of voltage change is used as an index and is defined for both voltages as follows:

$$P_p = \frac{V_0 - v_p(t)|_{t=(\alpha+\mu)/\omega}}{V_0} \times 100\% \tag{3.26}$$

$$P_n = \frac{v_n(t)|_{t=(\alpha+\mu)/\omega} - V_0}{V_0} \times 100\% \tag{3.27}$$

v_n can be calculated by substituting (3.3) and (3.4) into (3.2) and then take definite integral with respect to t

$$v_n(t) = v_p(t) + \frac{I_d}{C}(t - \alpha/\omega) \tag{3.28}$$

Then by calculating (3.26) and (3.27) using (3.8) and (3.28), the percentage of voltage reduction as a function of capacitor values can be obtained.

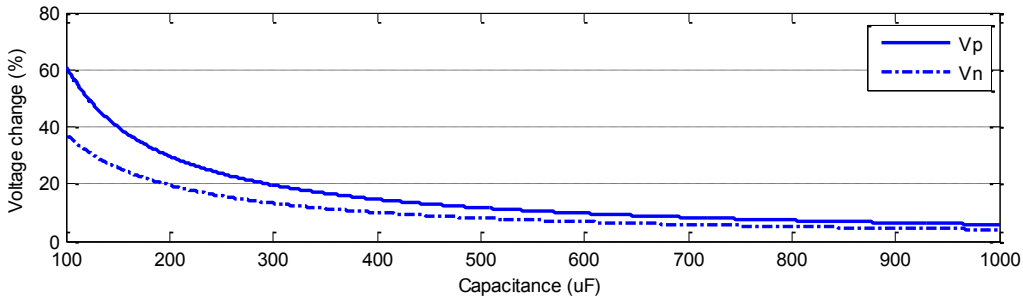

Figure 3-12 Percentage of voltage change under three-phase to ground fault

Figure 3-12 shows the change of percentage of voltage reduction with varying capacitor value. It can be seen from the figure that for all values of capacitor, the voltage increase of v_n is always smaller than the voltage reduction of v_p. It means that there will be a net voltage reduction for all the capacitor modules after each cycle and additional balancing actions are definitely needed. Also it can be seen that in order to get reasonable voltage reduction during fault cases, the capacitor value cannot be too small.

3.5.2 Single-phase Fault

The same calculations for three-phase fault can also be applied to the single-phase fault case but use different solution of $v_p$under single-phase fault. It should be noted that additional phase shift also need to be considered for this calculation. Figure 3-13 shows the calculated results for single-phase fault. By comparing the results with three-phase fault case, it can be found that with reasonably large capacitor value, the voltage change for both fault cases are similar. Also by comparing the results of different firing angles under single-phase fault, it can be found that the variation of firing angle does not have a significant impact on the capacitor voltage change.

Finally based on the results for both cases, if a maximum 10% of voltage change is chosen, the capacitor value for each module is selected to be 585 μF, which is illustrated in Figure 3-13(a).

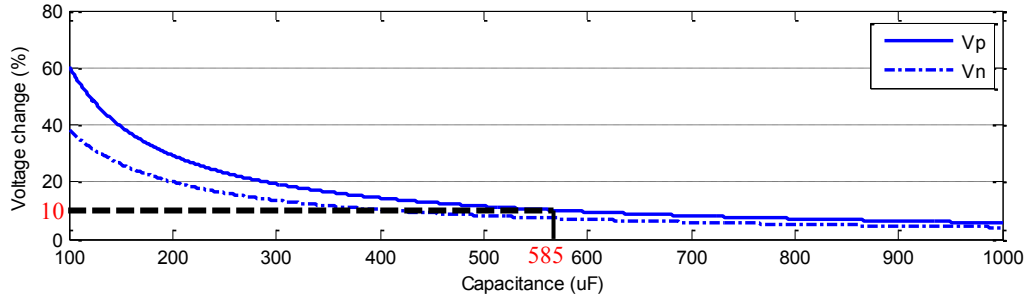

(a)

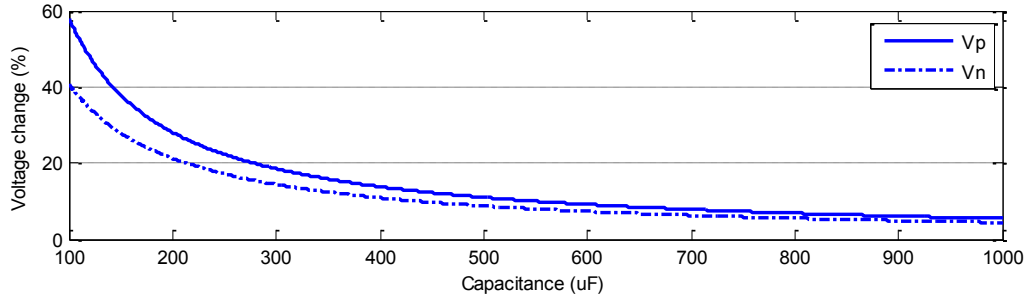

(b)

Figure 3-13 Percentage of voltage change for single-phase fault. (a) With firing angle of 140^0; (b) With firing angle of 160^0.

3.6 Simulation Results

In order to verify the performance of the proposed method, simulation studies are carried out on the CIGRE HVDC benchmark model. The benchmark model is modified to include the proposed capacitor modules and the component parameters are got from theoretical calculations. The whole system is setup in RTDS and so as to achieve better accuracy the HVDC system including the capacitor modules are modelled inside the 'VSC small time-step box'. The time-step achieved is 3.6μs. The capacitor modules are simulated using the full bridge sub-module topology as shown in Figure 3-1(b). The capacitors are the ideal capacitors whose voltage and current relationship is described by the following function:

$$i = C\frac{dU}{dt} \tag{3.29}$$

where i is the instantaneous current going through capacitor, C is the capacitance value and U is the instantaneous voltage across the capacitor.

The IGBT switches are simulated as very large resistances during the off state and very small resistances during the on state. Each IGBT is controlled to be on and off by its own firing pulse and hence detailed switching actions are also simulated.

It should be noted that the conventional way of testing commutation failure is to simulate the system performance under different levels of voltage reduction at inverter AC bus. The different levels of voltage reduction are achieved by applying fault at different electrical distances. The point-on-wave way of fault application is normally used and then the probability of commutation failure can be plotted.

For the proposed method, since commutation failures can be eliminated, only the worst cases of faults, i.e. zero impedance single-phase and three-phase faults, are shown. In addition, the rectifier firing angle is temporarily limited to 60^0 when the rectifier DC current is higher than 2.5kA. The main reason is that the DC current can then be kept at a relatively high value in the fault. Otherwise the rectifier controller will significantly increase its firing angle and results in a very low DC voltage and DC current. In this way a reasonable DC current can be kept during the fault cases and can help the system recover after the fault is cleared.

3.6.1 Single-phase Fault

Figure 3-14 shows the results of system response under a 50ms zero impedance single-phase to ground fault. It can be seen from the figure that one of the phase voltages drops to zero during the fault but the DC voltage can still be kept positive. From Figure 3-14(c) it can be clearly seen that there is no commutation failures happening during the fault period. Consequently the HVDC system is able to transmit about 40% of the rated active power

during the fault period. Figure 3-14(d) shows that the system is able to recover to 90% of the rated power in about 80ms when the fault is cleared. The performance of the proposed capacitor voltage balancing strategy can be observed in Figure 3-14(e). It demonstrates that all the capacitor voltages are balanced at the reference value under steady state and fault conditions.

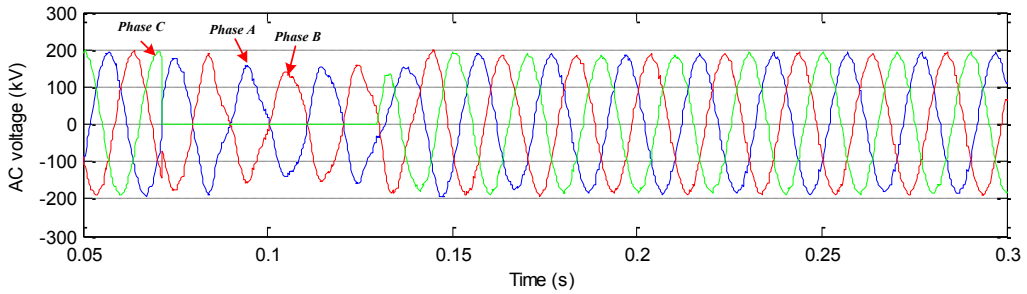

(a)

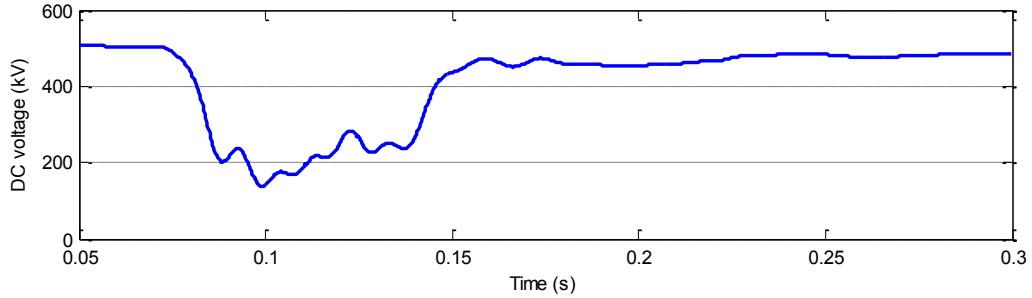

(b)

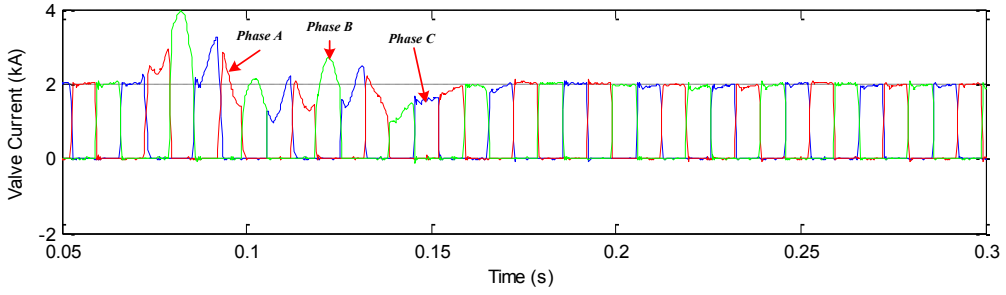

(c)

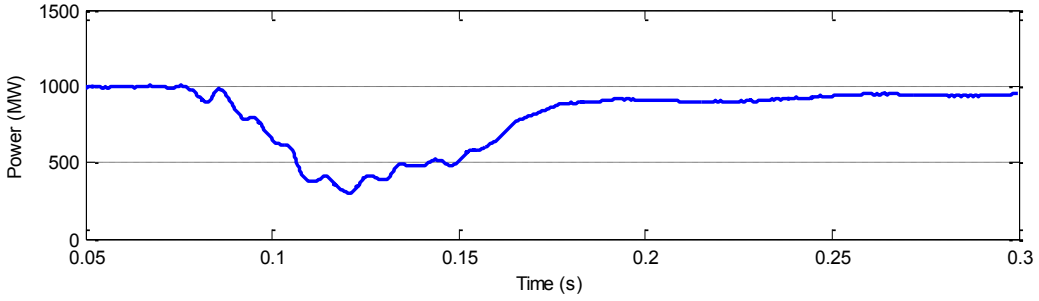

(d)

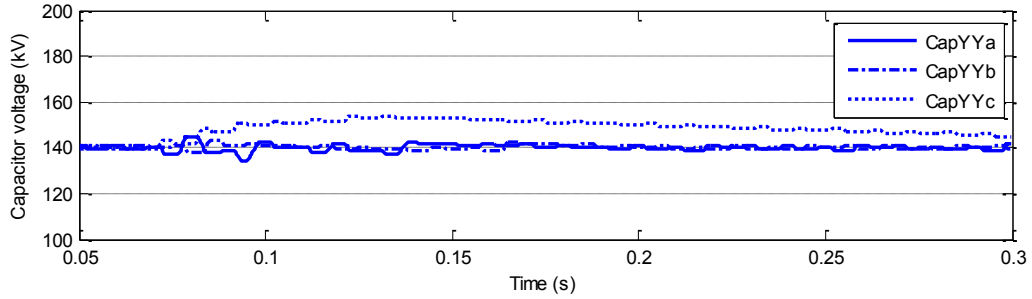

(e)

Figure 3-14 System responses under 50ms zero impedance single-phase to ground fault. (a) AC voltages; (b) Inverter DC voltage; (c) Valve currents; (d) Active power; (e) Capacitor voltages.

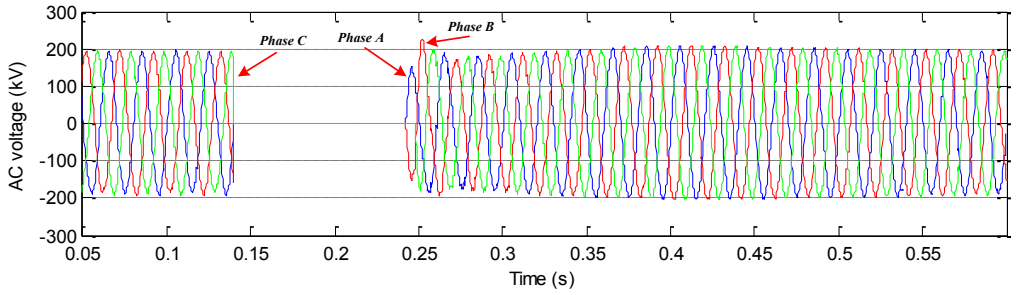

(a)

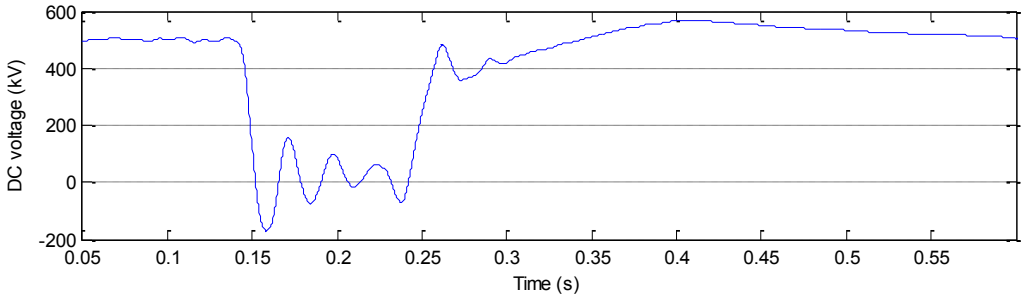

(b)

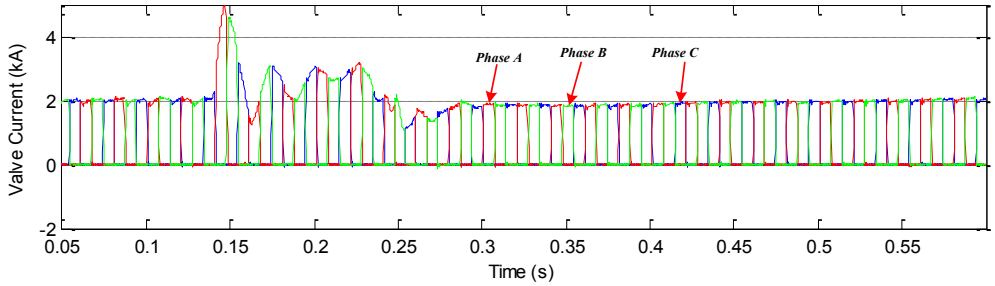

(c)

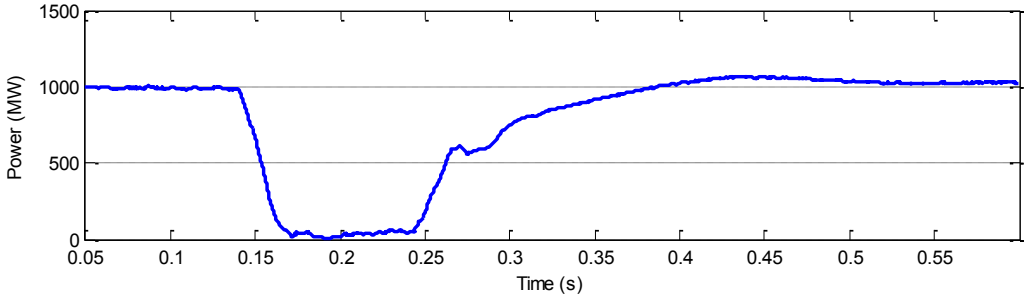

(d)

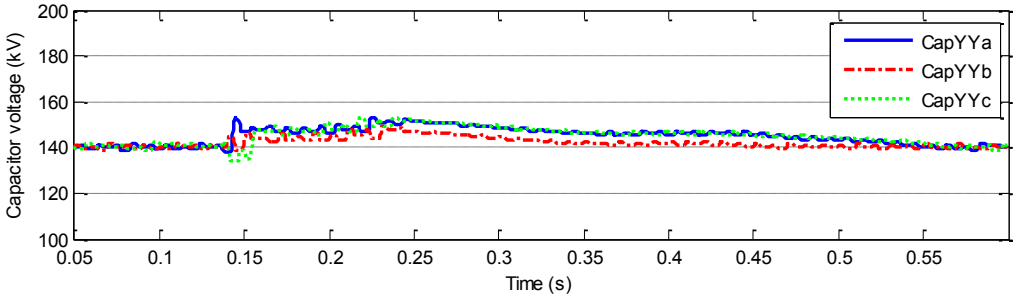

(e)

Figure 3-15 System responses under 100ms zero impedance three-phase to ground fault. (a) AC voltages; (b) Inverter DC voltage; (c) Valve currents; (d) Active power; (e) Capacitor voltages.

The system responses under a 100ms zero impedance three-phase to ground fault is shown in Figure 3-15. In this case, during the fault period, natural commutation voltages from the AC side are zero and the commutations are completely driven by the inserted capacitors. It can be seen from Figure 3-15(c) that all the commutations are successful in the complete absence of AC voltage. Although the transmitted power during the fault case is zero but the system is able to recover to 90% of its rated power in about 100ms. Similar to single-phase fault, the capacitor voltages are well balanced as shown in Figure 3-15(e).

3.6.2 Harmonic Comparisons

Since the proposed method is using dynamic insertion of capacitors in the commutation loops, it is essential to check that the Total Harmonic Distortion (THD) of AC voltage at inverter side is not significantly increased. Table 3-1 shows the calculated THD of inverter AC voltage for both the original benchmark system and the proposed configuration. It can be

seen from the table that although additional switching actions do increase the THD level, the increase is not significant and is within 1.5% at inverter AC bus [120].

Table 3-1 THD comparison

Test System	AC Voltage THD
Benchmark System	0.9631%
Proposed System	1.12%

3.6.3 Voltage Across Thyristors

To enable a full comparison of the proposed system with the original CIGRE HVDC benchmark system, the valve forward voltages from the two systems are measured and compared with each other as shown in Figure 3-16. It can be seen from the figure that the valve forward voltages are also comparable with the original benchmark system.

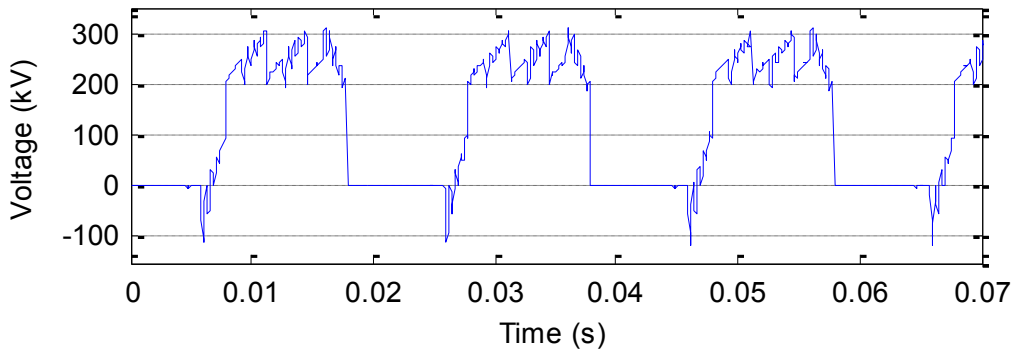

(a)

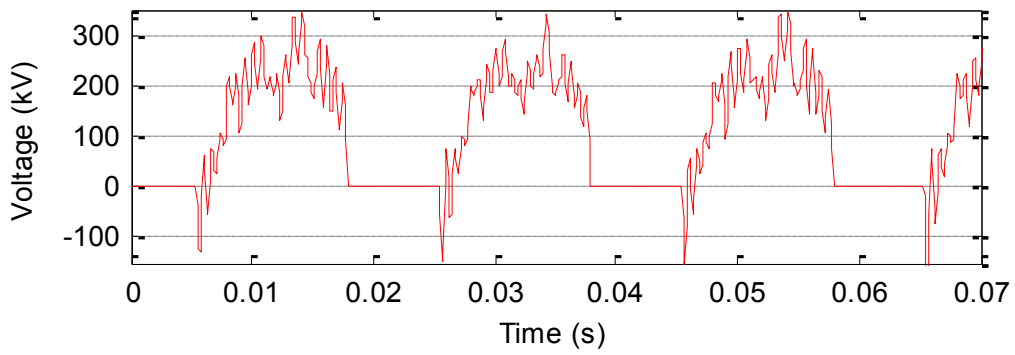

(b)

Figure 3-16 Valve forward voltages. (a) Original benchmark system; (b) Proposed hybrid HVDC system.

3.7 Summary

Parallel connection of voltage regulation devices at inverter side can only mitigate commutation failures under remote AC faults. In order to completely eliminate commutation failures, series connected devices with the ability of providing commutation voltage should be adopted. Therefore the hybrid HVDC with dynamic series insertion of capacitors are utilised to provide the commutation voltage, which is the most dominant factor affecting the onset of commutation failure.

The proposed insertion strategies insert the capacitors during commutation with their inserted orientation in favour of the commutation process. The proposed voltage balancing method pre-insert the capacitors into the commutation loop for a short period of time before the commutation starts.

Detailed analysis has been carried out and showed that if the capacitor voltage levels and capacitor values are correctly chosen, complete immunity to commutation failure under zero impedance single-phase and three-phase to ground faults can be achieved. Formulations are then derived to select the required capacitor voltage level and capacitor values.

Finally simulation results in RTDS of the system under two different kinds of faults are presented, which validate the performance of the proposed configuration and the proposed control methods.

CHAPTER 4 Reactive Power and AC Voltage Control of the Hybrid HVDC System

4.1 Introduction

In this chapter reactive power control and AC voltage control of the hybrid HVDC system are investigated. In section 4.2, various aspects of reactive power control for LCC HVDC system are discussed. In section 4.3, detailed theoretical analysis of how the proposed insertion strategy affects the average DC voltage and how reactive power is related to the firing angle and extinction angle are carried out. In section 4.4, the required capacitor voltage is selected based on the mathematical analysis for acceptable system performance. In section 4.5, the proposed new extinction angle measurement, reactive power controller and the AC voltage controller are explained and designed. In section 4.6, a number of simulation case studies are carried out to validate the performance of the proposed system and controllers. Finally in section 4.7, major results and conclusions of this chapter are summarized.

4.2 Reactive Power Control of LCC HVDC

Reactive power requirement of LCC HVDC is inherent for both rectifier and inverter sides. It originates from the fact that firings of thyristors happen after the commutation voltage becomes positive, which in effect delayed the current waveform with respect to the voltage waveform. This delay is largely related to the firing angle and overlap angle and is normally around 30^0 during rated operating. It causes both rectifier and inverter sides absorb about 60% of reactive power under normal operation. As being discussed in earlier chapters, in most of

the cases reactive power compensation devices are installed to provide the needed reactive power locally.

However it should be mentioned that to the rectifier side AC systems, the rectifier terminal acts as a lagging power factor load and it is natural that it absorbs some reactive power just like other loads. On the other hand, from the point of view of the receiving end AC system, the inverter is like a power producer and should provide the reactive power to the load. However, instead of producing, it absorbs significant amount of reactive power. So the level of absorption should be minimised.

It is a common practice for a back-to-back HVDC scheme to have some ability of reactive power control at inverter side of the system [125, 126]. It is because in this case the two converter stations are essentially located at the same site and the problems of tele-communication and the risk of losing communication between the control systems at rectifier side and inverter side is minimised. Another advantage is that the measurements from both terminals are available for both control systems. Therefore it is not difficult to design reactive power controllers at inverter side to control its reactive power consumption. One possible method is to control the reactive power consumption by modifying its extinction angle. The danger of commutation failure caused by small extinction angle can be mitigated by the modifying operating conditions of rectifier side. As a result, the AC voltage stability is improved at inverter side. However considerable steady state reactive power consumption is still needed and this type of control strategy is limited to back-to-back schemes.

When it comes to point to point HVDC schemes, due to the normally long distance of LCC, the communication delay and the requirement for the system to operate without communications make it impossible to design appropriate reactive power controller at inverter side. Further considering the fact that extinction angle cannot be too small to prevent

commutation failures, controllers aiming to realize reactive power control seems hard to achieve.

Using the proposed hybrid HVDC system with its ability of commutation failure elimination, it is now possible to design reactive power controller at inverter side. In addition if the capacitor voltage level is appropriately chosen, even AC voltage can be controlled by the inverter side to improve stability of receiving AC system. At the same time, problems of commutation failure should be eradicated as well.

4.3 Mathematical Analysis

The hybrid circuit configuration is the same as shown in Figure 3-1. The principles of operation together with the capacitor voltage balancing methods are also described in section 3.2 and will not be repeated here. This section is dedicated to deriving mathematical relationships between reactive power and other system variables for the proposed system. It is important to point out that the proposed capacitor insertion strategies and voltage balancing methods affect the system from three different aspects:

- The commutation overlap angle is smaller due to the resulting higher commutation voltages.
- The average voltage across the bridge is slightly increased due to the different of capacitor voltage change during commutations.
- The average DC voltage is further increased because of the per-insertion of capacitors for balancing purpose.

Analytical derivations will be presented for all three aspects and then the relationship between firing angle and power factor will be shown to facilitate controller designs. Also capacitor voltage selection for commutation elimination is presented.

4.3.1 Commutation Overlap

To calculate commutation overlap angle for the proposed system, commutation period from *TY1* to *TY3* is again considered, which is shown in Figure 3-8. So the same results for v_p and i_3 are obtained:

$$v_p = C_1 cos\omega_n t + C_2 sin\omega_n t + Bsin\omega t + D \tag{4.1}$$

$$i_3 = -C(-C_1\omega_n \sin\omega_n t + C_2\omega_n \cos\omega_n t + B\omega\cos\omega t - \frac{I_d}{2C}) \tag{4.2}$$

Where the definition of coefficients are the same as (3.9)-(3.15).

If the commutation overlap angle is denoted as μ, then at the end of commutation $t = (\alpha + \mu)/\omega$. At the same time $i_3 = I_d$, which indicates the completion of commutation. Re-write (4.2) for the end of commutation we get

$$I_d = -C(-C_1\omega_n \sin\omega_n \frac{\alpha+\mu}{\omega} + C_2\omega_n \cos\omega_n \frac{\alpha+\mu}{\omega} + B\omega\cos\omega\frac{\alpha+\mu}{\omega} - \frac{I_d}{2C}) \tag{4.3}$$

This equation can be used to calculate the relationship between overlap angle and capacitor voltages under different values of firing angle. The capacitor value used is 585μF, which is the same as that in the last chapter.

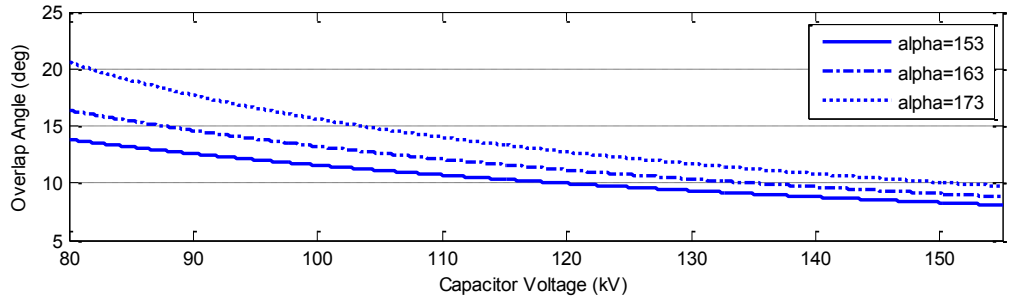

Figure 4-1 Variation of overlap angle against different capacitor voltage

Figure 4-1 shows the results for three different firing angles. It can be seen from the figure that as the capacitor voltage level increases, overlap angle decreases to around 10^0 at higher capacitor voltages. Further increase of capacitor voltage and firing angle do not affect the overlap angle as much. It is mainly because the leakage reactance of transformer cannot be completely eliminated by the inserted capacitor.

4.3.2 Pre-insertion of Capacitors

It has been discussed that the capacitors need to be pre-inserted into the circuit for charging purposes. The duration of pre-insertion depends on the level of its voltage reduction over a cycle. Consider the same commutation process from *TY1* to *TY3*, the voltage increment in the outgoing phase is

$$\Delta V_{in} = v_n(\frac{\alpha+\mu}{\omega}) - V_0 \tag{4.4}$$

The voltage decrease in the incoming phase is

$$\Delta V_{de} = V_0 - v_p(\frac{\alpha+\mu}{\omega}) \tag{4.5}$$

Then by substituting (3.3) and (3.4) into (3.2) and integrate over the whole commutation period gives the relationship between the two capacitor voltages after commutation,

$$v_n(\frac{\alpha+\mu}{\omega}) = v_p(\frac{\alpha+\mu}{\omega}) + \frac{I_d\mu}{\omega C} \tag{4.6}$$

Since for each cycle each capacitor is inserted four times with two voltage increases and two voltage decreases, the net decrease of voltage is

$$\Delta V_{total} = 2\Delta V_{de} - 2\Delta V_{in} \tag{4.7}$$

Now by substituting (4.4)-(4.6) into (4.7), the net capacitor voltage can be re-written as

$$\Delta V_{total} = 4V_0 - 4v_p(\frac{\alpha+\mu}{\omega}) - \frac{2I_d\mu}{\omega C} \tag{4.8}$$

So the pre-insertion time required for each cycle can be calculated as

$$\Delta t = \frac{\Delta V_{total} \times C}{I_d} \tag{4.9}$$

Consequently the average DC voltage increase due to the pre-insertion of capacitors is

$$\Delta V_{pre} = \frac{V_0 \times \Delta V_{total} \times \omega C}{2\pi I_d} \tag{4.10}$$

(4.10) can be calculated using the overlap angle result from (4.3).

4.3.3 Commutation Process

Commutation process affects the average DC voltage by different capacitor voltage changes. Still considering the same commutation period, the lower point voltage for the 6-pulse group is

$$V_{low} = \frac{(e_a - v_n) + (e_b + v_p)}{2} \tag{4.11}$$

So the average voltage increase over a cycle due to the increase of bridge voltage during commutation can be calculated as

$$\Delta V_{\mu} = \frac{\int_{\frac{\alpha}{\omega}}^{\frac{\alpha+\mu}{\omega}} \frac{e_a + e_b}{2} dt - \int_{\frac{\alpha}{\omega}}^{\frac{\alpha+\mu}{\omega}} \frac{(e_a - v_n) + (e_b + v_p)}{2} dt}{\pi/3} \tag{4.12}$$

By substituting (3.2) and (3.3) into (4.12), it can be simplified to

$$\Delta V_{\mu} = \frac{3\mu^2 I_d}{4\pi\omega^2 C} \tag{4.13}$$

Similar to (4.10), (4.13) can be calculated using the commutation overlap results from (4.3).

4.3.4 Power Factor

The power factor of the hybrid HVDC system can be calculated by calculating the change of DC voltage since the RMS AC current going out of the converter station is the same for both systems.

Without capacitor insertions the average DC voltage is given by

$$V_{original} = \frac{3\sqrt{6}}{\pi} \frac{\cos(\alpha) + \cos(\alpha + \mu)}{2} E_{LN} \tag{4.14}$$

where

E_{LN} is the RMS line to neutral voltage.

So by considering the increase of average DC voltage from (4.10) and (4.13) and use the decreased overlap from (4.3), the average DC voltage for the proposed hybrid HVDC is

$$V_d = |V_{original}| + \Delta V_{pre} + \Delta V_{\mu} \tag{4.15}$$

In (4.15), the absolute value of original average DC voltage is used because the calculated $V_{original}$ is negative using (4.14) at inverter side.

By neglecting the active power losses, the AC power and DC power should be equal:

$$3E_{LN} I_{L1} \cos\phi = V_d I_d \tag{4.16}$$

where

I_{L1} is the RMS value of the fundamental frequency current;
$\cos\phi$ is the power factor.

From the classic HVDC theories, it is well know that I_{L1} can be approximated by the fundamental frequency current when the overlap angle is zero

$$I_{L1} = \frac{\sqrt{6}}{\pi} I_d \tag{4.17}$$

The accuracy of this approximation decreases as overlap angle increases, but for hybrid HVDC, since the overlap angle is smaller than normal value, this approximation is quite accurate.

Now by substituting (4.15) and (4.17) into (4.16), the power factor for the proposed system can be calculated as

$$\cos\phi = \frac{\pi V_d}{3\sqrt{6} E_{LN}} \tag{4.18}$$

By calculating (4.18), the variations of power factor as a function of firing angle and extinction angle are shown in Figure 4-2. It can be seen from Figure 4-2(a) that the power factor can be favourably controlled to unity by controlling the firing angle to be close to 180^0. From Figure 4-2(b) it can be clearly seen that with a close to unity power factor, the extinction angle effectively becomes negative, which indicates that the commutation process completes after the natural commutation voltage becomes negative. So in this case the success of commutation has to rely on the inserted capacitor voltages. Also it motivates the need of designing a new extinction angle measurement mechanism which can accommodate negative extinction angle values. For normal extinction angle measurement when

commutation extends beyond 180^0 the output value will be zero, which cannot be used for the proposed system.

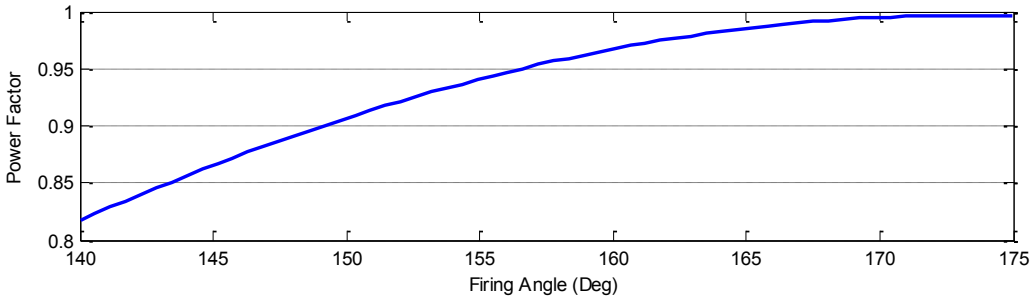

(a)

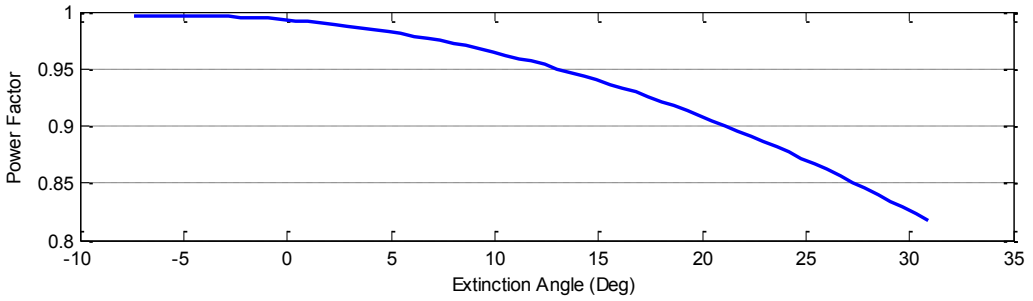

(b)

Figure 4-2 Variation of power factor against firing angle and extinction angle. (a) Power factor against firing angle; (b) Power factor against extinction angle.

4.4 Capacitor Voltage Level Selection

In simulation studies, two different control modes, i.e. constant unity power factor control and inverter AC voltage control will be presented. So in this section, the capacitor voltage level selection is presented for both control modes.

4.4.1 Constant Power Factor Control

For the constant power factor control, the aim is to control the reactive power consumption of the inverter at zero and eliminate commutation failures at the same time. So under this control mode, seen form the AC system, the inverter is outputting pure active power with unity

power factor. In this case it is clear that the minimum required capacitor level is determined by commutation failure elimination under the most serious fault. From the analysis in chapter 3, it is the single-phase fault that requires the highest capacitor voltage level for successful commutation due to the additional phase shift to the other unfaulty phases. Hence it will be used to calculate the required capacitor voltage.

Considering the commutation period from *TY1* to *TY3* with zero impedance phase A to ground fault, the fault current in *TY3* i_{3_fault} can be calculated as

$$i_{3\_fault} = -C[-C_1'\omega_n \sin\omega_n t + C_2'\omega_n \cos\omega_n t - B'\omega \sin(\omega t - 30^o) - \frac{I_d}{2C}] \tag{4.19}$$

where the coefficients are defined in (3.11)-(3.13) and (3.22)-(3.24).

If the maximum DC fault current I_{dcmax} is chosen to be 4kA and the maximum overlap angle μ_{max} is chosen to be 40^0, the necessary condition for successful commutation in this case can be formulated as

$$i_{3\_fault}\Big|_{t=\frac{\alpha+\mu_{\max}}{\omega}, I_d = I_{d\max}} \geq I_{d\max} \tag{4.20}$$

So now the required capacitor voltage level for complete elimination of commutation failure under single phase fault can be calculated by solving (4.20) for a range of firing angles. It should be mentioned that in this case the converter transformer turns ratio is modified so that the same power transfer at the same DC and AC voltage level is achieved.

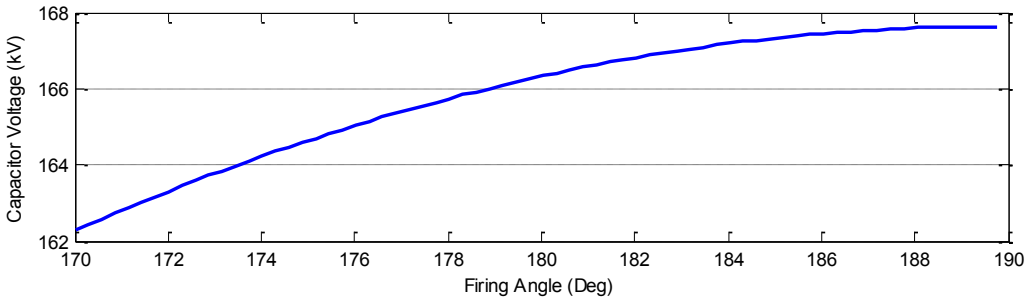

Figure 4-3 Required capacitor voltage level for commutation failure elimination at constant power factor control

Figure 4-3 shows the results of the required capacitor voltages for different firing angles. In the figure the firing angle is ranging from 170^0 to 190^0 and it can be seen that the required capacitor voltage level is higher than that under normal operating conditions. The capacitor value of 168kV is selected for simulation studies.

4.4.2 Inverter AC Voltage Control

Under the inverter AC voltage control mode, the required capacitor voltage level is determined by the operating range of firing angles. In this control mode, the normal operating point is such that when the inverter is outputting rated active power the reactive power consumption is zero. The required capacitor voltage level for commutation elimination under single phase fault also needs to be considered in this case.

At rated condition with zero reactive power consumption, firing angle is close to 180^0 and a maximum firing angle of 190^0 is chosen for the capacitor voltage selection. Similar to previous cases, a maximum overlap angle of 40^0 is chosen for safe commutation.

The result of calculation is shown in Figure 4-4. It shows that without considering the fault cases, the required capacitor voltage level can be significantly lower for inverter AC voltage control. If commutation failure elimination is required then the capacitor voltage need to be selected according to Figure 4-3. However in this case since the focus is on AC voltage

control rather than fault analysis, the capacitor voltage level of 110kV is chosen for successful control of AC voltage at different loading conditions.

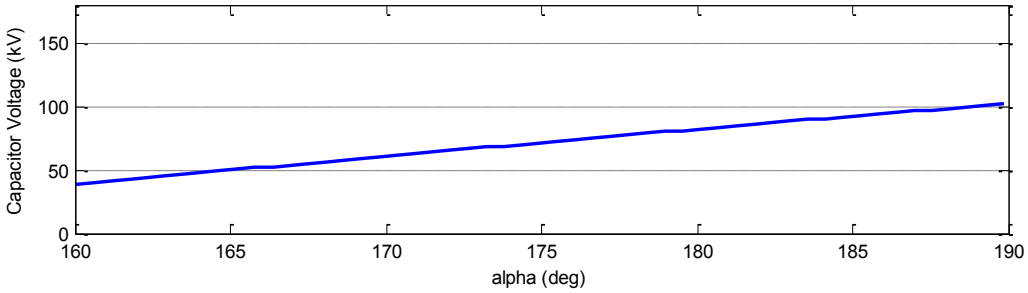

Figure 4-4 Required capacitor voltage for AC voltage control

4.5 Reactive Power Controller & AC Voltage Controller

In this section, the design of reactive power controller and AC voltage controller will be presented. In addition the proposed new extinction angle measurement method which can accommodate negative extinction angle values are explained to facilitate the design of both controllers.

4.5.1 New Extinction Angle Measurement

As for the conventional extinction angle measurement, the extinction angle for a specific valve is calculated by measuring the time between the commutation completion and the point when valve voltage becomes positive. It has been shown that for the proposed system with the ability of exporting reactive power to the AC system, extinction angle can sometimes be negative so a new way of measurement is proposed.

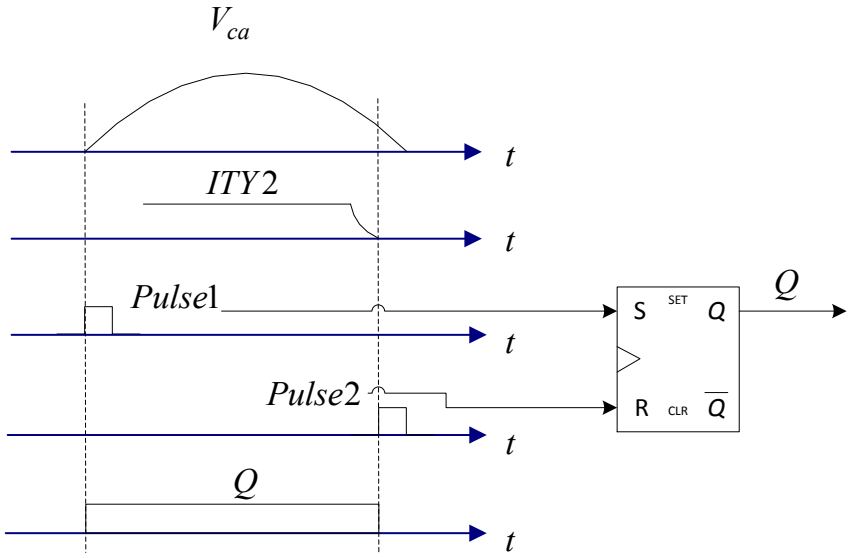

(a)

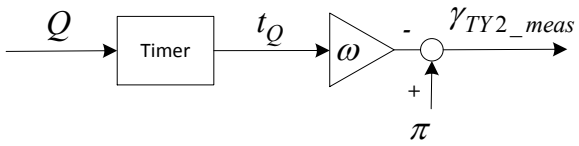

(b)

Figure 4-5 Proposed extinction angle measurement for TY2. (a) Pulse Q generation; (b) Extinction angle calculation for TY2

The new way of extinction angle measurement can be best understood with reference to Figure 4-5, which shows the extinction angle measurement for *TY2*. A pulse Q is firstly initiated when commutation voltage V_{ca} becomes positive. When *TY2* current is decreased to zero, which indicates the end of commutation, another pulse is activated and resets Q. So now the length of pulse Q represents the addition of firing angle and overlap angle. Then by subtracting the time represented by Q from 180^0, the extinction angle for *TY2* can be calculated. The main logics for calculation process are shown in Figure 4-5(b). Similar ways of extinction angle calculation can be applied to all the other valves and the final extinction angle value send to the inverter control system is obtained by taking the minimum of all the extinction angles over a cycle. In this way if the commutation period extent beyond 180^0, a

negative extinction angle which measures the difference in time between valve voltage zero-crossing point and completion of commutation is utilized for control system.

4.5.2 Proposed Reactive Power Controller

It was shown in section 4.4 that reactive power can be effectively controlled by varying the firing angle so that the resulting extinction angle can be changed. With the original benchmark system in constant extinction angle control, the proposed method of reactive power control is achieved by adding an additional outer reactive power control loop to the existing extinction angle control. The original extinction angle reference value is no longer a fixed value pre-set by the designer but a dynamic control variable which is generated by the outer reactive power control loop. A block diagram showing the structure of the proposed reactive power controller at inverter side is shown in Figure 4-6. The parameters for PI controllers are tuned through trial and error by carrying out a number of simulation studies of reactive power reference step changes. It can be seen from the figure that the extinction angle order γ_{order} is calculated by minimising the reactive power error Q_{error} between the measured value Q_{meas} and its reference value Q_{ref}. This is because the power factor at inverter side can be controlled by controlling the extinction angle as shown in Figure 4-2(b). Then this extinction angle order is used in the same way as the original extinction angle measurement to get the inverter side firing angle. The *CEC* in the figure represents the current error signal which is derived from the current controller at inverter side [56]. The extinction angle measurement γ_{meas} for the controller is the measurement from the proposed strategy so that negative values can also be fed back. For existing controllers, negative extinction angle cannot be measured and hence similar reactive power controller cannot be implemented.

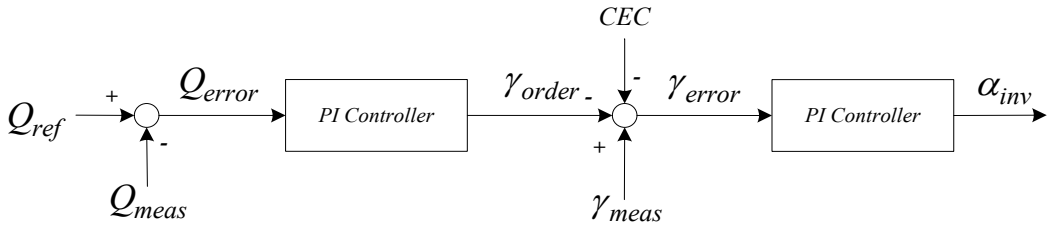

Figure 4-6 Proposed reactive power controller

4.5.3 AC Voltage Controller

Under the AC voltage control mode the inverter bus AC voltage is controlled to be at the rated value. The control of AC voltage is achieved by controlling the reactive power consumption at inverter side. So theoretically the same control structure can be applied to achieve the AC voltage control with the extinction angle reference generated by the AC voltage error. However in order to increase the stability of connected AC system, a faster AC voltage controller is desirable. So the proposed inverter AC voltage controller calculates the firing angle directly by minimising the RMS voltage error. A block diagram showing the controller structure is drawn in Figure 4-7, where the parameters for PI controller are obtained through trial and error by carrying out a number of simulation studies of voltage reference step changes. It can be clearly seen from the figure that the firing angle at inverter side is obtained directly by minimising the voltage reference.

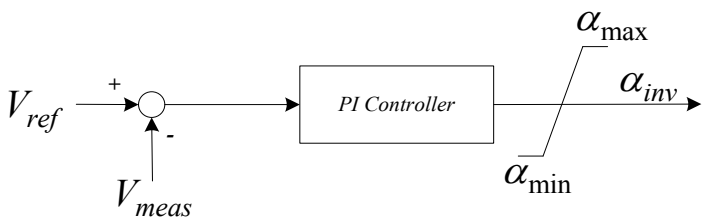

Figure 4-7 Proposed AC voltage controller

4.6 Simulation Results

In this section, simulation results are presented to verify the performance of the proposed hybrid HVDC system and the designed controllers. Firstly the reactive power control capability is demonstrated with changing reactive power reference using the designed reactive power controller. The nominal operating point of the system is such that the inverter terminal absorbs zero reactive power. Secondly different fault cases are simulated to demonstrate the system's immunity to commutation failures. Finally a series of load switching are simulated to demonstrate the effectiveness of the designed AC voltage controller. For all the simulated cases, the capacitor banks are removed due to the zero reactive power consumption and the transformer turns ratio is modified to meet the rated working condition [77]. The capacitor values are chosen to be $585\ \mu F$ which is the same as that being calculated in section 3.5.2, and its voltage level is 168 kV. The rest of the system is the same as the CIGRE HVDC benchmark model.

The whole test system is modelled in RTDS and for the accuracy of simulation results, the capacitor modules and all the thyristor bridges are modelled inside the RSCAD "VSC small time-step box". The achieved simulation time step is $3.6\ \mu s$.

4.6.1 Test System Configuration

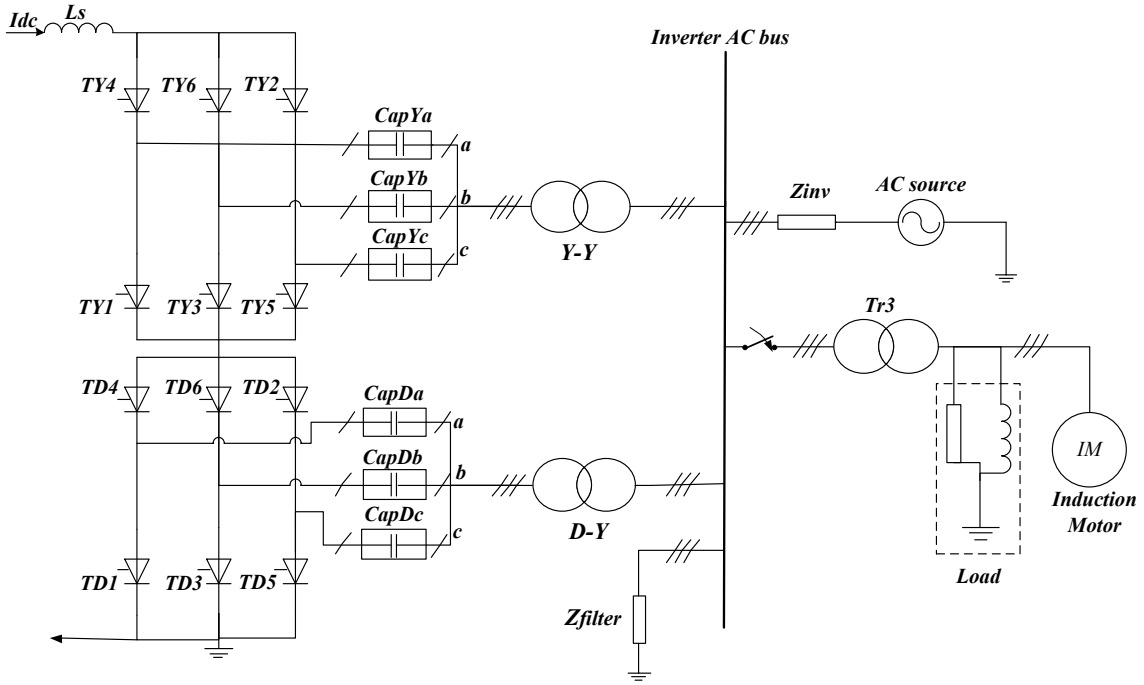

Figure 4-8 Hybrid HVDC and the connected AC system at inverter side

The test system for simulation study is shown in Figure 4-8. The main components and their notations are the same as those for Figure 3-1. The series connected capacitor modules are also modelled using full bridge configuration as shown in Figure 3-1(b). The main modification made to the original benchmark system is that additional passive loads and an induction motor are connected to the inverter AC bus through a transformer. Also the transformer turns ratio is changed so that rated power is transmitted at similar DC and AC voltage as the original benchmark system.

4.6.2 Reactive Power Tracking

Figure 4-10 shows the simulated system response with reactive power step changes. The flow chart for the step changes of reactive power reference is shown in Figure 4-9. The reactive power reference changes are realized by changing Q_{ref} in the proposed reactive power

controller as shown in Figure 4-6. A negative value of reactive power indicates that inverter is exporting reactive power to the connected AC system. In this case study, as shown in the flow chart, reactive power reference is firstly set to zero and changes to -200 MVar at 3.1s, then increases to 200 MVar at 4.6s and finally changes back to zero at 6.1s. It can be clearly seen from Figure 4-10(a) that the measured inverter reactive power successfully tracks the reference value. Because this change of reactive power consumption is achieved by modifying inverter side firing angle, DC voltage changes accordingly as shown in Figure 4-10(c). DC current is controlled at rated value by the rectifier side current controller, which is shown in Figure 4-10(d). So the transmitted active power by the HVDC system, shown in Figure 4-10(e), has similar shape as the DC voltage. Finally the measured extinction angle using the proposed extinction angle measurement is shown in Figure 4-10(f). It can be observed that the ability to measure negative extinction angle enables the controller to control the system to export reactive power. At the same time the negative value of extinction angle measurement validates the effectiveness of the proposed measuring method.

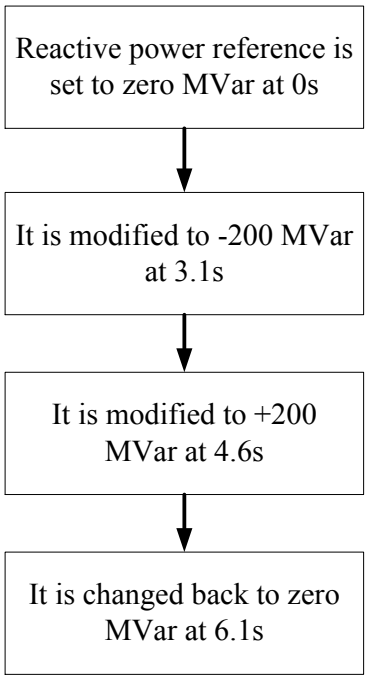

Figure 4-9 Reactive power reference changes

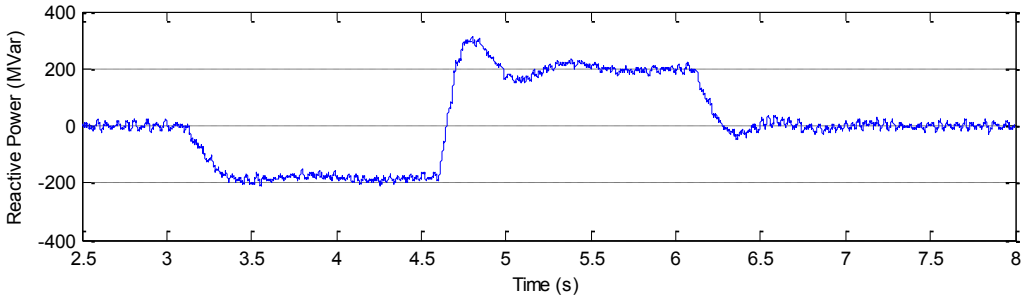
Reactive Power (MVar)
400
200
0
-200
-400
2.5
3
3.5
4
4.5
5
5.5
6
6.5
7
7.5
8
Time (s)

(a)

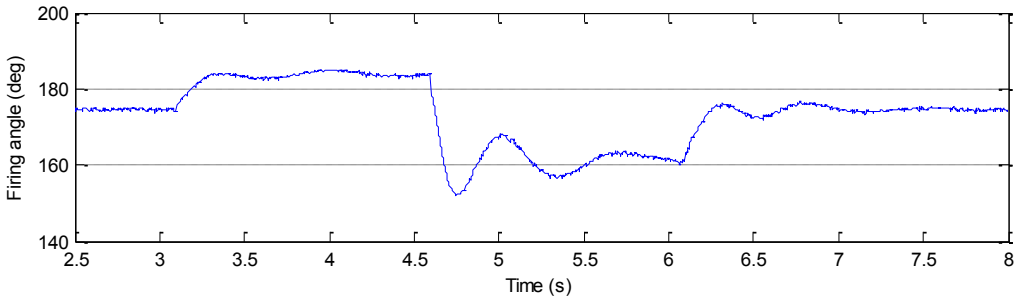
Firing angle (deg)
200
180
160
140
2.5
3
3.5
4
4.5
5
5.5
6
6.5
7
7.5
8
Time (s)

(b)

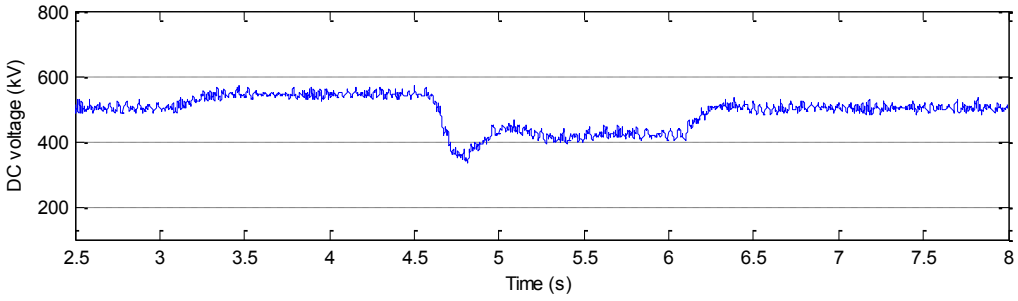
DC voltage (kV)
800
600
400
200
2.5
3
3.5
4
4.5
5
5.5
6
6.5
7
7.5
8
Time (s)

(c)

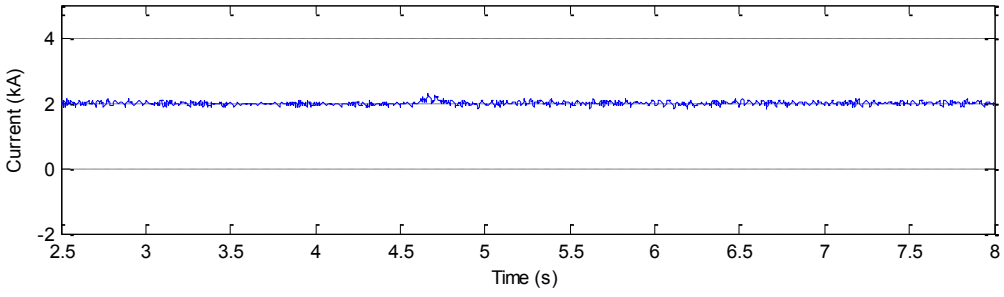
Current (kA)
4
2
0
-2
2.5
3
3.5
4
4.5
5
5.5
6
6.5
7
7.5
8
Time (s)

(d)

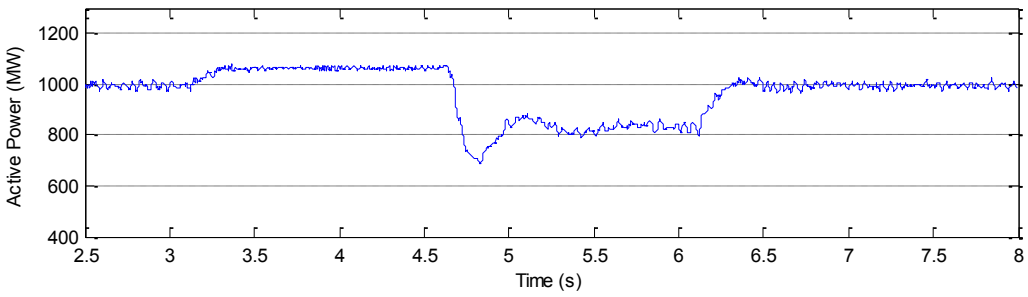
Active Power (MW)
1200
1000
800
600
400
2.5
3
3.5
4
4.5
5
5.5
6
6.5
7
7.5
8
Time (s)

(e)

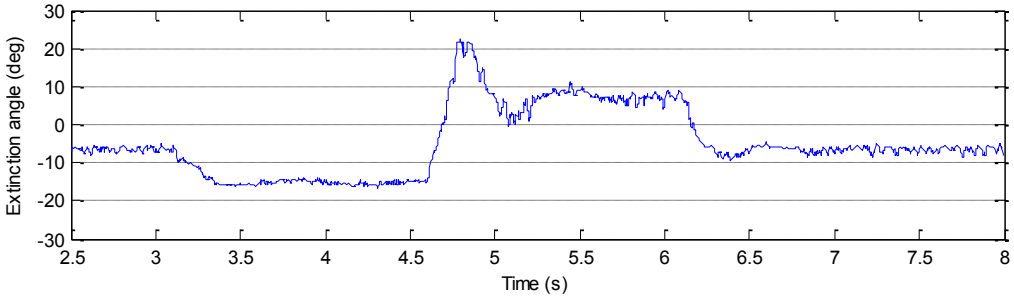

(f)

Figure 4-10 System responses with reactive power step changes. (a) Inverter reactive power consumption; (b) Inverter firing angle; (c) DC voltage; (e) Active power; (f) Extinction angle.

4.6.3 Commutation Failure Immunity

In order to test the system's immunity to commutation failure under the most serious faults, test cases for zero impedance single-phase to ground fault and three-phase to ground fault are carried out.

Figure 4-11 and Figure 4-12 show the system responses under a 50ms zero impedance single-phase to ground fault at inverter AC bus. From Figure 4-11 it can be clearly seen that when one phase voltage drops to zero commutation failures do not happen and the DC voltage is kept positive at about 200 kV throughout the fault. Moderate rise of DC current can be seen from Figure 4-11(b). As a result, about 40% of the rated active power can still be transmitted during fault, which can be seen in Figure 4-12(a). The main factors that affect the level of active power transfer during single-phase fault are the voltage levels of the remaining two phases. If their voltage levels are controlled to be near the rated value by external voltage control devices, e.g. FACTS devices, the active power flow level during single-phase fault can be maximised. In Figure 4-12, the active power responses from the original benchmark system are also depicted as a comparison to the proposed system. From Figure 4-12(a) it can be clearly observed that the proposed system is able to recover to about 90% of the rated active power in about 50ms after the fault is cleared, while it takes about 85ms for the

benchmark system due to successive commutation failures. The limited reactive power consumption at inverter side for the proposed system, which is shown in Figure 4-12(b) helps the recovery of the system from fault. It also demonstrates that the controller is working correctly by controlling the reactive power consumption to be zero.

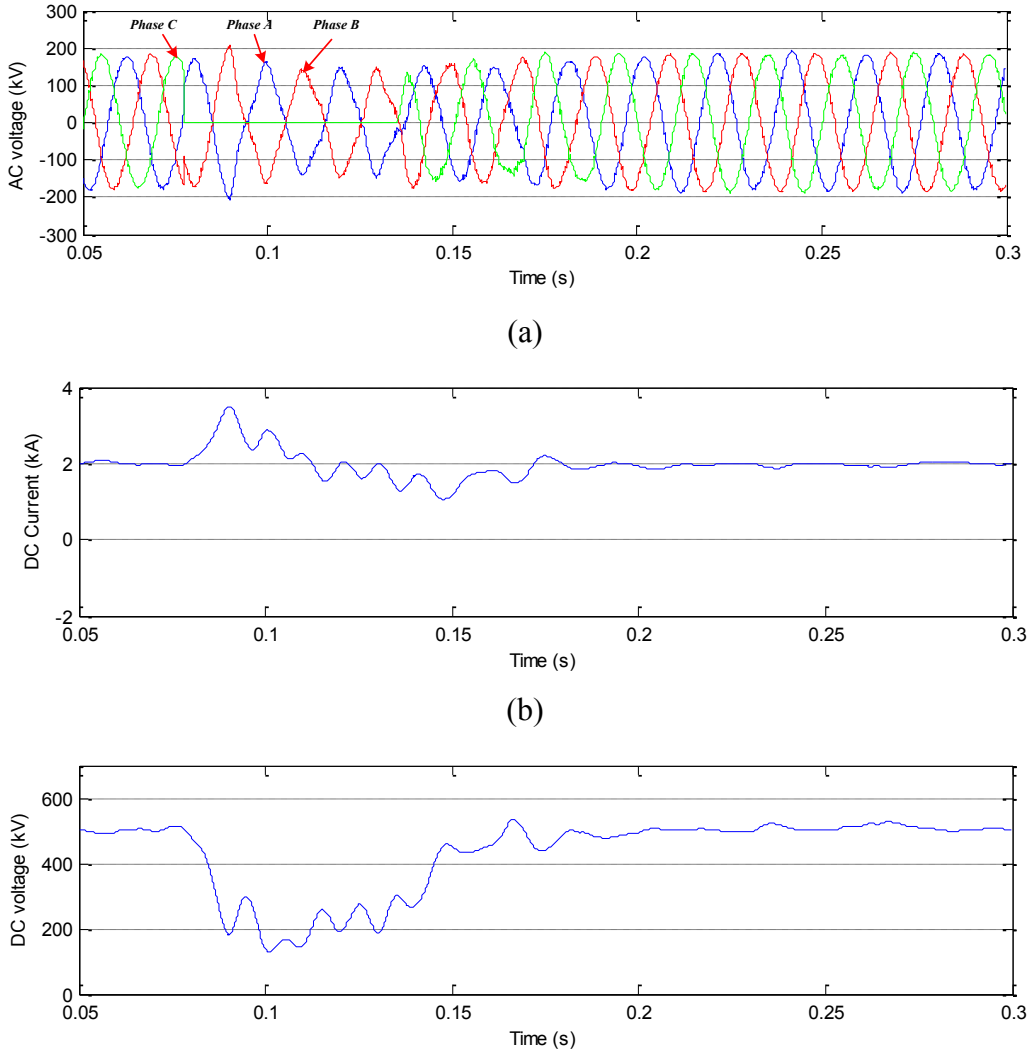

Figure 4-11 System responses with 50ms single-phase to ground fault. (a) AC voltage; (b) DC current; (c) DC voltage.

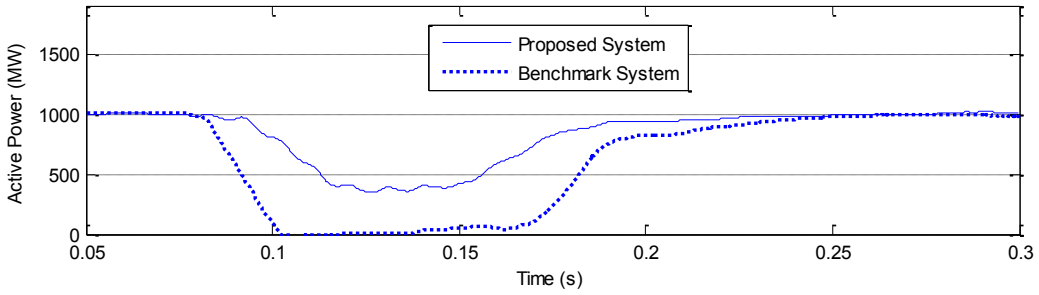

(a)

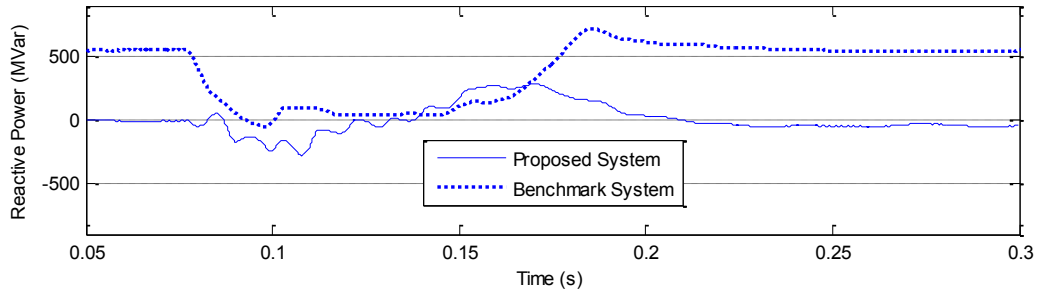

(b)

Figure 4-12 Active and reactive power response with single-phase fault. (a) Active power; (b) Reactive power

Figure 4-13 and Figure 4-14 show the system responses under a 100ms zero impedance three-phase to ground fault at inverter AC bus. From Figure 4-13(d) it can be seen that under the zero impedance three-phase to ground fault, when there is no natural commutation voltage from the AC side, commutations are all successful. Since the capacitors are mostly inserted during the commutation period, they do not provide any additional DC voltage at inverter side. Hence the DC voltage drops to zero and no active power can be transmitted during fault. Also the lack of inverter DC voltage drives up the DC current, which is shown in Figure 4-13(c), with a maximum value of nearly 5kA. However from Figure 4-14(a) it can be seen that the active power of the proposed system is able to recover to about 90% of the rated value in about 100ms after the fault is cleared, which is faster than that for the benchmark system. Similar to the single-phase fault case, the reactive power consumption of inverter side is well controlled to about zero during fault, which facilitates a fast recovery.

From the above two simulations it can be seen that complete immunity to commutation failure is preserved when the inverter side is in reactive power control. It also shows that reactive power can be successfully tracked by the controller or can be controlled to be zero making inverter work at unity power factor. Limited reactive power consumption of inverter helps the recovery of AC voltage after fault is cleared hence facilitates a quick recovery of the HVDC system.

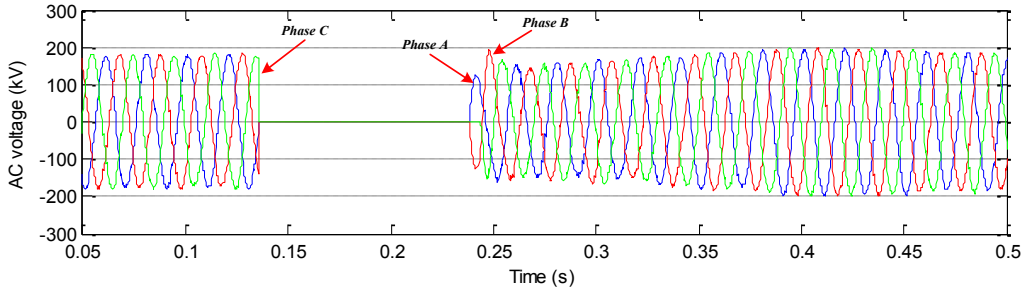

(a)

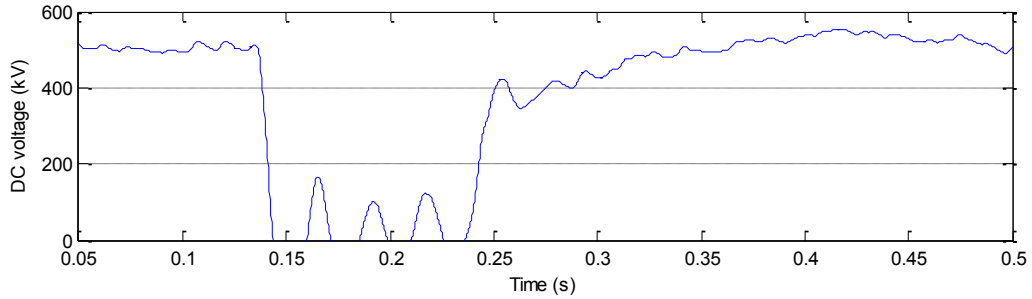

(b)

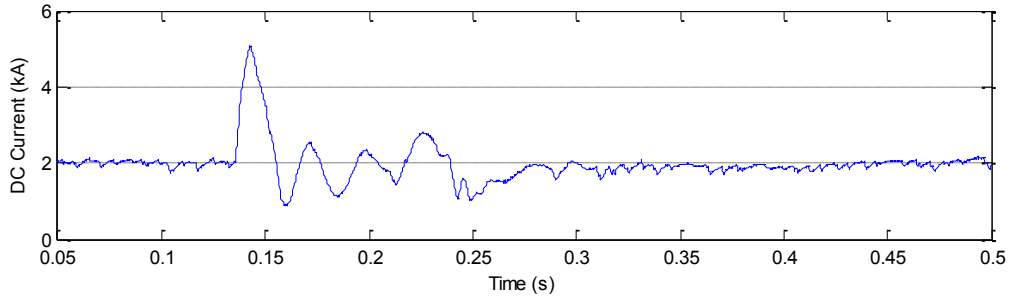

(c)

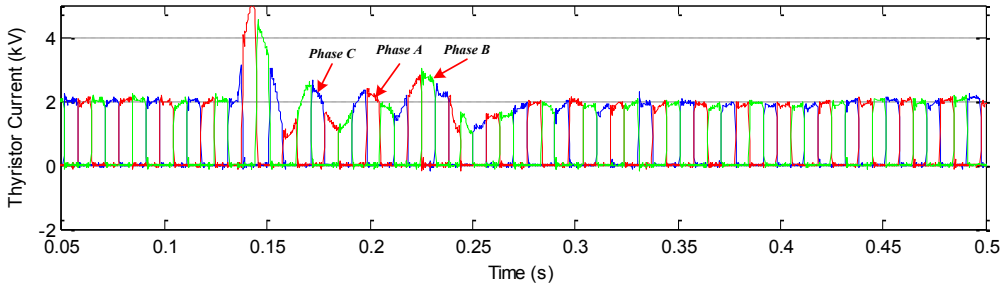

(d)

Figure 4-13 System responses under 100ms three-phase to ground fault. (a) AC voltage; (b) DC voltage; (c) DC current; (d) Thyristor currents

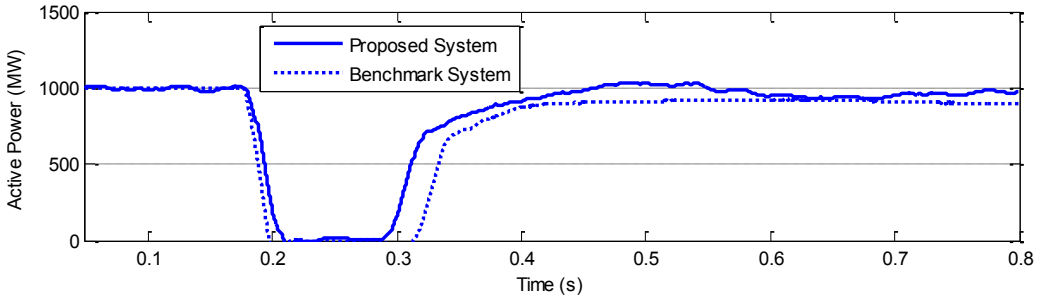

(a)

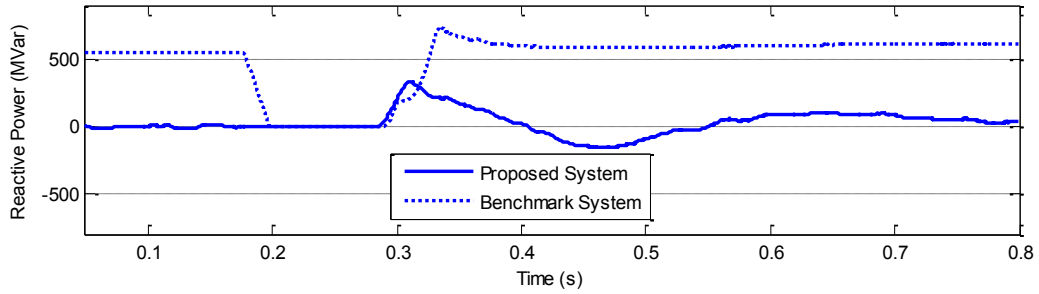

(b)

Figure 4-14 Active and reactive power responses under three-phase grounding fault. (a) Active power; (b) Reactive power.

4.6.4 AC Voltage Control

In order to demonstrate the effectiveness of the proposed AC voltage controller, different load switching cases are simulated. In this particular case, three different types of loads are considered which are listed in Table 4-1. Two of them are passive loads and one is an induction machine. The induction machine is chosen according to [113], and its rated power is being proportionally increased as the rated power of the HVDC benchmark system is larger

than the HVDC system being used in that reference. The technical data for the induction machine is listed in Appendix B.1. All the loads are switched in and out by controlling the connected circuit breakers. The detailed switching sequence for this study is listed in Table 4-2.

Table 4-1 Types of loads

Load	Load type	MVA	Power factor
1	Passive	487	0.9
2	Passive	344	0.95
3	Induction machine	99.7MW	0.935

Table 4-2 Switching sequence

Time (s)	**1.6**	**2.6**	**3.6**
Event	Switch in Load 1	Switch in Load 2	Switch in Load 3
Time (s)	4.6	5.6	6.6
Event	Switch out Load 1	Switch out Load 2	Switch out Load 3

Figure 4-15 shows the simulation results by applying this switching sequence. When Load 1 is switched in at 1.6s, the AC voltage drops as shown in Figure 4-15(a) due to the large reactive power absorption of load. In response to the change of AC voltage, firing angle at inverter side increases, which is shown in Figure 4-15(b), to lower its reactive power consumption in order to bring back the AC voltage. It can be clearly seen from Figure 4-15(a) that the AC voltage is quickly controlled to be the reference value. Similar to the switching in of Load 1, when Load 2 and Load 3 are switched in, the AC voltage drops initially due the additional reactive power load but the controller acts quickly to bring it back. As a result, the inverter firing angle is increased and its reactive power consumption decreases to balance the reactive power. It should be mentioned that when Load 3 (induction machine) is initially

switched in, it absorbs a large amount of reactive power as shown in Figure 4-15(d). In order to control the AC voltage, the inverter temporarily exports about 250 MVar of reactive power to the AC system to control the AC bus voltage. The high-frequency harmonics in Figure 4-15(d) is due to the *LC* oscillation between capacitor banks and inductors in the load. As the system settles to a new steady-state, the oscillation reduces. Later on when the loads are switched out, the AC voltage tends to increase due to the reactive power surplus and the firing angle is decreased to match the reactive power requirement. Consequently it can be seen from Figure 4-15(a) that the AC voltage is well controlled in all the cases. Finally as shown in Figure 4-15(g), the DC current is successfully controlled by the rectifier side current controller throughout the whole simulation period. The large smoothing reactor on the DC side also helps to limit the change of DC current when inverter AC load is switched in.

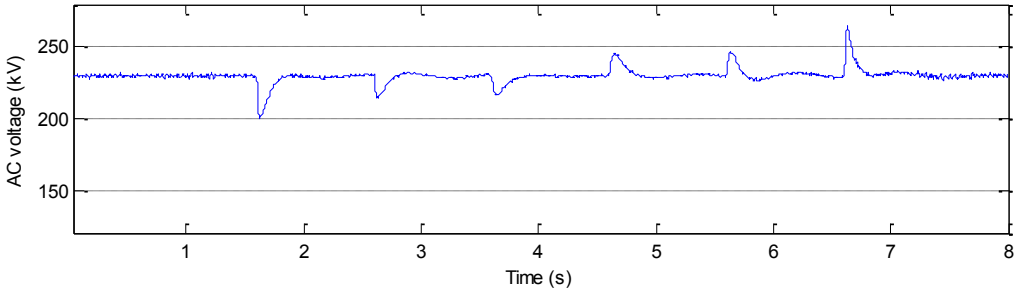

(a)

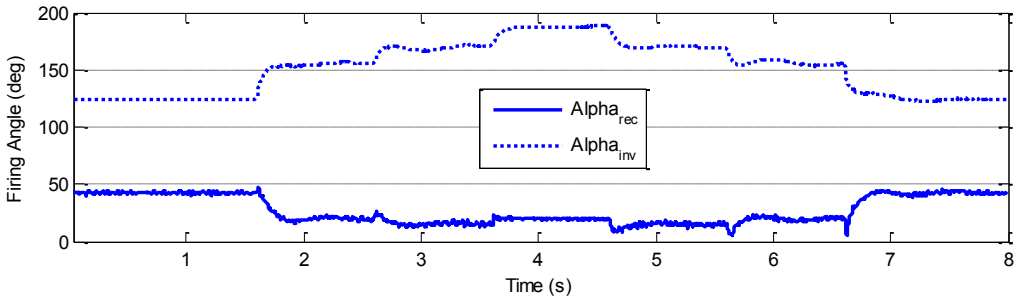

(b)

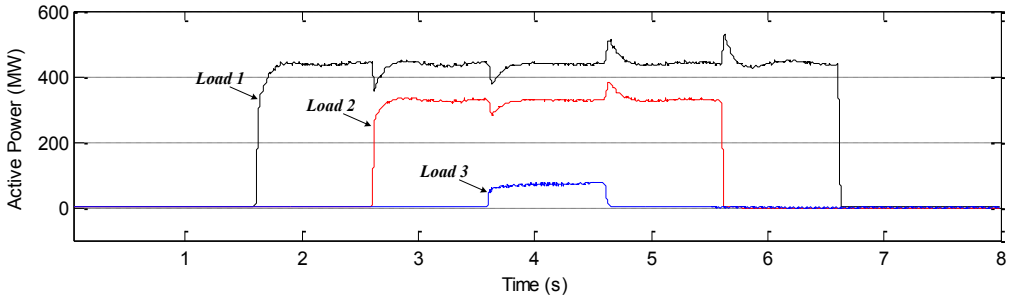
Active Power (MW)
600
400
200
0
Load 1
Load 2
Load 3
1
2
3
4
5
6
7
8
Time (s)

(c)

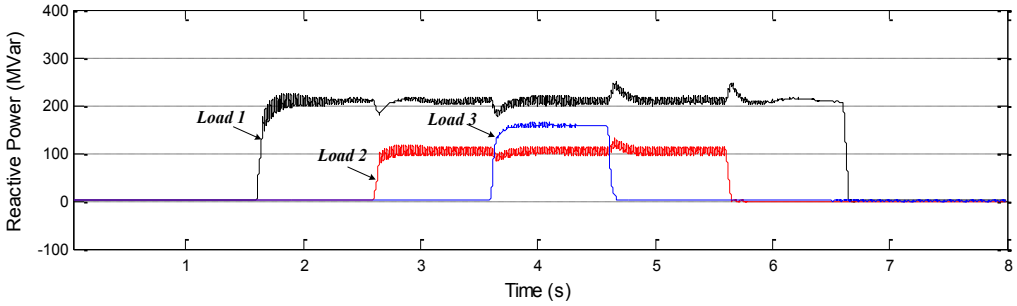
Reactive Power (MVar)
400
300
200
100
0
-100
Load 1
Load 3
Load 2
1
2
3
4
5
6
7
8
Time (s)

(d)

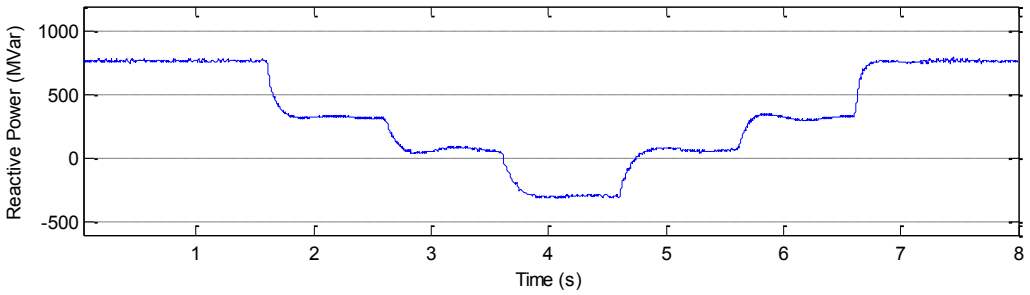
Reactive Power (MVar)
1000
500
0
-500
1
2
3
4
5
6
7
8
Time (s)

(e)

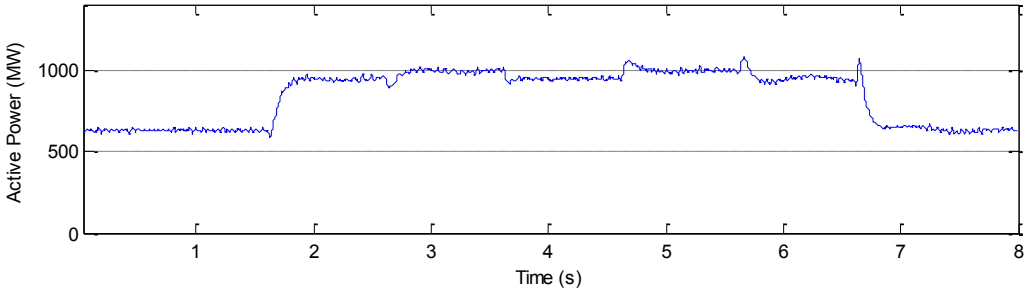
Active Power (MW)
1000
500
0
1
2
3
4
5
6
7
8
Time (s)

(f)

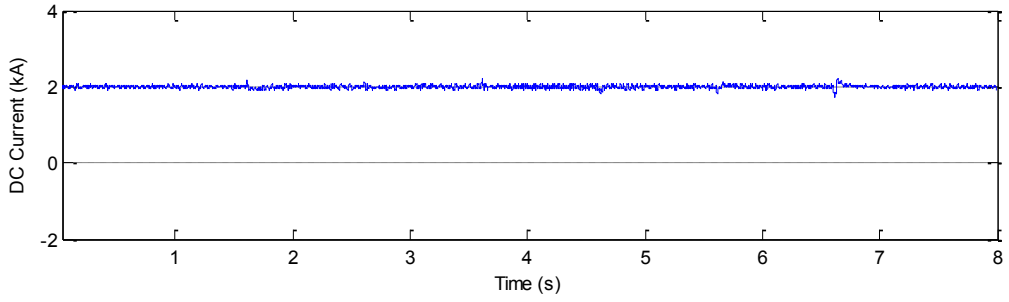
DC Current (kA)
4
2
0
-2
1
2
3
4
5
6
7
8
Time (s)

(g)

Figure 4-15 System responses with various load switching. (a) Inverter AC bus voltage; (b) Rectifier and inverter sides firing angles; (c) Load active power; (d) Load reactive power; (e) HVDC inverter reactive power; (f) HVDC active power; (g) DC current.

4.7 Summary

In this chapter, the reactive power controllability of the proposed hybrid HVDC system is analysed and demonstrated. Reactive power control at inverter side is made possible by dynamic insertion of capacitors to help the commutation process.

Detailed analysis is carried out to investigate the reactive power characteristic of the proposed system. It has been found that by controlling the inverter firing angle to be close to 180^0, inverter power factor can be controlled at unity. At the same time extinction angle is negative and cannot be measured using the conventional methods. A new extinction angle measurement which can accommodate negative extinction angle is then proposed to facilitate the controller designs.

Two different types of controllers, i.e. reactive power controller and AC voltage controller are designed based on the reactive power controllability of the proposed system. Reactive power controller can be used to track the reactive power reference changes and in particular to control the inverter side to operate at unity power factor for different active power levels. The AC voltage controller is used to control the inverter AC bus voltage to increase the voltage stability of the connected AC system.

Simulation case studies are carried out in RTDS to test the effectiveness of the proposed system and the designed controllers. It can be concluded that reactive power controller successfully controls the reactive power consumption of inverter side to follow the reference

value. Also this limited reactive power consumption can help the system's recovery from fault, which is validated by comparisons with original benchmark system. Complete commutation failure immunity is achieved by choosing the appropriate capacitor voltage level. Finally the AC voltage controller is tested by simulating a series of passive and dynamic load switching. The results demonstrate that the voltage controller can successfully control the AC bus voltage at reference value for different load switching cases.

CHAPTER 5 Black Start Using the Hybrid HVDC System

5.1 Introduction

This chapter discusses the black start of an AC system using the proposed Hybrid HVDC system. In section 5.2, the procedures for traditional LCC HVDC black start are described. In section 5.3, various issues with the hybrid HVDC black start are presented and discussed with detailed analysis for no load start up and load pickup process. Based on the analysis the inverter AC voltage controller is also proposed for the hybrid HVDC system. In section 5.4, simulation results for no load start and load pickup cases are presented to demonstrate the effectiveness of the proposed system and its controller. Finally the main results of this chapter are summarized in section 5.5.

5.2 Conventional LCC-HVDC Black Start

It has been generally accepted that traditional LCC-HVDC system cannot supply active power to a passive AC network where no synchronous generators are available. The use of line commutated thyristor semi-conductors requires a relatively stiff AC voltage for successful commutations. However in some special applications where the HVDC system is needed to supply power to an island system or a remote community, the black start capability is essential. In this case the common choice is to install enough synchronous compensators and diesel generators at inverter side. The synchronous compensators are essential to provide the necessary AC commutation voltage for black start. The traditional black start sequence can be summarized as follows:

- The diesel generator is started to provide the auxiliary power to the converter station and the associated control & protection systems.
- When converter control and protection systems are back on line, synchronous compensators are energized using starting motors. Then the excitation systems are energized to regulate the AC commutation voltage.
- When the AC commutation voltages generated by synchronous compensators are stable, firing pulses of inverter side are released. Now the starting motors can be disconnected.
- As the HVDC system is initially energized, active power from the rectifier side can be used to supply the power for synchronous compensators, its own power losses and auxiliary power. Now the active power transfer through the HVDC link is very low with a low DC current. Due to the harmonics in the DC current, operation with discontinuous DC current is needed.
- The loads are able to be connected in sequence. As a result the DC current increases and more active power is drawn from the rectifier side to the inverter passive system.

It can be clearly seen from the above descriptions that the procedures are quite complex and require careful coordination between different electrical components. The time it requires for successful load pick up can be quite long and there is a possibility of commutation failures when large loads are switched in. Furthermore if the rectifier side is used to control the DC current to regulate the inverter AC voltage, a reliable tele-communication is required, which is a significant disadvantage for the black start case.

The complexity of black start and inability to transmit power to a passive network under normal operation motivates the development of new system configuration and controllers to solve these problems.

5.3 Black Start with Hybrid HVDC

To analyse the black start situation in detail, the main differences in operations compared to normal case should be identified first. It acts as an essential foundation for the understanding of system dynamics during black start and for the controller designs. Then the steady state operation and no load start of the system are investigated, which lead to the design of start-up sequence and inverter AC voltage controller.

5.3.1 Special Considerations for Black Start with Hybrid HVDC

Due to the complete absence of commutation voltage from AC side, there are some major differences between the normal case and black start case, which are listed as follows:

- There are no AC reference voltages which can be utilized by PLL for the synchronization of firing pulses. In this case to control the connected AC system frequency, all the thyristor valves have to be fired by fixed interval firing pulses synchronized to an external 50 Hz or 60 Hz clock. This is the main difference from the normal operation of LCC HVDC.
- The inverter AC voltage is now established by the injected currents passing through system impedances. Since the AC system impedances cannot be controlled, the control of AC voltage can only be achieved by controlling the injected current. With the traditional LCC where the rectifier side is controlling the DC current, tele-communications are needed to send the measured AC voltage signal back to rectifier side.
- Under black start case, the extinction angle is largely dependent on the AC system impedance angle. Hence the change of firing angle during black start does not have any effects on the steady state operation of the system. The more resistive the AC

system is, the smaller the extinction angle will be, which can endanger the success of commutations.

- During very light load after initial start-up, because the loads have not been added, extinction angle can be close to 90^0. Therefore continuous operation with high extinction angle is required, which is not desirable. It results in high voltage stress of valves and higher ratings for the surge arresters.
- The control of AC voltage is at priority for the black start case for normal operation of the connected loads. Acceptable dynamic control of AC voltages during load switching should also be achieved to avoid temporary overvoltage.
- If the inverter current entering into the AC system is denoted as the positive direction, the phase displacement between the AC voltage and AC current is closely related to the system impedance angle and current should lead voltage by a sufficient amount to avoid commutation failures. This requirement poses a fundamental limitation on the type of loads that can be connected at AC side for normal operation.

From the above descriptions, if an LCC-HVDC system is to carry out black start without any synchronous compensators at AC side, the following difficulties can be identified [110]:

- Successful initial commutations without any AC commutation voltage from the AC side.
- The control of AC voltage should not depend on the current controller at rectifier. Firstly, the communication system at inverter side can be out of power during a black out case. Secondly, communication delays can lead to slow controller reactions, which can degrade controller performances. It should be mentioned that for point to point LCC HVDC connection the transmission distance is usually more than 1000 km [120].

- Continuous operation of the system with high extinction angle should be avoided to limit the investment cost.
- The ability of transmitting wide range of active power within the rated value without suffering commutation failures. The dependence of extinction angle on the AC system impedance can limit the maximum amount of power than can be safely transferred.
- Acceptable dynamic response under large load switching.

The aims of the proposed system configuration and control method are to solve these difficulties.

5.3.2 Steady State Operation

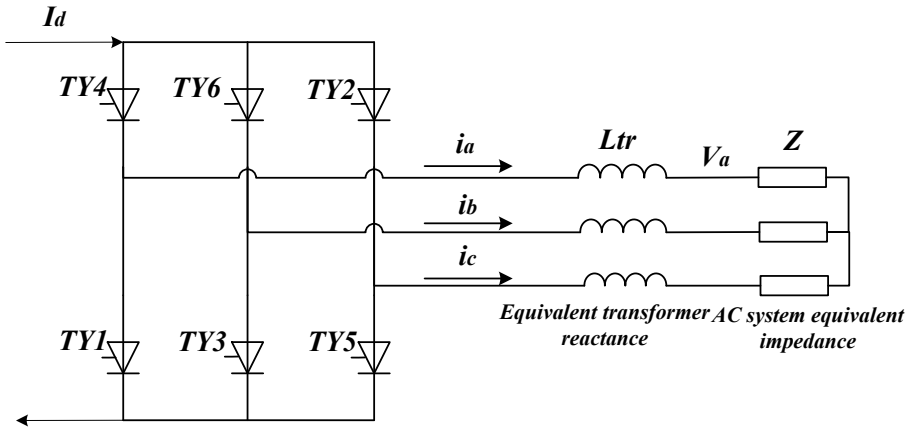

Figure 5-1 Inverter side 6-pulse bridge

The steady state operation is presented first to show a more detailed relationship between the inverter side system variables. In the following analysis only the 6-pulse group is considered, which can be easily extended to the 12-pulse case. The equivalent circuit of inverter side 6-pulse bridge used for the following analysis is shown in Figure 5-1. During steady state operation, inverter acts as a current source converter and injects alternating current into the AC system. Assuming a constant DC current, the injected currents are of square wave shape with a significant fundamental component and higher order harmonic content. The AC

voltage being developed will be of sinusoidal shape because most of the harmonic currents are filtered out by the installed harmonic filters at inverter AC bus. As a result the current entering into the AC system will be of fundamental frequency, which leads to a fundamental frequency AC voltage at inverter AC bus. According to the analysis carried out in section 1.1.4, which shows that the firing pulses can only be issued after the voltage across the valve becomes positive, it can be seen that the total impedance of inverter AC system is capacitive at fundamental frequency under steady-state operation.

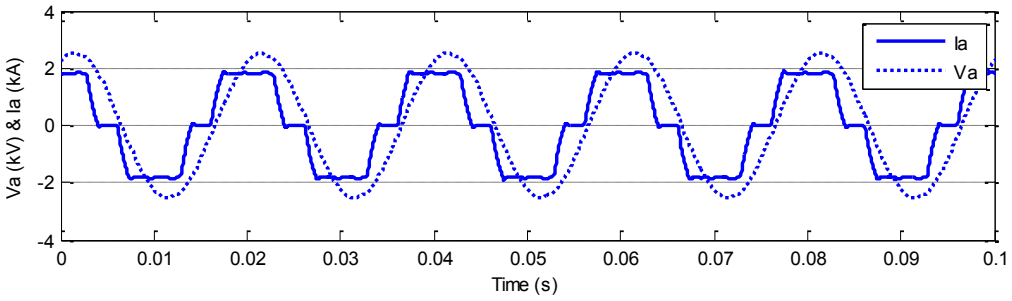

Figure 5-2 Steady state AC voltage and AC current

Figure 5-2 shows the inverter side AC voltage and the injected square wave current. The inverter firing angle being used is about 140^0. It can be clearly seen from the figure that under steady state operation the current leads the AC voltage, which is determined by the AC system impedance for a passive network. When the impedance Z is purely resistive, the current and voltage will be in phase with each other; if Z is more capacitive, the current has a higher leading phase to the AC voltage; if Z is inductive, the current lags the AC voltage. It should be mentioned that for traditional LCC-HVDC system the injected AC current always leads the voltage because the equivalent impedance of the AC system is capacitive due to the connected filter and capacitor banks. A smaller or zero leading angle is impossible for steady state operation because the resulting extinction angle is too small and successive commutation failures will happen. Thus it is essential that the equivalent AC system is

capacitive for successful initial commutation under black start case. This point will be explained in more detail in the following paragraphs.

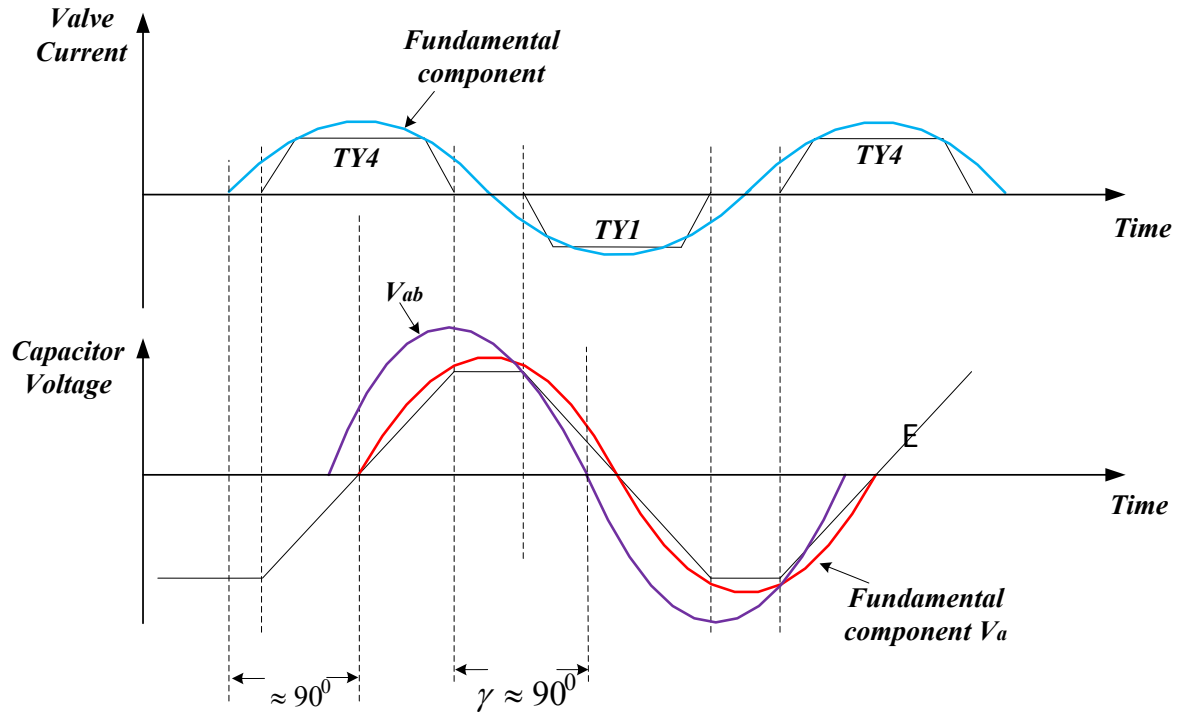

Figure 5-3 Current and voltage waveform with pure capacitive network

Now consider the AC system impedance is purely capacitive, which means that Z is capacitive. The detailed waveform relationship for this case is shown in Figure 5-3. Under steady state operating condition, the AC voltage is of trapezoidal shape as shown in the figure. When the valves connected to that phase is conducting, the capacitor charges or discharges according the direction of current and it holds its voltage level when there is no current conducting in that phase. The fundamental frequency current and voltage are drawn to visualize the phase relationship. The commutation voltage V_{ab} for commutation from *TY4* to *TY6* is also shown. It can be seen from the figure that in this case the injected AC current is leading the AC voltage by 90^0 and the extinction angle is also about 90^0. If the overlap angle is neglected, the extinction angle is expected to be at 90^0. When the AC system impedance is less capacitive, the leading phase of current is smaller, which results in a decrease of extinction angle. This situation is encountered as more resistive loads are connected to the

AC system and eventually when the system loads reach a certain level, the extinction angle can be so small that additional active power load can directly leads to commutation failures due to loss of commutation margin.

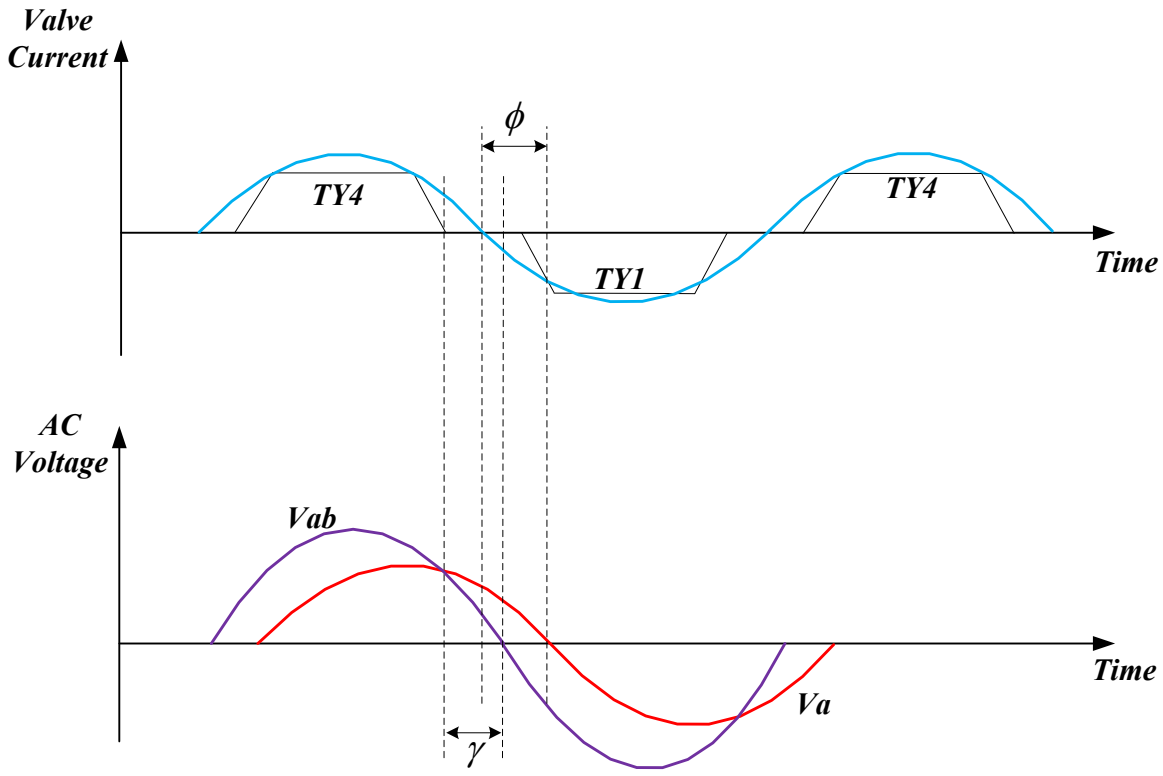

Figure 5-4 Current and voltage waveform with less capacitive network

When AC system impedance is less capacitive, the current and voltage waveforms are shown in Figure 5-4. The same waveforms as Figure 5-3 are shown and the only difference is that the AC system impedance is less capacitive. It can be caused by the switching in of more resistive power loads. From the figure it can be seen that the phase displacement between the fundamental frequency current and voltage are close to the extinction angle. It further demonstrates that a capacitive network at fundamental frequency is required for commutation with a passive AC system. Also the system impedance angle can be used as an immediate indication of the commutation margin of thyristors.

The above analysis shows that when the LCC HVDC system is inverting into a dead AC network, normal operation is only possible with a sufficiently large extinction angle. In other words, the injected AC current has to lead the AC voltage by a sufficient amount. Consequently, a capacitive AC network is essential for black start without additional electronic devices to generate commutation voltages.

5.3.3 No Load Start

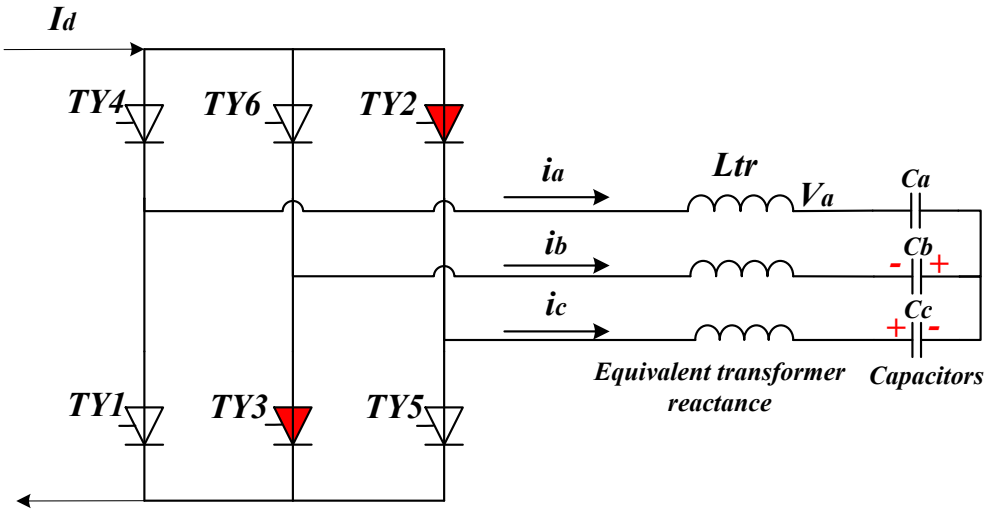

Figure 5-5 Initial start-up when TY2 and TY3 are on

According to the analysis from last section, no load start is only possible with all or part of the capacitor banks in service to provide capacitive network impedance. For the initial start-up process, both filter banks and capacitor banks are similar because they are all designed to be capacitive at fundamental frequency. Assuming that for the initial start-up, the rectifier side is already deblocked, the capacitors at the inverter side are connected and loads are not connected. Some level of DC current and DC voltage are then established by the rectifier side and the inverter side thyristors can be turned on. Assume without losing generality that *TY2* and *TY3* are fired first as shown in Figure 5-5. The DC current path at this time is *TY2-Cc-Cb-TY3*. Due to the direction of this current, the capacitors connected to phase B and phase C are charged to the polarities as shown in the figure. The phase A capacitor is not charged

since there is no current in that phase. 60^0 later the next thyristor in the conduction sequence, which is *TY4,* is issued with a firing pulse and is turned on. At this time the commutation from *TY2* to *TY4* takes place and three thyristors are conducting at the same time as shown in Figure 5-6. At this point, it is important to mention that the commutation voltage V_{ca} is provided by the capacitors only. Since the phase A capacitor is not charged, only the phase C capacitor *Cc* is providing the commutation voltage. Hence a proper selection of capacitor value is vital for the success of initial commutation. At the same time, *Cb* is continued to be charged in the same polarity since *TY3* is still conducting and *Ca* is charged to the polarity as shown in the figure due to the conduction of *TY4*. At the end of commutation, *Cb* has the highest voltage level and the voltage level at *Cc* is reduced due to the direction of commutation current.

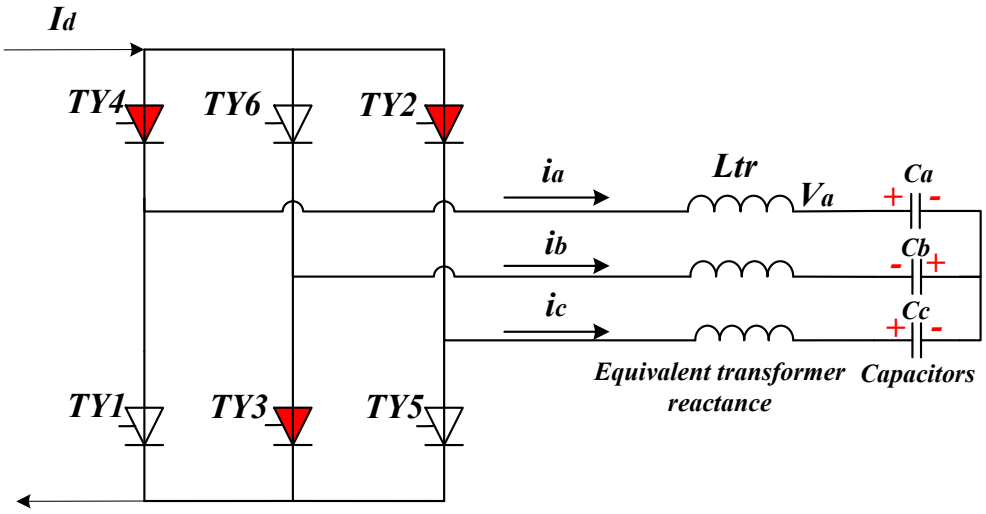

Figure 5-6 Commutation from TY2 to TY4 for initial start-up

When the commutation from *TY2* to *TY4* completes and after another 60^0, *TY5* is fired. This initiates the commutation process from *TY3* to *TY5*. From Figure 5-7, it can be clearly seen that the voltage polarities in *Cb* and *Cc* are all in favour of the commutation process. Also with higher capacitor voltages, the commutation is expected to be much easier for the first

commutation from *TY2* to *TY4,* which results in a smaller commutation overlap angle. For subsequent commutations, there will always be two charged capacitors with voltage polarities in favour of commutation. The no load steady state is reached when the DC current becomes constant and the capacitors in all three phases are equally charged.

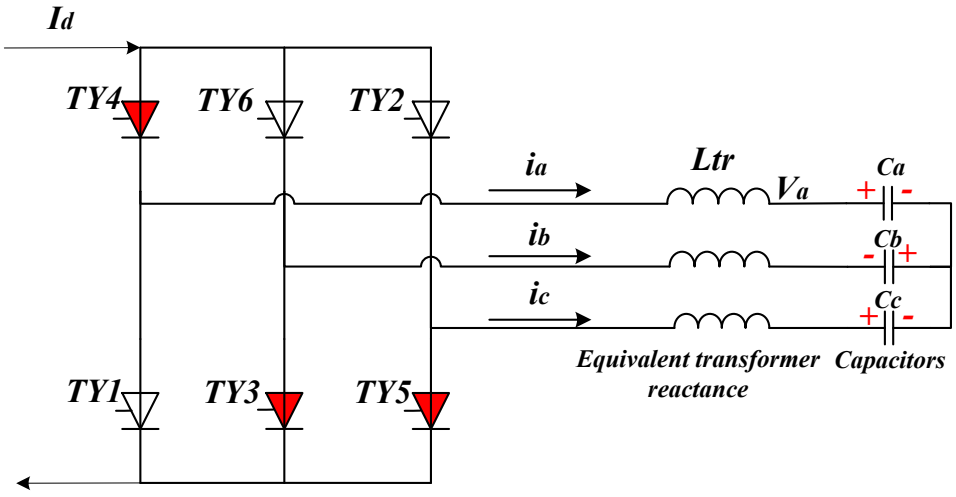

Figure 5-7 Commutation from TY3 to TY5 for initial start-up

From the above analysis for no load start-up procedure, it can be found that the existence of capacitive element in the AC system gives a significant advantage for initial commutation process. Those capacitors are able to provide the needed commutation voltage and with a properly chosen capacitor value, the difficult initial commutations can be successful.

Also it can be seen that if any resistances are connected at the initial start-up, they will be effectively in parallel with the capacitors and can discharge the capacitor energies. Therefore it lowers the possibility of successful initial commutation and is not desirable.

5.3.4 Load Pickup

Once steady state is reached under the no load condition, resistive loads can start to be connected. Assuming a stiff DC current is supplied by the rectifier side, when additional

loads are switched in, it causes the equivalent impedance in the AC network to drop. This causes a dip in the AC voltage. At the same time the DC voltage will increase to meet the increasing active power load since the DC current is more or less unchanged. From another perspective, the DC voltage is given by [62]:

$$V_{dc} = 1.35 V_{ac} \cos\gamma - \frac{3}{\pi} I_d X_{tr} \tag{5.1}$$

Where

V_{ac} is the RMS line-to-line voltage at inverter AC side;
γ is the extinction angle;
I_d is the DC current;
X_{tr} is the transformer impedance.

It has been discussed in previous sections that when the load are added, the system impedance angle will decrease, which will result in a decrease of the extinction angle. Hence from (5.1) it can be observed that when the extinction angle is decreased, the DC voltage increases. So if the current is properly controlled, the increase of active power load at inverter side is met by the increase of DC voltage. As more loads are switched in, the DC voltage will be higher towards the rated DC voltage and the inverter extinction angle will be smaller and will be similar in value to the system impedance angle. From the transient perspective, the DC current will experience a sudden dip due to the increased inverter DC voltage, but can be controlled at the desired value. Also the AC voltage at rectifier side can be changed due to the change of rectifier firing angle. However given the normally strong rectifier side AC system, the change is not significant.

5.3.5 Proposed Inverter AC Voltage Controller

A stable and controllable AC voltage is vital for acceptable and economical operation of an AC system. For steady state operation, the AC voltage level directly determines the healthy operation of different kinds of loads. Under transient operations, the level of AC voltage change affects the protection and insulation of the system largely. Thus inverter side AC voltage control is the most important control objective for LCC HVDC black start cases and a reliable and fast AC voltage controller is necessary.

It has been analysed in former sections that the inverter AC voltage is mainly determined by the magnitude of the injected AC current. So it is straightforward to control the AC voltage by controlling the DC current level, because the magnitude of injected current is directly related to the DC current level. However, since the rectifier is normally controlling the DC current, this control strategy relies heavily on a fast and reliable telecommunication system. It is extremely undesirable for a black start case, since the telecommunication system at inverter can also be affected when a black out happens. On the other hand, if the DC current controller is moved to the inverter side with the rectifier side controlling the DC voltage, the DC fault current level could be extremely high when there is a DC fault or inverter side AC fault. So it would be best to control the AC voltage at inverter side, but since the firing pulses are issued based on an independent clock, the change of firing angle is now irrelevant.

The proposed method works by controlling the phase angle difference between the injected AC currents from each 6-pulse group. This method only works for 12-pulse based HVDC system but since all of the HVDC systems are utilizing the 12-pulse technology for partial harmonic cancellation, it is indeed a general method for all the LCC HVDC systems. Normally for a 12-pulse scheme such as the CIGRE benchmark system, the injected currents from the two 6-pulse bridges have zero phase shifts between them to maximise the usage of

DC current. However when it comes to the black start case, it can be effectively used to control the inverter AC voltage.

In order to better illustrate the control strategy, a 12-pulse system shown in Figure 5-8 is considered. I_d is the DC current and is assumed to be constant; I_{up} and I_{down} are the injected AC currents from the upper 6-pulse bridge and lower 6-pulse bridge. I_{conv} is the total current entering into the AC system. V_{inv} is the inverter AC bus voltage established by I_{conv} and the system impedance.

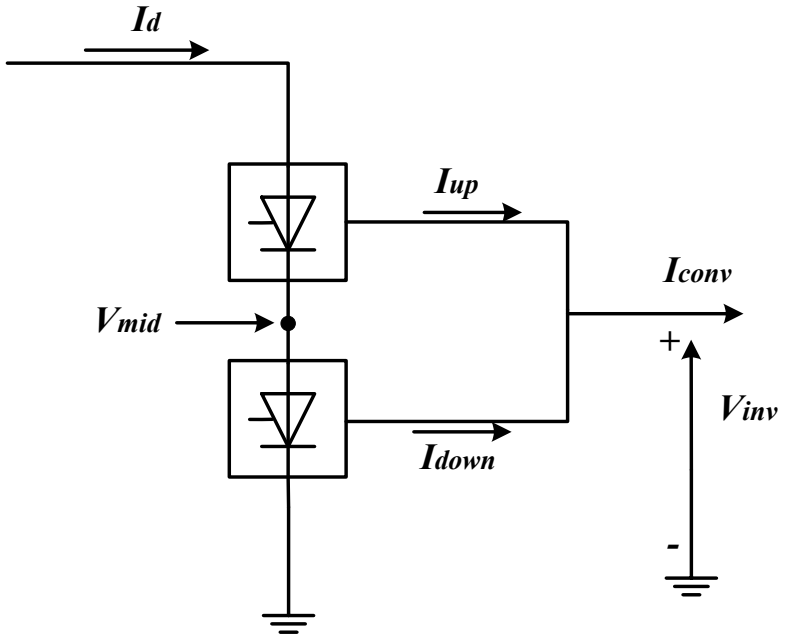

Figure 5-8 Inverter 12-pulse system

When the system reaches steady state under no load condition with only the capacitors being connected, I_{conv} should lead V_{inv} by 90^0 as shown in the phasor diagram of Figure 5-9. While the phase relationship between I_{conv} and V_{inv} are fixed, there are infinite numbers of combinations of I_{up} and I_{down} to achieve the same phase orientation of I_{conv}. Two different combinations of I_{up} and I_{down} that can make up the same I_{conv} direction are also shown in the figure. Having different phase displacements between the two injected currents, the

resulting I_{conv} has the same 90^0 leading angle but with a different magnitude. It should be noted that since I_{up} and I_{down} are from the same DC current, if their transformers are using the same connection topology, their fundamental frequency current magnitudes will be the same. So by controlling the phase difference between the two injected currents, the magnitude of total current injection can be modified. A larger phase difference result in a smaller current magnitude and vice versa. Furthermore, because the AC voltage magnitude is developed by the multiplication of impedance magnitude and injected current magnitude, this method of control can then be effectively used to control the AC voltage.

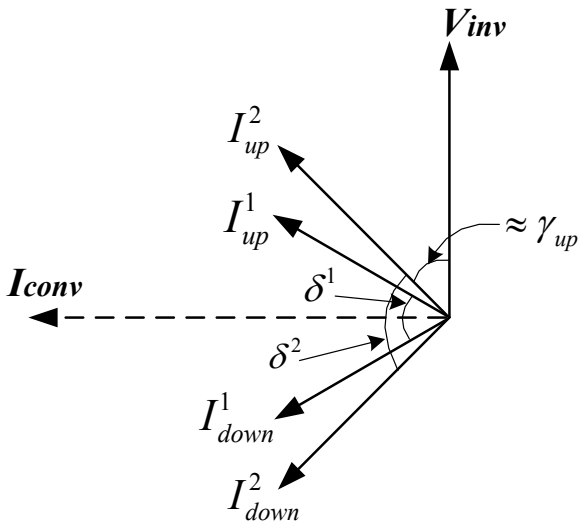

Figure 5-9 Phasor diagram of no load start up

From the above analysis the inverter AC voltage controller is designed as shown in Figure 5-10. The parameters of this PI controller are determined through trial and error by carrying out a series of simulations of voltage reference step changes. When the voltage reference is larger than the measured AC voltage, the phase displacement angle δ is controlled to be smaller to increase the voltage; when the reference voltage is smaller than the measured AC voltage, δ is then decreased to lower down the AC voltage.

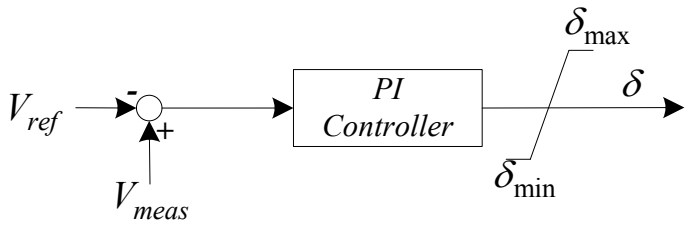

Figure 5-10 Inverter AC voltage controller for black start

For this controller, three important aspects need to be pointed out. First is about the maximum phase displacement angle δ_{max}. Ideally it can be up to 180^0, which will result in a zero inverter side AC voltage. Under this situation all of the power coming from the upper 6-pulse bridge goes to the lower 6-pulse bridge and no power is fed to the connected AC system. The upper 6-pulse is working at inverting mode and lower 6-pulse bridge is actually working in rectifier mode with a negative mid-point voltage V_{mid}. However, since thyristors need a minimum voltage to be turned on, the ideal 180^0 cannot be achieved for practical systems. Given a minimum firing angle of 5^0, δ_{max} is around $180^0 - 2 \times 5^0 = 170^0$.

The second aspect is the δ_{min}, at which the maximum AC voltage is produced. The ideal minimum displacement angle is 0^0 and can be safely achieved. However, when the DC current magnitude is fixed, the maximum AC voltage level achievable is limited by the DC current level. On the other hand, the steady state AC voltage under no load start is higher than that when the load is on. So initially the phase displacement needs to be relatively large to keep the AC voltage at the reference value. As loads are switched in, phase displacement becomes smaller to control the AC voltage. Consequently, as long as the voltage can be controlled at rated value under rated loading condition, it can be well controlled at all the lower loading conditions using the proposed control method.

Last but not least, it needs to be pointed out that at a higher phase displacement angle, the upper 6-pulse bridge is working at inverting mode with a small extinction angle as shown in Figure 5-11. If the AC system is heavily loaded, extinction angle for that bridge can be so

small that normal operation cannot be possible due to commutation failures. However for the proposed hybrid HVDC system, it should not be a problem, since commutation failure can be perfectly eliminated by the inserted capacitors. So the maximum ideal phase displacement angle of 170^0 can be safely achieved using the proposed system.

Finally according to the above analysis, the proposed AC voltage controller is able to control the AC voltage in a wide range under the black start case. It should be emphasized that the proposed controller is only applicable to the proposed Hybrid HVDC system, since only in this case can the commutation failure problems be solved.

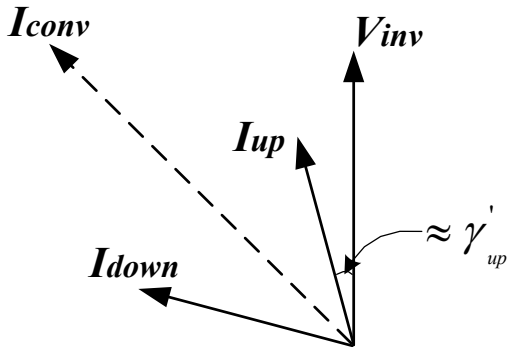

Figure 5-11 Phase diagram at higher loading conditions

5.3.6 Proposed Start-up Sequence

With the proposed inverter side AC voltage controller, the proposed start-up sequence is listed as follows and the associated flow chart is shown in Figure 5-12 for better illustration:

1. Before converter stations are deblocked, capacitor banks at inverter side are connected to the inverter AC bus. This is to provide a capacitive network for the difficult initial commutations.
2. Then the rectifier side of the system is deblocked. The main control function is current control with a current reference of rated value. So the firing angle of rectifier will decrease to increase the DC voltage and DC current.

3. Shortly after the rectifier side is deblocked, the inverter side is deblocked with firing pulses from an independent 50/60 Hz clock signal. Also the AC voltage controller output is released at the same time. At this time, since the AC voltage is very low, the voltage controller output will be zero displacement angle. The initial commutations will energize the AC system and gradually establish the AC voltage. The inverter side DC voltage is raised due to the commutations and results in an increase of rectifier DC voltage to control the DC current.
4. Then a short period later when the AC voltage is relatively stable, the capacitor voltage balancing controller is deblocked to charge the capacitors to its rated voltage level. This is mainly used to eliminate commutation failures when the steady state is reached under no load condition. As has been analysed in previous sections, phase displacement needs to be quite large to control the no load steady state voltage at reference value.
5. Later on when the no load steady state is reached, the load can start to be connected. Each time when the load is switched in, the AC voltage drops and the controlled phase displacement becomes smaller to stabilize the AC voltage. As the system becomes more resistive, the extinction angle of the upper 6-pulse bridge becomes smaller according to the system impedance angle. The increased load requirement is met by the increase of DC voltage, while the DC current is controlled at the rated value by the rectifier current controller.

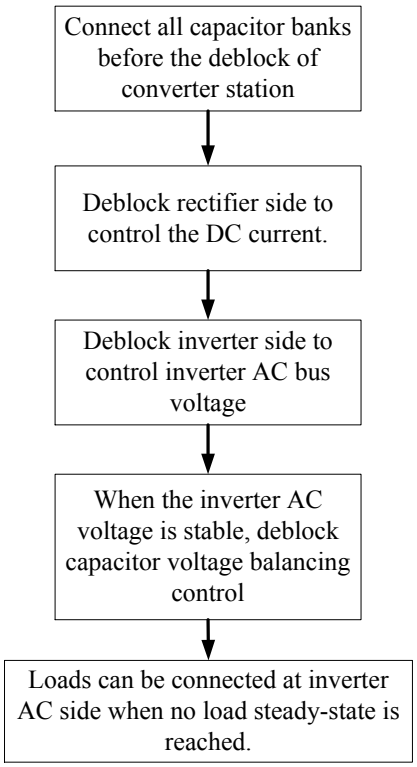

Figure 5-12 Proposed black-start sequence

5.4 Simulation Results

This section provides the simulation results to validate the black start capability of the proposed system using the proposed inverter AC voltage controller. The test system is established in RTDS and the no load start and load pickups are simulated separately.

5.4.1 System Configuration

The test system configuration for black start simulation is shown in Figure 5-13. The system topology of inverter side is identical to the one shown in Figure 3-1(a). The main differences are that at inverter AC side, voltage source is removed and various loads are connected to the inverter AC bus. The switch of load is controlled by the associated circuit breakers. The rest of the system parameters including the filters are the same as those in the CIGRE HVDC benchmark model.

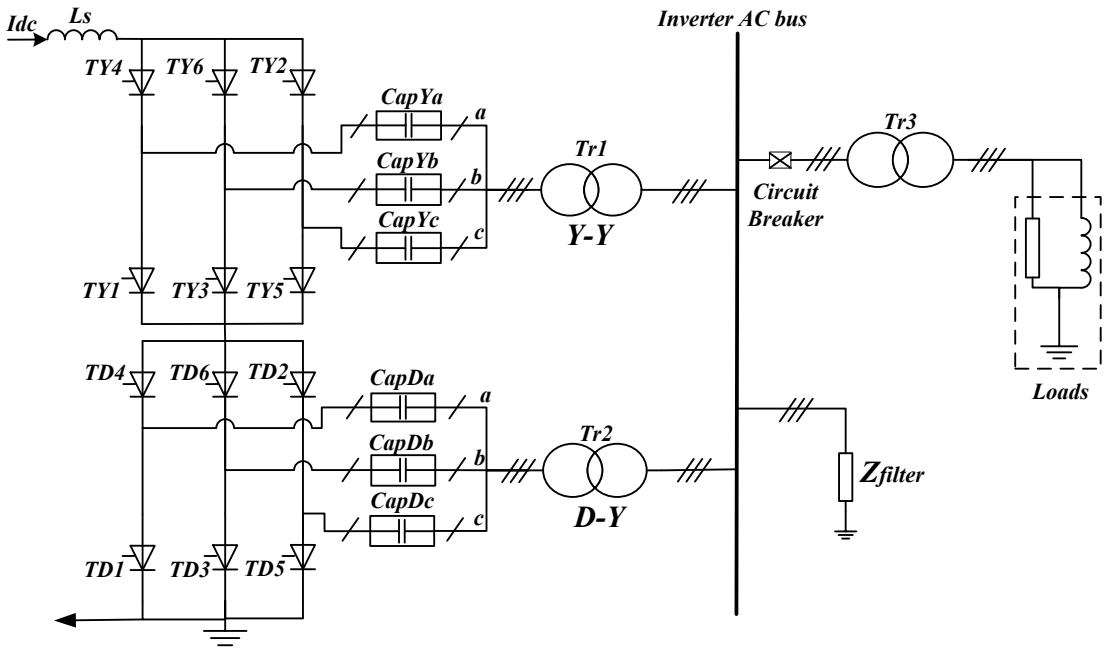

Figure 5-13 Black start test system configuration

5.4.2 No Load Black Start

In this section, no load start of the Hybrid HVDC system using the proposed voltage controller is presented. The same sequence as shown in Figure 5-12 is applied and simulation results are shown in Figure 5-14. As discussed before, the filter banks are connected to the inverter AC bus before the rectifier side is deblocked. At 1.4s the rectifier is deblocked with its current controller being released. Since at this time the inverter is blocked and its DC voltage is zero, the rectifier firing angle decreases to increase the DC current. Shortly after the rectifier is deblocked, the inverter side is deblocked with fixed frequency firing pulses from external clocks. This makes the inverter side starts to inject AC current into the receiving system and the inverter AC voltage is increased, which can be seen from Figure 5-14(c). From Figure 5-14(e) it can be seen at the same time the extinction angle jumps to about 90^0 because the AC system is now capacitive with only the filter banks connected. Both DC voltage and DC current experience a short transient due to the deblock of inverter

station. But the DC current will continue to rise according to the ramping speed set by the rectifier side current controller. Then after 1s at about 2.4s, the capacitor balancing controllers are released and the capacitor voltages quickly rise to the reference value as shown in Figure 5-14(f). After that DC current continues to increase and results in a further increase of inverter AC voltage. Finally the system achieves the no load steady state with the rated DC current. Because no loads are connected, the DC voltage keeps at a very low value and the transmitted active power is only compensating the system losses. Inverter extinction angle, which is largely determined by the AC system impedance angle, is at very high value. Meanwhile it can be seen that the inverter AC voltage is well controlled by the proposed voltage controller.

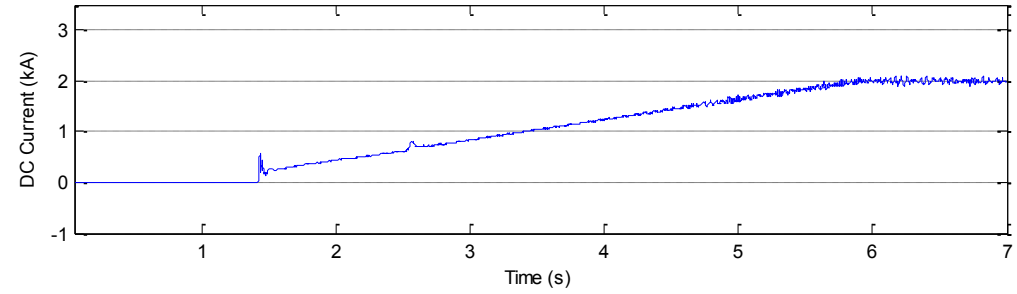

(a)

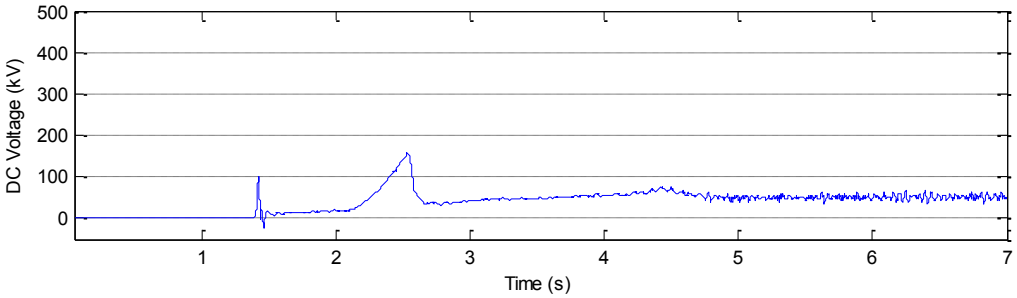

(b)

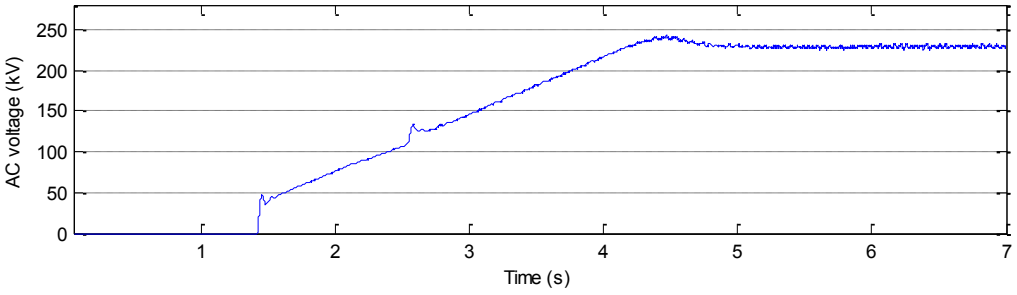

(c)

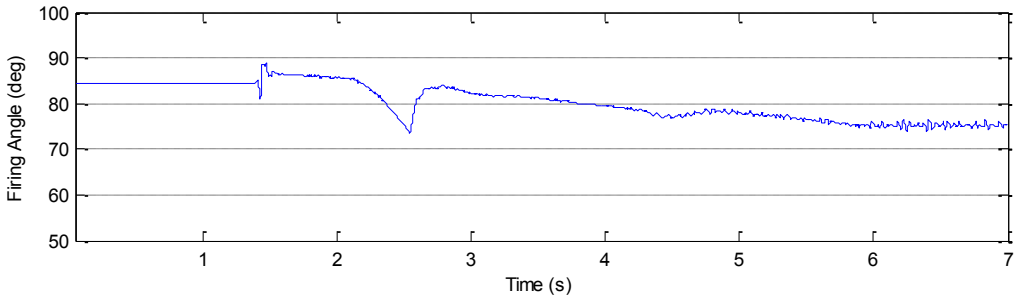

(d)

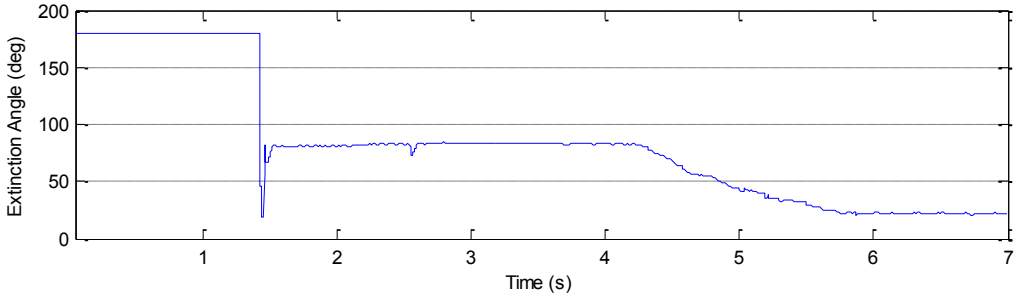

(e)

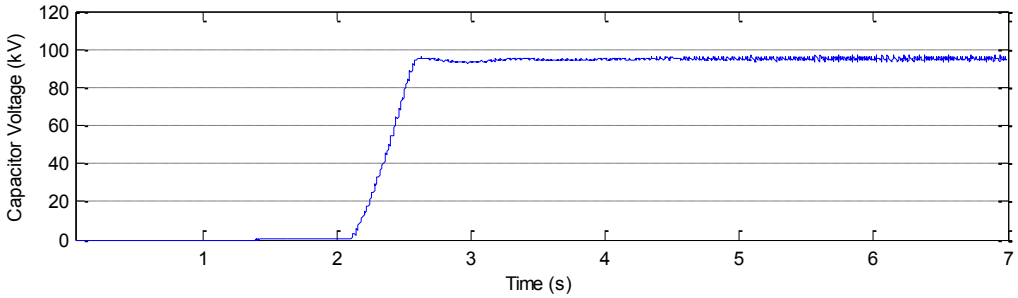

(f)

Figure 5-14 System responses for no load start. (a) DC current; (b) DC voltage; (c) AC voltage; (d) rectifier firing angle; (e) Extinction angle of upper 6-pulse bridge; (f) Capacitor voltage for CapYa.

5.4.3 Load Switching

This section presents the simulation results when the loads are switched in after the no load steady state is reached. Three resistive loads are considered and they are listed in Table 5-1. They will be switched in and out to demonstrate the effectiveness of the proposed inverter AC voltage controller. The switching sequence of loads is shown in Table 5-2.

Table 5-1 List of loads

Load	Load type	MW
1	Passive	415
2	Passive	290.5
3	Passive	290.5

Table 5-2 Load switching sequence

Time (s)	1	2	3	4
Event	Switch in Load 1	Switch in Load 2	Switch in Load 3	Switch out Load 3

Simulation results are presented in Figure 5-15. It can be clearly seen that each time when load is connected, it causes a temporary AC voltage drop. The controller then quickly recovers the voltage magnitude by decreasing the phase displacement angle as shown in Figure 5-15(c). The DC power is increased by an increased DC voltage to meet the load requirement, which can be seen from Figure 5-15(b). This increase of DC voltage causes the firing angle at rectifier side to drop to raise its DC voltage so that DC current can be well controlled. As explained earlier, extinction angle decreases as more load is switched in, which is shown in Figure 5-15(e). It should be noted that when Load 3 is switched in, the extinction angle for the upper 6-pulse bridge decreases to zero and will certainly cause commutation failures for the conventional LCC HVDC system. However, in this case for the hybrid HVDC system no commutation failures are happening and the AC voltage is well controlled by the proposed voltage controller. When all the loads are switched in, the HVDC system is transferring its rated active power at rated DC current and DC voltage. Finally when Load 3 is switched out, it causes a temporary AC voltage increase, which again quickly corrected by the controller through increasing phase displacement angle. Throughout the

whole simulation period, the DC current is well controlled by the rectifier current controller as shown in Figure 5-15(a) and capacitor voltage levels are well controlled by the capacitor voltage balancing controllers.

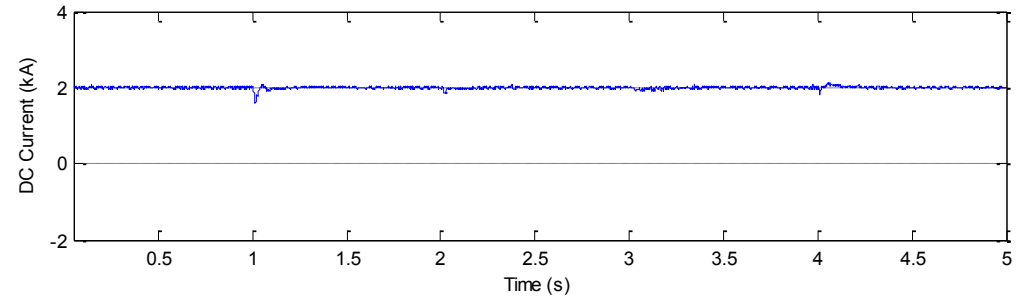

(a)

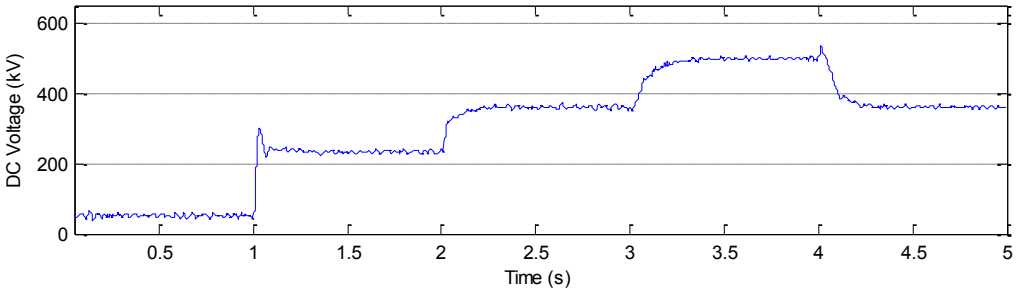

(b)

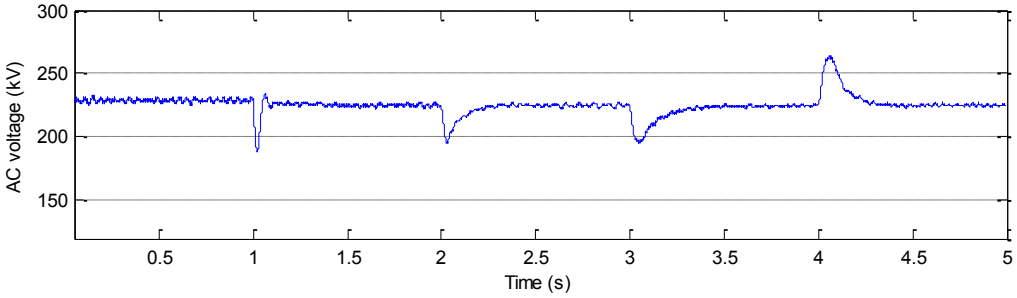

(c)

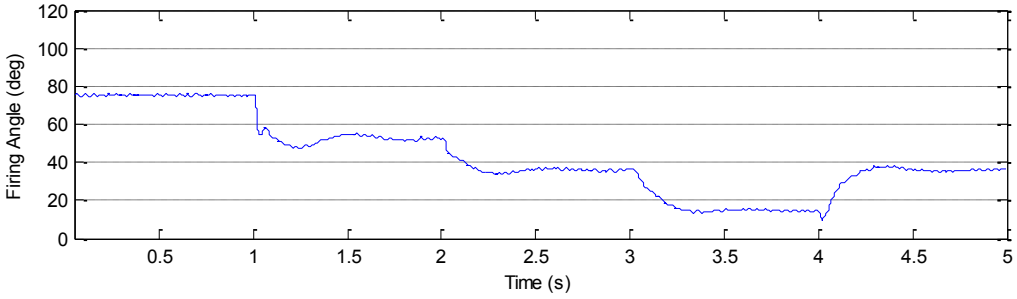

(d)

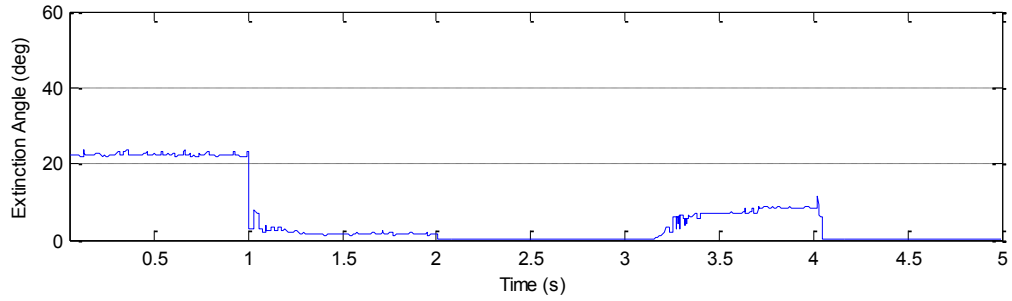
Extinction Angle (deg)
60
40
20
0
0.5
1
1.5
2
2.5
3
3.5
4
4.5
5
Time (s)

(e)

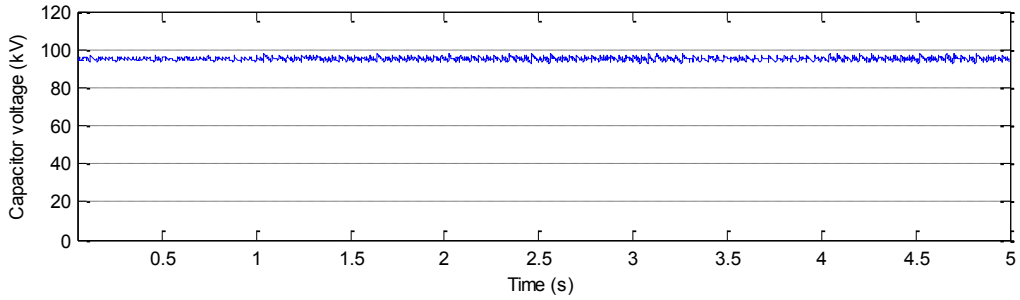
Capacitor voltage (kV)
120
100
80
60
40
20
0
0.5
1
1.5
2
2.5
3
3.5
4
4.5
5
Time (s)

(f)

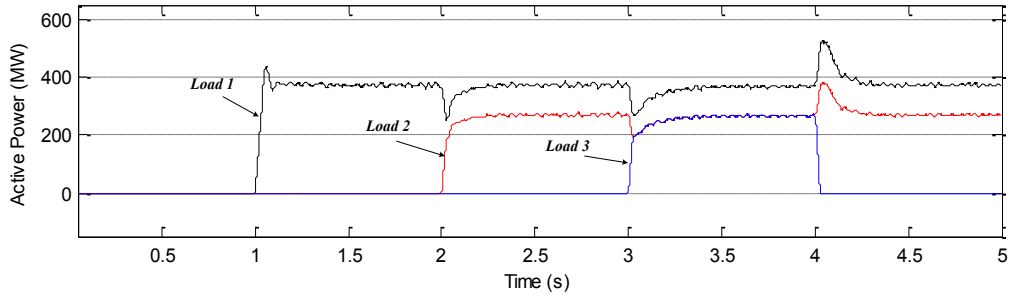
Active Power (MW)
600
400
200
0
Load 1
Load 2
Load 3
0.5
1
1.5
2
2.5
3
3.5
4
4.5
5
Time (s)

(g)

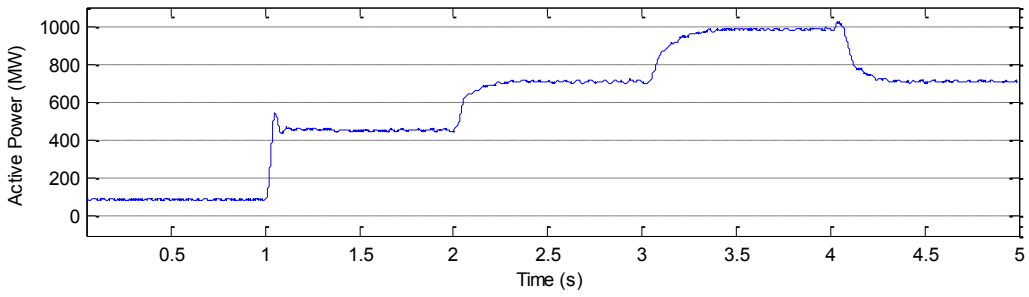
Active Power (MW)
1000
800
600
400
200
0
0.5
1
1.5
2
2.5
3
3.5
4
4.5
5
Time (s)

(h)

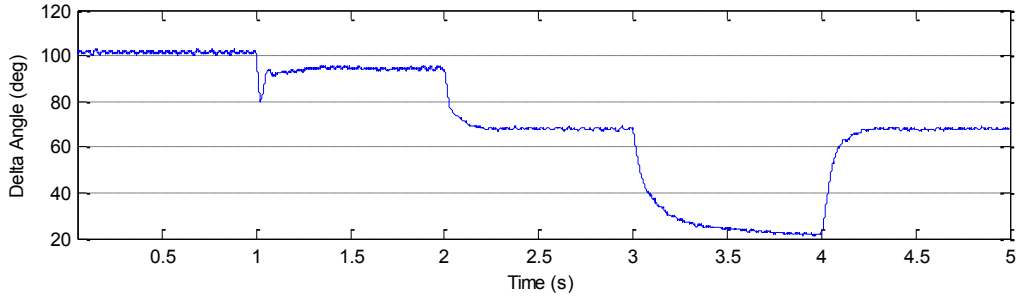
Delta Angle (deg)
120
100
80
60
40
20
0.5
1
1.5
2
2.5
3
3.5
4
4.5
5
Time (s)

(i)

Figure 5-15 System responses of load switching for black start. (a) DC current; (b) DC voltage; (c) AC voltage; (d) Rectifier firing angle; (e) Upper bridge extinction angle; (f) Capacitor voltage; (g) Load active powers; (h) DC power; (i) Phase displacement angle.

5.5 Summary

In this chapter the black start of the proposed hybrid HVDC system is investigated. It has been found through detailed steady-state analysis in section 5.3.2 that for successful initial commutations the inverter AC system has to be capacitive at fundamental frequency (the injected AC current has to lead the AC voltage by a sufficient amount). This requires the filter banks to be in service before the inverter station is deblocked. Considering the communication delays, the inverter AC voltage controller is designed to be at inverter side by controlling the phase displacement angle between the 6-pulse bridges. Although with this control strategy the upper 6-pulse bridge can easily reach the operation zone in which its extinction angle is very small, commutation failure is eliminated by the additional commutation voltages from inserted capacitors. Based on the detailed analysis, a black start sequence is proposed for the hybrid HVDC system and simulation results for both no load start and load pickup cases are presented to demonstrate the system and controller performances.

CHAPTER 6 Conclusions and Future Works

6.1 Conclusions

Because of the depletion of fossil fuels and concerns about increasing greenhouse gas emissions from the traditional electricity generations, more and more countries around the world have shifted to renewable energy based electricity generations. Renewable energies have the advantages of much less environmental harms, near zero greenhouse gas emissions and are mostly sustainable. Unfortunately they are mostly located at geographically remote areas and far from the load centres. For example, the hydro powers are normally located at remote inland areas and offshore wind powers are located off in the sea. This leads to the necessity of long distance bulk power transmissions for renewable integration, and HVDC technologies are the best candidates for this application in terms of total investment cost, power loss levels and power control capability. Although the recent development in VSC technology has made it better suited for offshore windfarm integration and realization of DC grid, but the traditional LCC HVDC is still the best choice for long distance bulk power transmission due to its higher efficiencies. Also the power handling capability of thyristor technology is much higher than the IGBTs. So it can be expected that with the increase of renewable energy integrations, LCC is going to play an even more important role in the future power systems. However there are several major disadvantages associated with LCC ever since it was first developed. They results in higher investment cost and limited the further application of this technology.

First and the most important problem is commutation failure. It is the most fundamental problem of LCC HVDC system and affects various aspects of system operations. It leads to a

DC short circuit and overheating of the valves. In order to achieve a complete elimination of commutation failures, this thesis proposed a new hybrid HVDC system based on the traditional LCC HVDC technology. With the dynamic series insertion of charged capacitors, the required commutation voltage during fault conditions can be provided by the capacitor voltages. With a sufficient commutation voltage, commutation failure can be eliminated. So the resulted insertion strategy is to insert the capacitors during commutation overlap period. In order to maximize the usage of each capacitor and limit the number of semiconductor switches, the capacitors are designed to be inserted at the secondary side of inverter transformers. In this way only one capacitor module is needed for each phase to handle the commutations associated with two valve groups of that phase.

The success of commutation failure elimination largely depends on the selected capacitor voltage levels. To facilitate the capacitor voltage level selection, mathematical formulations of the commutation period of the proposed hybrid HVDDC system are carried out. The minimum capacitor voltage level required for complete commutation failure immunity under zero impedance single-phase fault and zero impedance three-phase fault is used to calculate the capacitor voltage level. In addition, the maximum overlap angle and peak DC current is considered in the derivations. The effectiveness of the proposed method is verified by simulation results from RTDS.

With dynamic capacitor insertions, it is critical to keep all capacitor voltages balanced. According to the detailed analysis of system operation, it has been found that because of the position of capacitor modules, the direction of currents flowing through it changes periodically as the valve in conduction alters. So the capacitor voltages over one cycle should be partially balanced thanks to the conduction sequence of valves. Through mathematical calculations, it was found that for each commutation, the capacitor voltage decrease in the

incoming phase is always larger than the capacitor voltage increase in the outgoing phase. This indicates a net capacitor voltage reduction over each commutation cycle so additional switching actions are needed to keep the capacitor voltage at reference value. For the simplicity of implementation, a continuous PI controller is designed to keep the capacitor voltages balanced. The designed control strategy is to insert the outgoing capacitor into the circuit a short time before the commutation starts and then bypass it when commutation completes. The capacitors are designed to be inserted when one of the upper three valve groups is conducting to limit the number of switching actions.

The second problem associated is the significant reactive power consumption of converter terminals. It not only results in considerable investment cost but also affect the stability of the connected AC system. In this thesis, the proposed hybrid HVDC system is further exploited for the reactive power control at inverter side. Detailed analysis has been carried out to find the relationship between the reactive power consumption and other system variables. It has been proved that the system is indeed capable of achieving reactive power control. With appropriate choice of capacitor voltage level, the reactive power consumption can be effectively controlled through modification of firing angles. Moreover, the inverter system is even able to temporarily export reactive power to the AC system to improve the system stability if needed.

The inverter reactive power controller was then designed based on the mathematical calculations. It can be used to achieve reactive power tracking by adjusting inverter firing angles. Particularly, with a zero reactive power reference, the constant unity power factor at inverter side is achieved. This means that the reactive power consumption can be limited to zero regardless of the active power transfer level. This can significantly help the system recovery from fault. In addition, the inverter AC voltage controller is designed based on the

reactive power controllability of the proposed system. It aims to control the inverter AC voltage at reference value under different load conditions. Various simulation results have been presented which demonstrate the performance of the proposed controllers. At the same time zero impedance single-phase fault and zero impedance three-phase fault are also applied and immunity to commutation failure is preserved.

In order to use the described reactive power and AC voltage controller, the traditional measurement of extinction angle is no longer effective. It is because a zero extinction angle will be the output value when commutation extends beyond the voltage zero crossing point. However, for the proposed controller, a negative extinction angle should be used. So a new extinction angle measurement method was proposed which is able to calculate negative extinction angles for normal operation of the designed controllers. Simulation results have been used to show the effectiveness of this method.

The third problem is the black start of LCC HVDC. It is generally accepted that LCC is not able to energize a dead network without external AC commutation voltages, while VSC is able to achieve black start with its voltage generating capability. However, in this thesis with the proposed hybrid HVDC system, black start is possible. Firstly through the analysis it has been found that PLL can no longer be used to synchronize the firing pulses because there is not reference AC voltages from the AC side that can be used for synchronization. So the only way to control the AC system frequency is to fire the thyristors according an external independent 50/60 Hz clock.

Another important aspect in black start case is the AC voltage control. In order to avoid the dependence on communication system and to achieve a reliable and fast AC voltage control, the inverter side is used to control the AC voltage. The proposed method controls the inverter AC voltage by controlling the phase displacement angle between the injected AC currents of

the two 6-pulse bridges for a 12-pulse system. It has been recognized that one of the bridges tend to work under very low extinction angle to achieve the control objective and this angle can become even smaller as the loads are picked up. For traditional LCC HVDC systems this is obviously not acceptable, since successive commutation failures can happen. However with the proposed hybrid system this problem can be solved by the inserted capacitors. In this way the minimum phase displacement angle can be controlled at 0^0 and maximum at 170^0. 180^0 phase displacement cannot be achieved because the thyristors that is working under rectifier mode needs at least 5^0 to turn on. Various simulation results have been presented including no load start and load switching, which demonstrated that the AC voltage can indeed be well controlled by the proposed AC voltage controller.

6.2 Future Work

The following is a list of the possible future works:

- In this thesis the capacitor modules being used are of full-bridge topology. As the development of MMC technology, more and more variations of sub-module topology are proposed in the literature. They usually have their special features such as lower losses, less number of semi-conductor devices or higher output voltages. So it would be interesting to see what kinds of new functionalities in terms of control and protection can be introduced by utilizing those topologies in the proposed hybrid HVDC system.
- The proposed capacitor insertion strategy for the hybrid system inserts the capacitors primarily during commutation processes with only a very short time of insertion before commutation for charging purpose. This makes those capacitors only able to provide the commutation voltage with no DC voltage support. Therefore the

commutations can be successful but the DC fault current is large. So one of the possibilities is to investigate inserting capacitors during the non-commutation period to participate in the formation of average DC voltage. Hence the DC fault current can be effectively limited under inverter side faults. This can reduce the required capacitor voltage level for commutation failure elimination and in turn reduce the cost.

- For the reactive power control, only one control variable can be used which is the inverter side firing angle. So when the reactive power is controlled, the active power level also changes accordingly. This may not be desirable in some cases and independent active and reactive power control like VSC would be preferred. One of the options is to introduce additional capacitor switching when only two thyristors are conducting so that the DC voltage level can be controlled by the capacitor voltage level. As a result, one additional control variable which is the DC voltage level can be utilized to control the DC voltage and the reactive power. This feature can make independent active and reactive power control possible for the hybrid HVDC system by controlling the firing angle and capacitor reference voltages.
- As more and more HVDC systems are built, the possibility of several HVDC systems connecting to the same load area is high. This forms the so called multi-infeed HVDC system. With the advantages of the proposed hybrid HVDC system, it would be interesting to investigate the multi-infeed case with the proposed hybrid system. Mathematical analysis and simulation results can be used to study the dynamic and steady state impact of the proposed system on the connected HVDC and AC systems. Also coordination controls between the multi-infeed HVDC systems can be investigated to improve the system dynamic response.

APPENDIX A

A.1 LCC-HVDC System Configuration in PowerFactory

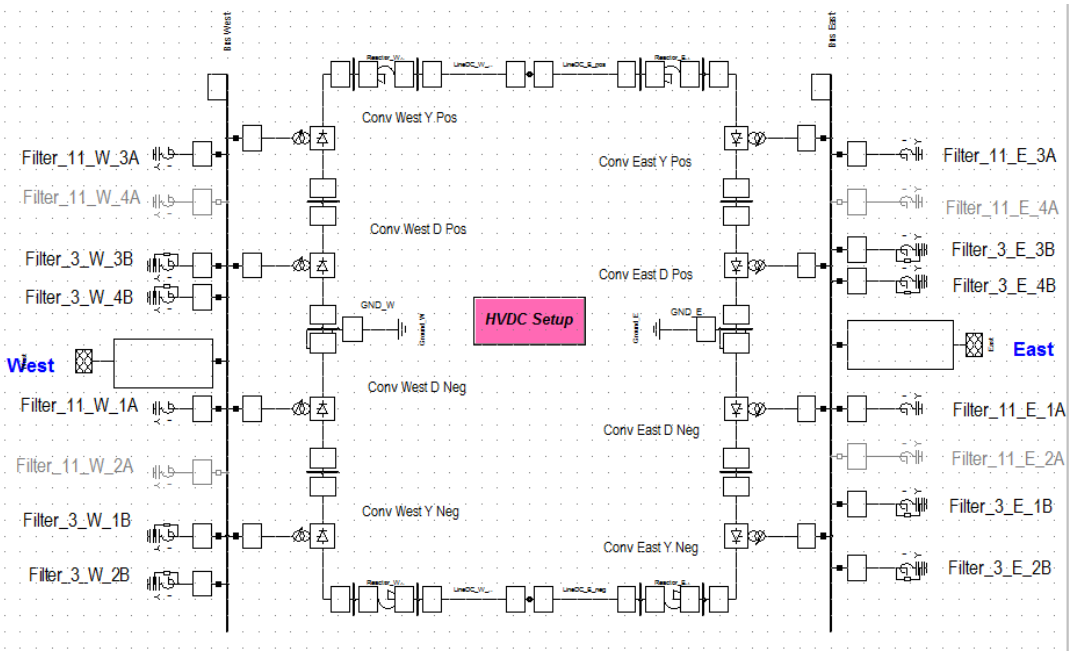

Figure A-1 LCC HVDC system in PowerFactory

A.2 DPL Command Object

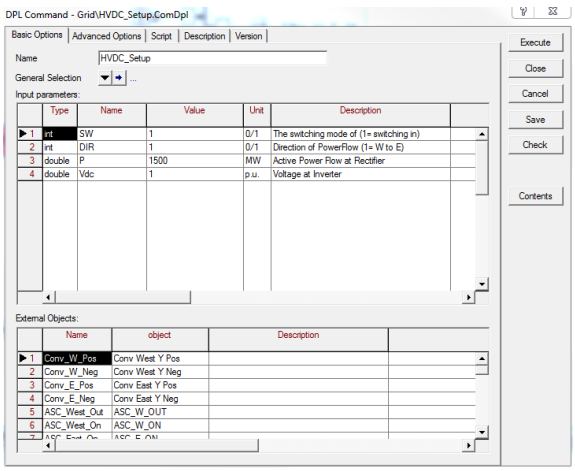

Figure A-2 DPL command object for HVDC setup

A.3 DSL Model for ASC

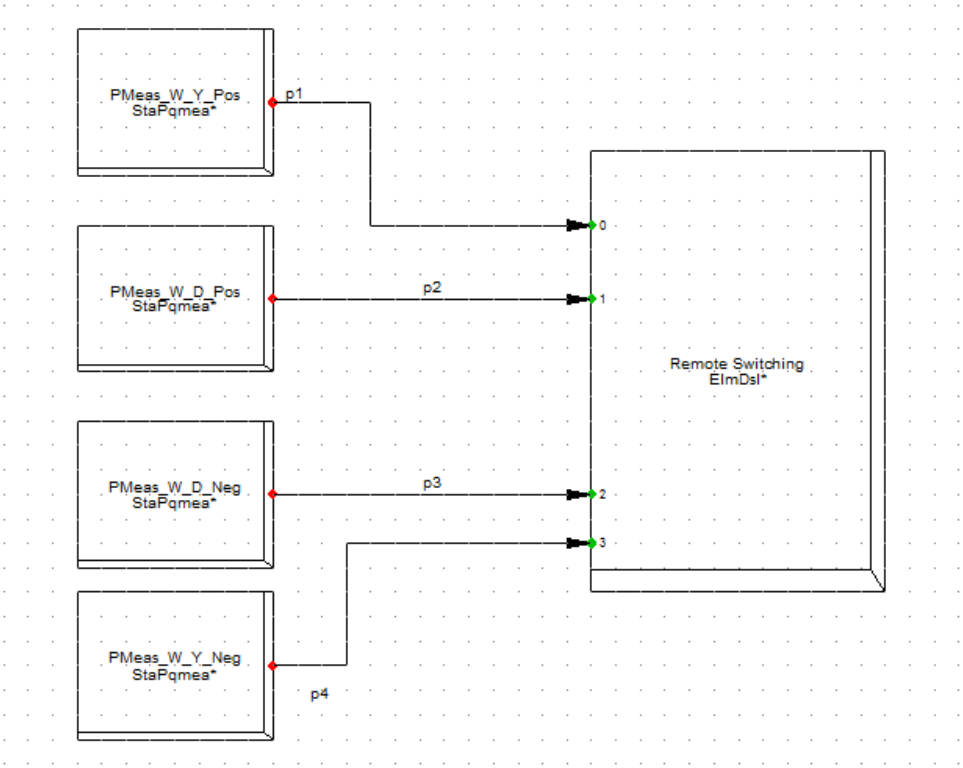

Figure A-3 DSL model for automatic switching control

A.4 OLTC Operating Flow Chart

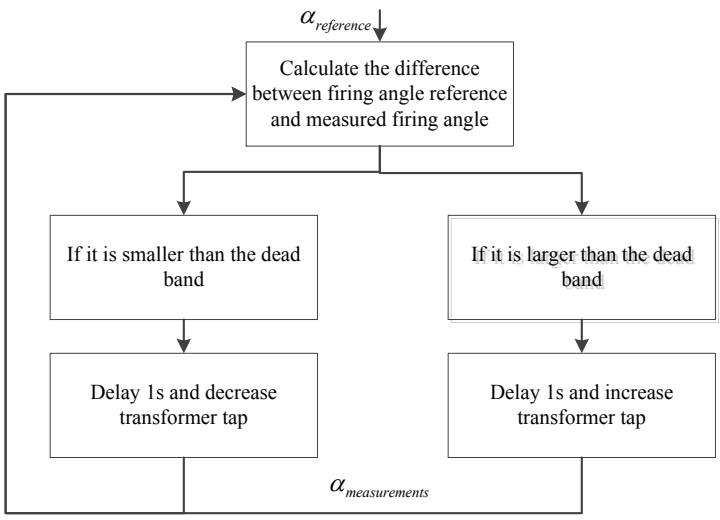

Figure A-4 Flow chart for OLTC operating method

APPENDIX B

B.1 Induction Machine Technical Data for Chapter 4

Table B-1 Induction Machine Technical Data

Rated stator voltage (L-L RMS) (kV)	**Turns ratio (rotor over stator)**	**Rated MVA**	**Stator resistance (p.u.)**	**Stator leakage reactance (p.u.)**
66	1.0	100	0.0125	0.0870
First cage rotor resistance (p.u.)	**First cage rotor leakage reactance (p.u.)**	**Second cage rotor resistance (p.u.)**	**Second cage rotor leakage reactance (p.u.)**	**Rotor mutual leakage reactance (p.u.)**
0.15	0.0658	0.05	0.0739	0
Neutral resistance (p.u.)	**Neutral reactance (p.u.)**	**Unsaturated magnetizing reactance (p.u.)**	**Rated frequency (Hz)**	
50000	0	4	50	

LIST OF PUBLICATIONS & OUTCOMES

1. X. P. Zhang, Y. Xue, GB Patent "Hybrid HVDC System," applied to the Intellectual Property Office, UK, Patent Application Number: GB1507669.8, 2015.05
2. Ying Xue, Dechao Kong, Ziming Song, Vandad Hamidi, Xiao-Ping Zhang, "Development of an advanced LCC-HVDC model for transmission system," *11th IET Int. Conf. AC DC Power Transmission, 2015*.
3. Mingyu Ou, Ying Xue, Xiao-Ping Zhang, "Iterative DC optimal power flow considering transmission network loss", *Electric Power Components and Systems.(under revision)*
4. Ying Xue, Xiao-Ping Zhang, Conghuan Yang, "Elimination of commutation failures of LCC HVDC system with controllable capacitors," *IEEE Transactions on Power Systems*. *(accepted for publication)*
5. Ying Xue, Xiao-Ping Zhang, "Reactive Power and Voltage Control of Hybrid HVDC System," *submitted to IEEE Transactions on Power Delivery*.
6. Ying Xue, Xiao-Ping Zhang, Conghuan Yang, "Investigation of commutation failure elimination by a novel hybrid HVDC system", *Power Systems Computation Conference, 2016*. *(Abstract accepted)*

REFERENCES

[1] M. Hook, J. Li, K. Johansson, and S. Snowden, "Growth Rates of Gloabal Energy Systems and Future Outlooks," *Natural Resources Research,* vol. 21, pp. 23-41, 2012.

[2] M. A. Maehlum. Fossil Fuels Pros and Cons [Online]. Available: http://energyinformative.org/fossil-fuels-pros-and-cons/ accessed on 11th Dec, 2015

[3] B. Schmitz. New Hydrogen-Powered Car Was Designed in the Cloud [Online]. Available: http://www.3dcadworld.com/new-hydrogen-powered-car-designed-cloud/ accessed on 11th Dec, 2015

[4] L. C. Ltd, "Rising Gas Prices for Home Heating in the UK," 2015.

[5] P. V. Nayagam. The End of Fossil Fuels up to 2088 [Online]. Available: http://vgaengine.blogspot.co.uk/2013/11/the-end-of-fossil-fuels-up-to-2088.html accessed on 11th Dec, 2015

[6] B. Harris. How Climate Change Threatens Food Security [Online]. Available: http://climateandcapitalism.com/2009/01/22/how-climate-change-threatens-food-security/ accessed on 11th Dec, 2015

[7] U. S. E. P. A. (EPA). Sources of Greenhouse Gas Emissions [Online]. Available: http://www.epa.gov/climatechange/ghgemissions/sources/electricity.html accessed on 11th Dec, 2015

[8] ENSG, "Our Electricity Transmission Network: A Vision For 2020," 2012.

[9] L. Zhen-ya, S. Yin-biao, Z. Wen-liang, and Z. Yun-zhou, "Study on Voltage Class Series for HVDC Transmission System," *Proceeding of the CSEE, 2008,* pp. 1-8.

[10] C. Spataru and M. Barrett, "The smart supper- European grid: Balancing demand and supply," in *3rd IEEE PES International Conference and Exhibition on Innovative Smart Grid Technologies (ISGT Europe)*, 2012, pp. 1-6.

[11] Andre and Canelhas. (2010). *High Voltage Direct Current (HVDC Technology)*. Available: http://www.alstom.com/Global/Group/Resources/Documents/Investors%20document/Investor%20events/Analysts%20presentation/Analyst%20Day%20-%20HVDC%20technology.pdf accessed on 11th Dec, 2015

[12] W. Peng, L. Goel, L. Xiong, and C. Fook Hoong, "Harmonizing AC and DC: A Hybrid AC/DC Future Grid Solution," *IEEE Power and Energy Magazine* vol. 11, pp. 76-83, 2013.

[13] ABB. Special Report-60 Years of HVDC [Online]. Available: https://library.e.abb.com/public/aff841e25d8986b5c1257d380045703f/140818%20ABB%20SR%2060%20years%20of%20HVDC_72dpi.pdf

[14] L. Zhang, "Modeling and Control of VSC-HVDC Links Connected to Weak AC Systems," PhD thesis, Royal Institute of Technology, Stockholm, 2010.

[15] R. Adapa, "High-Wire Act: HVdc Technology: The State of the Art," *IEEE Power and Energy Magazine,* vol. 10, pp. 18-29, 2012.

[16] V. F. Lescale, "Modern HVDC: state of the art and development trends," in *International Conference on Power System Technology*, 1998, pp. 446-450 vol.1.

[17] D. Jovcic, N. Pahalawaththa, and M. Zavahir, "Analytical modelling of HVDC-HVAC systems," *IEEE Transactions on Power Delivery,* vol. 14, pp. 506-511, 1999.

[18] C. Osauskas and A. Wood, "Small-signal dynamic modeling of HVDC systems," *IEEE Transactions on Power Delivery,* vol. 18, pp. 220-225, 2003.

[19] G. E. Gardner and D. Fairmaner, "Alternative convertor for h.v. d.c. transmission. Three single-phase bridges connected in series," *Proceedings of the Institution of Electrical Engineers,* vol. 115, pp. 1289-1296, 1968.

[20] T. Halder, "Comparative study of HVDC and HVAC for a bulk power transmission," in *International Conference on Power, Energy and Control (ICPEC)*, 2013, pp. 139-144.

[21] P. S. Maruvada, "800-kV HVDC transmission systems," in *IEEE/PES Transmission and Distribution Conference and Exposition T&D*, 2008, pp. 1-2.

[22] U. Astrom, B. Westman, V. Lescale, and G. Asplund, "Power transmission with HVDC at voltages above 600 kV," in *IEEE Power Engineering Society Inaugural Conference and Exposition in Africa*, 2005, pp. 44-50.

[23] W. Hermansson, B. Breitholtz, L. C. G. Zdansky, K. Andersson, L. F. Heijkenskjold, R. Revsater, and D. Sigurd, "A MOS-controlled high-voltage thyristor with low switching losses," *IEEE Transactions on Electron Devices,* vol. 45, pp. 957-965, 1998.

[24] H. Akagi, "Utility applications of power electronics in Japan," in *23rd International Conference on Industrial Electronics, Control and Instrumentation*, 1997, pp. 409-416 vol.2.

[25] T. Hasegawa, K. Yamaji, H. Irokawa, H. Shirahama, C. Tanaka, and K. Akabane, "Development of a thyristor valve for next generation 500 kV HVDC transmission systems," *IEEE Transactions on Power Delivery,* vol. 11, pp. 1783-1788, 1996.

[26] Ofgem, "Calculating Target Availability Figures for HVDC Interconnectors," 2012.

[27] F. M. Kasangala and G. Atkinson-Hope, "Electrical energy losses and costs evaluation of HVDC and UHVDC transmission lines," in *Proceedings of the 10th Industrial and Commercial Use of Energy Conference (ICUE)* 2013, pp. 1-7.

[28] W. Shanshan, T. Guangfu, and H. Zhiyuan, "Comprehensive evaluation of VSC-HVDC transmission based on improved analytic hierarchy process," in *Third International Conference on Electric Utility Deregulation and Restructuring and Power Technologies*, 2008, pp. 2207-2211.

[29] K. Eriksson, "Operational experience of HVDC Light," in *Seventh International Conference on AC-DC Power Transmission*, 2001, pp. 205-210.

[30] N. Flourentzou, V. G. Agelidis, and G. D. Demetriades, "VSC-Based HVDC Power Transmission Systems: An Overview," *IEEE Transactions on Power Electronics,* vol. 24, pp. 592-602, 2009.

[31] U. Axelsson, A. Holm, C. Liljegren, M. Aberg, K. Eriksson, and O. Tollerz, "The Gotland HVDC Light project-experiences from trial and commercial operation," in *16th International Conference and Exhibition on Electricity Distribution Part 1: Contributions. CIRED*, 2001, p. 5 pp. vol.1.

[32] D. Guanjun, T. Guangfu, H. Zhiyuan, and D. Ming, "New technologies of voltage source converter (VSC) for HVDC transmission system based on VSC," in *IEEE Power and Energy Society General Meeting - Conversion and Delivery of Electrical Energy in the 21st Century*, 2008, pp. 1-8.

[33] B. R. Andersen, L. Xu, P. J. Horton, and P. Cartwright, "Topologies for VSC transmission," *Power Engineering Journal,* vol. 16, pp. 142-150, 2002.

[34] F. Schettler, H. Huang, and N. Christl, "HVDC transmission systems using voltage sourced converters design and applications," in *IEEE Power Engineering Society Summer Meeting*, 2000, pp. 715-720 vol. 2.

[35] Z. Xiao-Ping, "Multiterminal voltage-sourced converter-based HVDC models for power flow analysis," *IEEE Transactions on Power Systems,* vol. 19, pp. 1877-1884, 2004.

[36] G. Asplund, "Application of HVDC Light to power system enhancement," in *IEEE Power Engineering Society Winter Meeting*, 2000, pp. 2498-2503 vol.4.

[37] A. Lesnicar and R. Marquardt, "An innovative modular multilevel converter topology suitable for a wide power range," in *IEEE Bologna Power Tech Conference Proceedings*, 2003, p. 6 pp. Vol.3.

[38] M. D. Manjrekar, P. K. Steimer, and T. A. Lipo, "Hybrid multilevel power conversion system: a competitive solution for high-power applications," *IEEE Transactions on Industry Applications,* vol. 36, pp. 834-841, 2000.

[39] M. Hagiwara and H. Akagi, "Control and Experiment of Pulsewidth-Modulated Modular Multilevel Converters," *IEEE Transactions on Power Electronics,* vol. 24, pp. 1737-1746, 2009.

[40] M. Saeedifard and R. Iravani, "Dynamic Performance of a Modular Multilevel Back-to-Back HVDC System," *IEEE Transactions on Power Delivery,* vol. 25, pp. 2903-2912, 2010.

[41] S. Allebrod, R. Hamerski, and R. Marquardt, "New transformerless, scalable Modular Multilevel Converters for HVDC-transmission," in *IEEE Power Electronics Specialists Conference*, 2008, pp. 174-179.

[42] T. Qingrui, X. Zheng, and X. Lie, "Reduced Switching-Frequency Modulation and Circulating Current Suppression for Modular Multilevel Converters," *IEEE Transactions on Power Delivery,* vol. 26, pp. 2009-2017, 2011.

[43] M. Hagiwara and H. Akagi, "PWM control and experiment of modular multilevel converters," in *IEEE Power Electronics Specialists Conference*, 2008, pp. 154-161.

[44] P. Fang Zheng, "A generalized multilevel inverter topology with self voltage balancing," *IEEE Transactions on Industry Applications,* vol. 37, pp. 611-618, 2001.

[45] M. Glinka and R. Marquardt, "A new AC/AC multilevel converter family," *IEEE Transactions on Industrial Electronics,* vol. 52, pp. 662-669, 2005.

[46] O. Kaijian, R. Hong, C. Zexiang, G. Haiping, L. Xuehua, G. Lin, T. Maguire, B. Warkentin, and C. Yuan, "MMC-HVDC Simulation and Testing Based on Real-Time Digital Simulator and Physical Control System," *IEEE Journal of Emerging and Selected Topics in Power Electronics,* vol. 2, pp. 1109-1116, 2014.

[47] P. S. Jones and C. C. Davidson, "Calculation of power losses for MMC-based VSC HVDC stations," in *15th European Conference on Power Electronics and Applications (EPE)*, 2013, pp. 1-10.

[48] J. Li, X. Zhao, Q. Song, H. Rao, S. Xu, and M. Chen, "Loss calculation method and loss characteristic analysis of MMC based VSC-HVDC system," in *IEEE International Symposium on Industrial Electronics (ISIE)*, 2013, pp. 1-6.

[49] U. N. Gnanarathna, S. K. Chaudhary, A. M. Gole, and R. Teodorescu, "Modular multi-level converter based HVDC system for grid connection of offshore wind power plant," in *9th IET International Conference on AC and DC Power Transmission*, 2010, pp. 1-5.

[50] I. Atkinson, M. Smith, P. Damgaard, M. Haeusler, M. Kuhn, P. Lips, and G. Balog, "Innovative technology in the Moyle Interconnector," in *Seventh International Conference on (Conf. Publ. No. 485) AC-DC Power Transmission*, 2001, pp. 66-71.

[51] J. Egan, P. O'Rourke, R. Sellick, P. Tomlinson, B. Johnson, and S. Svensson, "Overview of the 500MW EirGrid East-West Interconnector, considering System Design and execution-phase issues," in *48th International Universities' Power Engineering Conference (UPEC)*, 2013, pp. 1-6.

[52] T. Machida and Y. Yoshida, "A Method to Detect the Deionization Margin Angle and to Prevent the Commutation Failure of an Inverter for DC Transmission," *IEEE Transactions on Power Apparatus and Systems,* vol. PAS-86, pp. 259-262, 1967.

[53] N. G. Hingorani, R. H. Kitchin, and J. L. Hay, "Dynamic Simulation of HVDC Power Transmission Systems on Digital Computers - Generalized Mesh Analysis Approach," *IEEE Transactions on Power Apparatus and Systems,* vol. PAS-87, pp. 989-996, 1968.

[54] J. Reeve and S. C. Kapoor, "Dynamic Fault Analysis for HVDC Systems with ac System Representation," *IEEE Transactions on Power Apparatus and Systems,* vol. PAS-91, pp. 688-696, 1972.

[55] E. Rahimi, A. M. Gole, J. B. Davies, I. T. Fernando, and K. L. Kent, "Commutation Failure Analysis in Multi-Infeed HVDC Systems," *IEEE Transactions on Power Delivery,* vol. 26, pp. 378-384, 2011.

[56] E.W.Kimbark, *Direct Current Transmission,* vol. 1: Wiley-Blackwell, 1971.

[57] P. Li, X. Wu, Y. Zhang, X. Jin, C. Lu, and J. He, "Analysis of Modulation Controllers of Multi-infeed HVDC for CSG in 2008," in *International Conference on Power System Technology*, 2006, pp. 1-7.

[58] O. Kaijian, "Study on the Dynamic Performance of AC & DC Hybrid System in China Southern Power Grid," in *IEEE Power Engineering Society Conference and Exposition in Africa*, 2007, pp. 1-4.

[59] X. Zhou, "Simultaneous commutation failures and forced blocking of multi-in-feed HVDC in East China Power Grid," presented at the CIGRE Large Disturbances Workshop, Paris, 2014.

[60] C. V. Thio, J. B. Davies, and K. L. Kent, "Commutation failures in HVDC transmission systems," *IEEE Transactions on Power Delivery,* vol. 11, pp. 946-957, 1996.

[61] CIGRE Technical Brochure, "Commutation failures, causes and consequences," 1995.

[62] P. Kundur, *Power System Stability and Control*. New York: McGraw-Hill, 1994.

[63] M. Bahrman and P. E. Bjorklund, "The New Black Start: System Restoration with Help from Voltage-Sourced Converters," *IEEE Power and Energy Magazine,* vol. 12, pp. 44-53, 2014.

[64] J.-H. Ying, H. Duchen, M. Karlsson, L. Ronstrom, and B. Abrahamsson, "HVDC with voltage source converters - a powerful standby black start facility," in *IEEE/PESTransmission and Distribution Conference and Exposition*, 2008, pp. 1-9.

[65] M. Mohaddes, "Supplying Dead Load with a Conventional HVDC System," in *Proceedings of CIGRE Colloquium on Role of HVDC, FACTS and Emerging Technologies in Evolving Power Systems*, Bangalore, India, 2005

[66] H. P. Lips, "Aspects of Multiple Infeed of HVDC Inverter Stations into a Common A.C. System," *IEEE Transactions on Power Apparatus and Systems,* vol. PAS-92, pp. 775-779, 1973.

[67] S. Lefebvre, M. Saad, and R. Hurteau, "Adaptive Control for HVdc Power Transmission Systems," *IEEE Transactions on Power Apparatus and Systems,* vol. PAS-104, pp. 2329-2335, 1985.

[68] P. C. S. Krishnayya, R. J. Piwko, T. L. Weaver, M. P. Bahrman, and A. E. Hammad, "DC Transmission Terminating at Low Short Cirucit Ratio Locations," *IEEE Transactions on Power Delivery,* vol. 1, pp. 308-318, 1986.

[69] A. Gavrilovic, "AC/DC system strength as indicated by short circuit ratios," in *International Conference on AC and DC Power Transmission*, 1991, pp. 27-32.

[70] R. S. Thallam, "Review of the design and performance features of HVDC systems connected to low short circuit ratio AC systems," *IEEE Transactions on Power Delivery,* vol. 7, pp. 2065-2073, 1992.

[71] P. C. S. Krishnayya, S. Lefebvre, V. K. Sood, and N. J. Balu, "Simulator Study of Multiterminal HVDC System With Small Parallel Tap and Weak AC Systems," *IEEE Transactions on Power Apparatus and Systems,* vol. PAS-103, pp. 3125-3132, 1984.

[72] R. Bunch and D. N. Kosterev, "Design and implementation of AC voltage dependent current order limiter at Pacific HVDC Intertie," *IEEE Transactions on Power Delivery,* vol. 15, pp. 293-299, 2000.

[73] Y.-X. Ni and A. A. Fouad, "A Simplified Two-Terminal HVDC Model and Its Use in Direct Transient Stability Assessment," *IEEE Transactions on Power Systems,* vol. 2, pp. 1006-1012, 1987.

[74] K. R. Padiyar, Sachchidanand, A. G. Kothari, S. Bhattacharyya, and A. Srivastava, "Study of HVDC controls through efficient dynamic digital simulation of converters," *IEEE Transactions on Power Delivery,* vol. 4, pp. 2171-2178, 1989.

[75] J. Bauman and M. Kazerani, "Commutation Failure Reduction in HVDC Systems Using Adaptive Fuzzy Logic Controller," *IEEE Transactions on Power Systems,* vol. 22, pp. 1995-2002, 2007.

[76] A. Hansen and H. Havemann, "Decreasing the commutation failure frequency in HVDC transmission systems," *IEEE Transactions on Power Delivery,* vol. 15, pp. 1022-1026, 2000.

[77] D. Jovcic, "Thyristor-based HVDC with forced commutation," *IEEE Transactions on Power Delivery,* vol. 22, pp. 557-564, 2007.

[78] G. M. Kristmundsson and D. P. Carroll, "The effect of AC system frequency spectrum on commutation failure in HVDC inverters," *IEEE Transactions on Power Delivery,* vol. 5, pp. 1121-1128, 1990.

[79] Y. Z. Sun, P. Ling, M. Feng, G. J. Li, and P. F. Lv, "Design a Fuzzy Controller to Minimize the Effect of HVDC Commutation Failure on Power System," *IEEE Transactions on Power Systems,* vol. 23, pp. 100-107, 2008.

[80] S. Tamai, H. Naitoh, F. Ishiguro, M. Sato, K. Yamaji, and N. Honjo, "Fast and predictive HVDC extinction angle control," *IEEE Transactions on Power Systems,* vol. 12, pp. 1268-1275, 1997.

[81] W. Zhinong, Y. Yang, L. Xiao, W. Huawei, S. Guoqiang, and S. Yonghui, "Direct-Current Predictive Control Strategy for Inhibiting Commutation Failure in HVDC Converter," *IEEE Transactions on Power Systems,* vol. 29, pp. 2409-2417, 2014.

[82] C. Lei, P. Hao, D. Changhong, Z. Feng, L. Zhe, and G. Fang, "Study on the Application of a Flux-Coupling-Type Superconducting Fault Current Limiter for Decreasing HVdc Commutation Failure," *Canadian Journal of Electrical and Computer Engineering,,* vol. 38, pp. 10-19, 2015.

[83] J. He, Y. Tang, J. Zhang, Q. Guo, J. Yi, and G. Bu, "Fast Calculation of Power Oscillation Peak Value on AC Tie-Line After HVDC Commutation Failure," *IEEE Transactions on Power Systems,* vol. 30, pp. 2194-2195, 2015.

[84] H. Shao-feng, S. Hong-ming, F. Bin, and L. Ou, "Effect of commutation failure on the distance protection and the countermeasures," *IET Generation, Transmission & Distribution,* vol. 9, pp. 838-844, 2015.

[85] G. Chunyi, L. Yuchao, Z. Chengyong, W. Xiaoguang, and X. Weihua, "Power Component Fault Detection Method and Improved Current Order Limiter Control for Commutation Failure Mitigation in HVDC," *IEEE Transactions on Power Delivery,* vol. 30, pp. 1585-1593, 2015.

[86] J. Hyunsik and C. Hanju, "ITER VS converter control for circulation current and commutation failure," in *2015 IEEE Applied Power Electronics Conference and Exposition (APEC)*, 2015, pp. 3212-3216.

[87] Z. Lidong and L. Dofnas, "A novel method to mitigate commutation failures in HVDC systems," in *International Conference on Power System Technology*, 2002, pp. 51-56 vol.1.

[88] D. Jovcic, "Thyristor-based HVDC with forced commutation," *IEEE Transactions on Power Delivery,* vol. 22, pp. 557-564, 2007.

[89] G. Balzer and H. Muller, "Capacitor commutated converters for high power HVDC transmission," in *Seventh International Conference on (Conf. Publ. No. 485) AC-DC Power Transmission*, 2001, pp. 60-65.

[90] A. M. Gole and M. Meisingset, "Capacitor commutated converters for long-cable HVDC transmission," *Power Engineering Journal,* vol. 16, pp. 129-134, 2002.

[91] M. Meisingset and A. M. Gole, "A comparison of conventional and capacitor commutated converters based on steady-state and dynamic considerations," in *Seventh International Conference on (Conf. Publ. No. 485) AC-DC Power Transmission*, 2001, pp. 49-54.

[92] M. Meisingset and A. M. Gole, "Control of capacitor commutated converters in long cable HVDC-transmission," in *IEEE Power Engineering Society Winter Meeting*, 2001, pp. 962-967 vol.2.

[93] N. Ottosson and L. Kjellin, "Modular back-to-back HVDC, with capacitor commutated converters (CCC)," in *Seventh International Conference on (Conf. Publ. No. 485) AC-DC Power Transmission*, 2001, pp. 55-59.

[94] K. Sadek, M. Pereira, D. P. Brandt, A. M. Gole, and A. Daneshpooy, "Capacitor commutated converter circuit configurations for DC transmission," *IEEE Transactions on Power Delivery,* vol. 13, pp. 1257-1264, 1998.

[95] J. Reeve, J. A. Baron, and G. A. Hanley, "A technical assessment of artificial commutation of HVDC converters with series capacitors," *IEEE Transactions on Power Apparatus and Systems,* vol. PAS-87, pp. 1830-1840, 1968.

[96] T. Funaki and K. Matsuura, "Predictive firing angle calculation for constant effective margin angle control of CCC-HVDC," *IEEE Transactions on Power Delivery,* vol. 15, pp. 1087-1093, 2000.

[97] Y. Kazachkov, "Fundamentals of a series capacitor commutated HVDC terminal," *IEEE Transactions on Power Delivery,* vol. 13, pp. 1157-1161, 1998.

[98] D. F. Menzies, J. Graham, and F. U. Ribeiro, ""Garabi" the Argentina-Brazil 1000 MW Interconnection; Commissioning and Early Operating Experience," presented at the ERLAC Conference, Foz do Iguaçu, Brazil, May/June, 2001.

[99] J. Graham, D. Menzies, G. Biledt, A. R. Carvalho, W. W. Ping, and A. Wey, "Electrical system considerations for the Argentina-Brazil 1000 MW interconnection," presented at the Cigre 2000 conference, Paris, France, 2000.

[100] Z. Xu, *Voltage Source Converter Based High Voltage Direct Current Transmission Systems*. Beijing, China: China Machine Press, 2012.

[101] Z. Zheren, X. Zheng, X. Yinglin, and T. Geng, "DC-Side Harmonic Currents Calculation and DC-Loop Resonance Analysis for an LCC-MMC Hybrid HVDC Transmission System," *IEEE Transactions on Power Delivery,* vol. 30, pp. 642-651, 2015.

[102] X. Zheng, H. Hongyang, T. Geng, and Z. Yuzhi, "Two new techniques to solve the problems with multi-infeed HVDC systems," in *International Conference on Power System Technology (POWERCON)*, 2014, pp. 2075-2082.

[103] M. Jafar and M. Molinas, "A Transformerless Series Reactive/Harmonic Compensator for Line-Commutated HVDC for Grid Integration of Offshore Wind Power," *IEEE Transactions on Industrial Electronics,* vol. 60, pp. 2410-2419, 2013.

[104] L. Gyugyi, C. D. Schauder, and K. K. Sen, "Static synchronous series compensator: a solid-state approach to the series compensation of transmission lines," *IEEE Transactions on Power Delivery,* vol. 12, pp. 406-417, 1997.

[105] B. Singh, R. Saha, A. Chandra, and K. Al-Haddad, "Static synchronous compensators (STATCOM): a review," *IET Power Electronics,* vol. 2, pp. 297-324, 2009.

[106] A. Yazdani, H. Sepahvand, M. L. Crow, and M. Ferdowsi, "Fault Detection and Mitigation in Multilevel Converter STATCOMs," *IEEE Transactions on Industrial Electronics,* vol. 58, pp. 1307-1315, 2011.

[107] S. Wenchao and A. Q. Huang, "Fault-Tolerant Design and Control Strategy for Cascaded H-Bridge Multilevel Converter-Based STATCOM," *IEEE Transactions on Industrial Electronics,* vol. 57, pp. 2700-2708, 2010.

[108] M. N. Slepchenkov, K. Smedley, and W. Jun, "Hexagram-Converter-Based STATCOM for Voltage Support in Fixed-Speed Wind Turbine Generation Systems," *IEEE Transactions on Industrial Electronics,* vol. 58, pp. 1120-1131, 2011.

[109] Y. Xiaoran, Y. Fenyan, F. Xiazhou, and X. Zheng, "Principle and algorithm of reactive power management for LCC-based parallel MTDC transmission system," in *2014 International Conference on Power System Technology (POWERCON)*, 2014, pp. 2265-2271.

[110] H. M. Turanli, R. W. Menzies, and D. A. Woodford, "Feasibility of DC Transmission with Forced Commutation to Remote Loads," *IEEE Power Engineering Review,* vol. PER-4, pp. 37-38, 1984.

[111] O. B. Nayak, A. M. Gole, D. G. Chapman, and J. B. Davies, "Dynamic performance of static and synchronous compensators at an HVDC inverter bus in a very weak AC system," *IEEE Transactions on Power Systems,* vol. 9, pp. 1350-1358, 1994.

[112] Y. Zhuang, R. W. Menzies, O. B. Nayak, and H. M. Turanli, "Dynamic performance of a STATCON at an HVDC inverter feeding a very weak AC system," *IEEE Transactions on Power Delivery,* vol. 11, pp. 958-964, 1996.

[113] B. R. Andersen and X. Lie, "Hybrid HVDC system for power transmission to island networks," *IEEE Transactions on Power Delivery,* vol. 19, pp. 1884-1890, 2004.

[114] M. De Oliveira, M. Poloujadoff, A. Le Du, and P. G. Therond, "Supply of an entirely passive AC system through an HVDC link," *International Journal of Electrical Power & Energy Systems,* vol. 16, pp. 111-116, 1994.

[115] G. Chunyi and Z. Chengyong, "Supply of an Entirely Passive AC Network Through a Double-Infeed HVDC System," *IEEE Transactions on Power Electronics,* vol. 25, pp. 2835-2841, 2010.

[116] M. Andersson, R. Cai, and C. Yang, "Black start of a passive AC network using bipolar LCC HVDC," 2014.

[117] M. Szechtman, T. Wess, and C. V. Thio, "A benchmark model for HVDC system studies," in *International Conference on AC and DC Power Transmission*, 1991, pp. 374-378.

[118] DIgSILENT, "User Manual," vol. 2, 2014.

[119] D. Jovcic and K. Ahmed, *High Voltage Direct Current Transmission: Converters, Systems and DC Grids*: Wiley, 2015.

[120] Alstom Grid, *HVDC: Connecting to the future*, 2011.

[121] M. A. Perez, S. Bernet, J. Rodriguez, S. Kouro, and R. Lizana, "Circuit Topologies, Modeling, Control Schemes, and Applications of Modular Multilevel Converters," *IEEE Transactions on Power Electronics,* vol. 30, pp. 4-17, 2015.

[122] Jiangchao Qin, M. Saeedifard, A. Rockhill, and Z. Rui, "Hybrid Design of Modular Multilevel Converters for HVDC Systems Based on Various Submodule Circuits," *IEEE Transactions on Power Delivery,* vol. 30, pp. 385-394, 2015.

[123] A. Nami, L. Jiaqi, F. Dijkhuizen, and G. D. Demetriades, "Modular Multilevel Converters for HVDC Applications: Review on Converter Cells and Functionalities," *IEEE Transactions on Power Electronics,* vol. 30, pp. 18-36, 2015.

[124] S. Debnath, Q. Jiangchao, B. Bahrani, M. Saeedifard, and P. Barbosa, "Operation, Control, and Applications of the Modular Multilevel Converter: A Review," *IEEE Transactions on Power Electronics,* vol. 30, pp. 37-53, 2015.

[125] RP Burgess, JD Ainsworth, HL Thanawala, M Jain, and R. Burton, "Voltage/Var control at McNeill Back-to-Back HVDC converter station," *CIGRE Session,* pp. 14-104, 1990.

[126] B. Andersen, D. Monkhouse, and R. Whitehouse, "Commissioning the 1000MW Back to Back HVDC link at Chandrapur, India," *CIGRE paper,* pp. 14-114, 1998.